

Aus der Universitätsklinik für Thorax-, Herz- und
Gefäßchirurgie Tübingen
Sektion Medizinische Werkstoffkunde und Technologie

Application of QCM-D to simulate oral interfacial
interactions of bacteria, antibacterial agent and titanium
implant surfaces

Inaugural-Dissertation
zur Erlangung des Doktorgrades
der Zahnheilkunde

der Medizinischen Fakultät
der Eberhard Karls Universität
zu Tübingen

vorgelegt von
Xu, Zeqian

2020

Dekan: Professor Dr. B. Autenrieth

1. Berichterstatter: Professor Dr. F. Rupp
2. Berichterstatter: Professorin Dr. D. Wolff

Tag der Disputation: 04. 06. 2020

Contents

Contents	I
List of Tables	IV
List of Abbreviations	X
1. Introduction	1
1.1 Oral biofilm and pellicle	1
1.1.1 Pellicle and dental materials.....	1
1.1.2 Bacteria colonization and pellicle	1
1.1.3 Biofilm formation on teeth and dental implant	2
1.2 Dental implant and peri-implantitis	5
1.2.1 Ti and dental implant	5
1.2.2 Prophylaxis and treatment of Peri-implantitis	6
1.3 Antibacterial agent	7
1.4 QCM-D and application	8
1.4.1 Mechanism of QCM-D	8
1.4.2 QCM-D and bacterial adhesion	10
1.4.3 Combination of QCM-D with online microscopy	11
1.5 Aim of the study	11
2. Materials and Methods	13
2.1 Surface characterization of sensor surface	13
2.1.1 Contact angle and wettability analysis	13
2.1.2 Surface roughness analysis	14
2.2 Online sensor system-quartz crystal microbalance	14
2.3 QCM-D runs.....	16
2.3.1 Online assembling of the biosensor by human saliva	16
2.3.2 Bacterial suspension and antibacterial agent (ABA)	17
2.3.3 QCM-D and running sequences	18
2.4 Live/Dead staining and microscopic analysis	19

Contents

2.5 SEM and FE-SEM analysis	20
2.6 Helium Ion Microscope (HIM) analysis	22
2.7 Dissipation-frequency (ΔD - Δf) plots	24
2.8 Real-time combination with QCM-Microscopy setup	24
2.9 Statistical analysis	28
3. Results	29
3.1 Sensor surface characterization	29
3.2 QCM-D online experiments and Live/Dead staining.....	31
3.2.1 Online formation of saliva-coated Ti-based biosensors.....	31
3.2.2 ABA interacting with Ti sensors	32
3.2.3 ABA interacting with saliva-coated biosensors	34
3.2.4 Influence of salivary pellicle on <i>S. gordonii</i> adhesion.....	35
3.2.5 Impact of ABA application on <i>S. gordonii</i> adhesion.....	38
3.2.6 Summarized results of ABA and bacteria caused <i>f</i> and <i>D</i> shifts	47
3.3 SEM, FE-SEM and HIM analysis after QCM-D run	51
3.4 Dissipation-frequency (ΔD - Δf) plots and their interpretation	58
3.5 QCM-Microscopy set-up construction and application	63
3.5.1 Microscopic lens selection.....	63
3.5.2 Consecutive fluorescent microscopic photo making	67
3.5.3 Combination of bacterial count and QCM-D signal	71
3.5.4 Analysis of antibacterial function	74
4. Discussion	82
4.1 QCM-D and SPR	82
4.2 QCM-D and bacteria adhesion	83
4.3 Chlorhexidine (CHX) and Ti interaction	84
4.4 <i>S. gordonii</i> and pellicle interaction and mass-loss effects	85
4.5 Surface interaction of antibacterial agent and its impact on bacterial adhesion and vitality	89
4.6 HIM and applications	91

Contents

4.7 Real-time monitoring with QCM and the QCM-Microscopy set-up ...	93
5. Conclusion	95
6. Zusammenfassung	97
7. References	99
Declaration of Contribution	XII
Publication of the content of the dissertation.....	XIV
Acknowledgment	XV
Curriculum Vitae	XVII

List of Tables

Table 1: Summary of QCM-D frequency and dissipation shifts and Sauerbrey calculations of adsorbed mass upon different interaction sequences of ABA and *S. gordonii* and the bacterial viability.

List of Figures

Figure 1: Contact angle measurement through DSA 10-Mk2 drop shape analysis system.....	13
Figure 2: Overview of QCM-D Ti coated quartz crystal sensor surface.....	16
Figure 3: QCM-D devices setup (qCell T, 3T analytik, Tuttlingen, Germany).	16
Figure 4: Schematic and respective protocols showing the different experimental sequences.....	19
Figure 5: E 3100 Critical Point Dryer (Quorum Technologies, Laughton, UK)	21
Figure 6: Sputter Coater (SCD 050, Baltec, Germany).....	21
Figure 7: Scanning electron microscope (Leo 1430 SEM, Zeiss, Oberkochen, Germany).....	22
Figure 8: Field emission scanning electron microscope (Fe-SEM, JSM-6500F, Jeol, Japan).....	22
Figure 9: Zeiss ORION NanoFab HIM (Carl Zeiss Microscopy GmbH, Oberkochen, Germany).....	24
Figure 10: Construction of QCM-fluorescent microscope dynamic observation flow chamber.....	27
Figure 11: Different bacterial staining protocol for continuous flowing measurement in the QCM-fluorescent microscope dynamic observation flow chamber setup.....	28
Figure 12: Contact angle measurement through DSA 10-Mk2 drop shape analysis system (Kruess, Hamburg, Germany).....	29
Figure 13: AFM and WLI outcomes of the Ti- coated quartz crystal sensor surfaces.....	30
Figure 14: PSD function of the Ti-coated quartz crystal sensor surface.....	31

Figure 15: QCM-D running sequence protocol A: online formation of saliva-coated Ti-based biosensors.....32

Figure 16: Exemplary QCM-D curves: online formation of saliva-coated Ti-based biosensors (protocol A in **Figure 4**).....32

Figure 17: QCM-D running sequence protocol B: online interaction of ABA and Ti-based biosensors surface with (2) and without (1) saliva coating.....33

Figure 18: Exemplary QCM-D curves: interaction of ABA and Ti-based biosensors surface (protocol B1 in **Figure 4**).....34

Figure 19: Exemplary QCM-D curves: interaction of ABA and Ti-based biosensors surface coated with saliva (protocol B2 in **Figure 4**).....35

Figure 20: QCM-D running sequence first part of protocol D: *S. gordonii* interacting with Ti-based biosensors surface with (2) and without (1) saliva coating.....35

Figure 21: Exemplary QCM-D curves: *S. gordonii* interaction with Ti-coated sensor surface (first part of protocol D1 in **Figure 4**).....36

Figure 22: Exemplary image of Live/Dead stained *S. gordonii* after 120 min flowing on Ti-coated sensor surface (first part of protocol D1 in **Figure 4**)....36

Figure 23: Exemplary QCM-D curves: *S. gordonii* interacting with saliva coated biosensor surface (first part of protocol D2 in **Figure 4**).....37

Figure 24: Exemplary image of Live/Dead stained *S. gordonii* after 120 min flowing on saliva coated biosensor surface (first part of protocol D2 in **Figure 4**).....37

Figure 25: QCM-D running sequence of protocol C: impact of ABA on *S. gordonii* adhesion toward Ti-coated biosensors surface with (2) and without (1) saliva coating.....38

Figure 26: Exemplary QCM-D curves: *S. gordonii* interacting with Ti-coated sensor surface preconditioned with ABA (protocol C1 in **Figure 4**).....39

Figure 27: Exemplary image of Live/Dead stained *S. gordonii* after 120 min flowing over Ti-coated sensor surface preconditioned with ABA (protocol C1 in **Figure 4**).....39

Figure 28: Exemplary QCM-D curves: *S. gordonii* interacting with saliva-coated biosensor surface preconditioned with ABA (protocol C2 in **Figure 4**).....40

Figure 29: Exemplary image of Live/Dead stained *S. gordonii* after 120 min flowing over saliva-coated biosensor surface preconditioned with ABA (protocol C2 in **Figure 4**).....40

Figure 30: QCM-D running sequence of protocol D: ABA interacting with *S. gordonii* pre-adhered to Ti-coated sensors with (2) and without (1) saliva coating.....41

Figure 31: Exemplary QCM-D curves: ABA interacting with *S. gordonii* attached to Ti-coated sensor surface (protocol D1 in **Figure 4**).....42

Figure 32: Exemplary image of Live/Dead staining of ABA applying to Ti-coated sensor surface attached *S. gordonii* (protocol D1 in **Figure 4**).....42

Figure 33: Exemplary QCM-D curves: ABA interacting with *S. gordonii* attached to saliva-coated biosensor surface (protocol D2 in **Figure 4**).....43

Figure 34: Exemplary image of Live/Dead staining of ABA acting on *S. gordonii* attached to saliva-coated biosensor surface (protocol D2 in **Figure 4**).....43

Figure 35: QCM-D running sequence of protocol E: mixture of ABA and *S. gordonii* interacting with Ti sensors with (2) and without (1) saliva coating. P44

Figure 36: Exemplary QCM-D curves: mixture of ABA and *S. gordonii* interacting with Ti-coated sensor surface (protocol E1 in **Figure 4**).....45

Figure 37: Exemplary image of Live/Dead staining of mixture of ABA and *S. gordonii* interacting with Ti-coated sensor surface (protocol E1 in **Figure 4**)..45

Figure 38: Exemplary QCM-D curves: mixture of ABA and *S. gordonii* interacting with saliva-coated biosensor surface (protocol E2 in **Figure 4**). P46

Figure 39: Exemplary image of Live/Dead staining of mixture of ABA and *S. gordonii* interacting with saliva-coated biosensor surface (protocol E2 in **Figure 4**).....47

Figure 40: *S. gordonii* (left part) and ABA (right part) caused frequency

changes in different flowing sequences.....48

Figure 41: After PBS flowing, ABA interaction caused final frequency change on different surface situation.....49

Figure 42: SEM image of 120 min flow of *S. gordonii* adhered on saliva coated biosensor at the magnification of 5000x.....52

Figure 43: FE-SEM image of 120 min flow of *S. gordonii* adhered on saliva coated biosensor at the magnification of 40000x.....53

Figure 44: FE-SEM image of 120 min flow of *S. gordonii* adhered on saliva coated biosensor at the magnification of 120000x.....53

Figure 45: SEM image of 30 min ABA treated 120 min flow of *S. gordonii* adhered on saliva coated biosensor at the magnification of 5000x SEM.....54

Figure 46: FE-SEM image of 30 min ABA treated 120 min flow of *S. gordonii* adhered on saliva coated biosensor at the magnification of 10000x.....54

Figure 47: FE-SEM image of 30 min ABA treated 120 min flow of *S. gordonii* adhered on saliva coated biosensor at the magnification of 43000x.....55

Figure 48: FE-SEM image of 30 min ABA treated 120 min flow of *S. gordonii* adhered on saliva coated biosensor at the magnification of 150000x.....55

Figure 49: HIM cross-section image of ABA treated *S. gordonii* adhered on saliva coated biosensor surface.....56

Figure 50: HIM cross-section image of the single *S. gordonii* treated by ABA adhered on saliva coated biosensor surface.....57

Figure 51: HIM images of un-sputtered (no Au-Pd coating) ABA treated *S. gordonii* adhered on the saliva coated biosensor surface.....58

Figure 52: Exemplary $\Delta D-\Delta f$ plots of QCM-D sequence of applying *S. gordonii* on ABA preconditioned Ti-coated sensor surface (protocol C1 in **Figure 4:** ABA-S.g.).....60

Figure 53: Exemplary $\Delta D-\Delta f$ plots of QCM-D sequence of applying *S. gordonii* on ABA preconditioned saliva-coated biosensor surface (protocol C2 in **Figure 4:** Sal-ABA-S.g.).....61

Figure 54: Exemplary $\Delta D-\Delta f$ plots of QCM-D sequence of applying ABA on *S.*

gordonii adhered Ti-coated sensor surface (protocol D1 in **Figure 4**:*S.g.-ABA*).....61

Figure 55: Exemplary ΔD - Δf plots of QCM-D sequence of applying ABA on *S. gordonii* adhered saliva-coated biosensor surface (protocol D2 in **Figure 4**:*Sal-S.g.-ABA*).....62

Figure 56: QCM-D flow chamber exposed to fluorescent light for dynamic observation through microscopy.....63

Figure 57: Construction of the mirror lens (40x 0.50, Carl Zeiss Jena) and adjustment of the QCM-D flow chamber.....64

Figure 58: Focused fluorescent images in of different situations under different magnification of lens.....66

Figure 59: Adhesion experiment of SYTO 9 stained *S. gordonii* ($OD_{620\text{ nm}} = 0.1$) flowing for 3 hours over the Ti coated quartz.....68

Figure 60: Representative consecutive online fluorescent images of *S. gordonii* ($OD_{620\text{ nm}} = 0.1$) attached to Ti sensor surface.....70

Figure 61: Adhesion experiment of Syto-9 stained *S. gordonii* ($OD_{620\text{ nm}} = 0.1$) flowing for 2 hours over the golden quartz.....70

Figure 62: Online consecutive fluorescent photograph of the attached *S. gordonii* ($OD_{620\text{ nm}} = 0.1$) on golden quartz surface.....71

Figure 63: Correlating the consecutive fluorescent images with the same time points on the frequency curve.....72

Figure 64: Correlating the number of surface bound bacteria with the frequency change at each time point.....72

Figure 65: Correlation between the change of QCM-D signal and the amount of Ti sensor surface-bound *S. gordonii*.....73

Figure 66: Linear correlation between the number of surface-bound bacteria and frequency or dissipation change.....74

Figure 67: Glass slide test with different ABA and *S. gordonii* Live/Dead stain process under fluorescent microscope (400x).....76

Figure 68: SYTO 9 stained *S. gordonii* ($OD_{620\text{ nm}} = 0.74$) binding on ultrasonic

Contents

bath cleaned golden quartz followed with ABA+ PI mixture.....	77
Figure 69: Exemplary online fluorescent images (200x) of SYTO 9 stained <i>S. gordonii</i> ($OD_{620\text{ nm}} = 0.74$) binding on ultrasonic bath and plasma cleaned golden quartz and interact with ABA.....	78
Figure 70: FDA stained <i>S. gordonii</i> ($OD_{620\text{ nm}} = 1.4$) binding on ultrasonic bath and 15 min O_2 plasma cleaned golden quartz and interact with ABA.....	80
Figure 71: Exemplary online fluorescent photo of FDA/EB stained <i>S. gordonii</i> ($OD_{620\text{ nm}} = 1.4$) binding on golden quartz and interact with ABA.....	81
Figure 72: Schematic illustration of QCM-D signal patterns during two physiologically important oral situations.....	86

List of Abbreviations

ABA: antibacterial agent

AC: alternating current

AFM: atomic force microscopy

AgI/II: antigen I/II

ANOVA: one-way analysis of variance

CHX: chlorhexidine

CPC: Cetyl pyridinium chloride

EB: ethidium bromide

FDA: fluorescein diacetate

FE-SEM: field emission scanning electron microscope

gp-340: glycoprotein-340

HIM: Helium ion microscope

Hz: Hertz

LbL: layer by layer

NCSCs: neural crest-derived stem cells

OMPs: outer membrane proteins

PI: propidium iodide

PPP: platelet poor plasma

PRP: platelet rich plasma

PRPs: proline rich proteins

PSD: Power Spectral Density

QCM: Quartz crystal microbalance

QCM-D: QCM with dissipation monitoring

S. gordonii: *Streptococcus gordonii*

S.g.: *S. gordonii*

Sa: average 3D-roughness

Sal: saliva

SEM: scanning electron microscope

SFE: surface free energy

SPR: surface plasmon resonance

Sq: root mean square roughness

Srr: Serine-rich Repeat

TEM: transmission electron microscopy

Ti: titanium

WLI: white light interferometry

ΔD - Δf : Dissipation change to frequency change

1. Introduction

1.1 Oral biofilm and pellicle

1.1.1 Pellicle and dental materials

Saliva, one of the most important body fluids, shows various vital functions for human oral and systematic health [1]. It is closely related to the development of pellicle. Pellicle is an organic proteinaceous film forming on the surface of dental enamel or dental materials which are exposed to saliva in the oral environment by selective and spontaneous adsorption of salivary proteins [2]. The mechanism of salivary components binding to mucosal surface are covalent binding, however, on teeth and dental material surfaces, the pellicle formation depends on non-covalent binding [3-5]. Thus, the composition of the salivary pellicle is somehow influenced by the nature of the teeth and dental material surfaces [6]. The main salivary proteins found on the dental enamel surface (hydroxyapatite) are consisting of secretory IgA, statherins, proline rich proteins (PRPs), high molecular weight mucin MUC5B, cystatin SA-I, lactoferrin, amylase and lysozyme [7]. The so-called “acquired pellicle” converts the dental surface through this thin film and plays an important role in preventing wear, demineralization and dehydration [2, 8]. The pellicle forming on Ti surfaces is of structural heterogeneity [9]. The formation process includes two phases, the first phase is correlated with the initial adsorption process of discrete protein, followed by the second phase of micelle-like salivary protein aggregate adsorption [9-12]. This implies that the pellicle on Ti surface comprises a highly hydrated outer layer on top of a dense anchoring inner layer [9, 13, 14]. Additionally, the formation of pellicle is of the utmost importance in the plaque formation [15].

1.1.2 Bacteria colonization and pellicle

Over 600 different bacterial species exist in the human oral cavity and more than 100 species for individuals [16]. These gram-positive and

gram-negative microbes can specifically bind to the pellicle covered oral surfaces through electrostatic, hydrophobic, and ionic interactions with the bacterial surface specific adhesin molecules [17]. The Serine-rich Repeat (Srr) protein family is mostly expressed by streptococci, lactobacilli and staphylococci through forming fimbriae or fibrils on the bacterial surface with a length up to 600 nm, which makes a larger distance interaction between bacteria and pellicle possible. These Srr surface adhesins can specifically recognize the carbohydrate (saccharide) moieties as part of the glycosylated salivary constituents in the salivary pellicle [17]. The Srr proteins consist of two variants of Hsa and GspB on the surface of *Streptococcus gordonii* (*S. gordonii*), which can mediate the specific recognition and adhesion toward sialic-acid-containing components (salivary mucin MG2 and salivary agglutinin) in pellicle [18]. The antigen I/II (Agl/II) family proteins expressed on bacterial surfaces are able to recognize various receptors of the oral cavity [19]. Some of the Agl/II proteins, such as Hsa/GspB and SspA/SspB on *S. gordonii* surfaces and SpaP on *S. mutans* surfaces, can specifically interact with the salivary pellicle through the scavenger receptor of innate immunity glycoprotein-340 (gp-340) [17, 20]. Besides, the FomA produced by *Fusobacterium nucleatum*, as one of the major outer membrane proteins (OMPs) of gram-negative bacteria, mediates strong attachment to the salivary constituent statherin [17, 21]. The oral primary colonizer interacting specifically with pellicle through the surface protein plays an important role in the further construction of mature oral biofilm [9].

1.1.3 Biofilm formation on teeth and dental implant

Biofilm is a microbial-derived sessile community characterized by bacteria which are irreversibly bound to various characterized surfaces and aggregate to each other, embedding in a hydrated polymeric extracellular matrix produced by multi-species of bacteria [22-24]. Clinically, biofilm can easily form on various medical material surfaces, including artificial heart valves, catheters,

coronary stents, fracture fixation devices, intraocular lenses, cochlear implants, dental prosthesis and dental implants [23, 25], causing invasive microbial infections in bone, lung, skin, or blood. These infections are still a life threatening issue due to multifaceted reasons, including (I) insufficient approaches to attack bacteria embedded inside of the biomedical biofilms, (II) a resistance toward the effective antibiotics, and (III) incapability of developing adequate and efficient novel antibiotics [26-28].

In the field of dentistry, biofilm which is denoted as dental plaque widely exists on dental natural surfaces as well as on dental material surfaces such as crowns, bridges made from metal or ceramic materials and implant or abutment surfaces. The disease-associated oral biofilm has gained great concern for decades [29]. In the oral cavity, the formation of plaque on enamel and dental material surfaces consists of multiple stages [30]. Within several minutes, the surface exposed to the oral cavity will be covered with a thin layer of pellicle [1]. In the human oral cavity, every milliliter of saliva contains as many as roughly 10^8 bacteria [1, 23, 31]. Within 4 hours after formation of pellicle, the oral bacteria start the colonization on the pellicle surface [23]. Taking the teeth surface as an example, initially, the bacteria are associated with the pellicle surface loosely and reversibly through electrostatic and hydrophobic forces, then switch to a higher binding affinity state through specific and irreversible adsorption between multiple adhesins on the bacterial cell surface and the pellicle proteins [30, 32].

The proliferation of adhered bacteria contributes to the subsequent formation of distinct micro-colonies, developing into the attached plaque. The biofilm is well organized and consists of various species, which can specifically adhere to different surfaces and co-aggregate with other species specifically to form a dense plaque [22, 33]. The growth and maturation of the plaque is characterized by the primeval "circulation system" and performs as an "organism" [30]. The connected channels for nutrients circulation and microbial communities embeded inside the biofilm build up the complicated structures

and metabolism. This provides the possibility for rapid dispersion and proliferation of the planktonic bacteria and nonsessile individuals and for building up an growth protection mode for the microbes' survival from the host environment [22, 34].

At this stage, after a 2 to 4 week plaque formation, the diversity of bacterial species is increased and the mature plaque is dominated by gram-negative anaerobic species, which could induce gingivitis or the progress into periodontitis [35].

The biofilm on implant surfaces shows great similarity to sub-gingival dental plaque [36-39]. The primary colonizers on implant surfaces are mainly oral streptococci, including *Streptococcus gordonii*, *Streptococcus sanguis*, *Streptococcus oralis* and *Streptococcus mitis*, which predominate in plaque for at least 4 hours. The number of anaerobic species increases after 48 hours [38, 40-42]. *S. gordonii*, which is intrinsically an oral non-pathogenic bacteria, could construct the base layer of the plaque on implant surfaces [43]. These bacteria can also infiltrate into the bloodstream through the sub-gingival region, which might induce infective life-threatening endocarditis [44].

The early colonizers on the surface could provide a supportive environment for the late colonizers, which are much more depending on growing conditions than the early colonizers [45]. The main secondary colonizer, *Fusobacterium nucleatum*, communicates and interacts with other bacteria constructing the biofilm continuously with the late colonizers [46]. The late colonizers, for instance, the *Porphyromonas*, *Fusobacterium* and *Prevotella* species, which are the main periodontal pathogens, can bind to the surface through the early colonizers [41], causing periodontitis and peri-implantitis [47, 48]. It is reported that within 30 min after implant insertion, bacteria start colonizing on the implant surface [49]. The bacterial early colonization is influenced by the surface properties of the implant, but not for the plaque maturation process [42].

The formation of biofilm on the Ti surfaces is influenced by various factors,

including implant surface roughness, surface wettability, surface chemistry, or surface free energy (SFE) [50]. Ti surfaces with a roughness of $Ra \leq 0.088 \mu\text{m}$ exhibited significant inhibition effects towards the primary biofilm colonization and also the plaque maturation after 24 h [51]. Correspondingly, a higher level of primary colonization was found on Ti with high roughness or also with low wettability [52]. As the components of SFE, the polar (acid-base) parts as well as the nonpolar (Lifshitz-van der Waals) parts of the colonizing bacteria as well as implant surfaces play an important role in bacterial adhesion and biofilm formation [23, 50, 53-55]. And the acid-base characteristics of the surface are considered as a crucial factor in bacterial adherence [55]. The surface chemistry of Ti, which is usually negatively charged in the physiological environment (pH = 7.4) and the oral salivary environment (pH = 6.7 - 7.3) [56, 57], is vital for biological interactions of positively charged proteins and for further attachment of bacteria forming biofilm [50, 58]. Thus, various surface modifications toward Ti surfaces into bacteriostatic or bactericidal surfaces has been carried out to diminish bacterial colonization and inhibit biofilm formation, such as antimicrobial peptide coating [59], TiO_2 nanotube coating [60], Ag or Cu nanoparticle coating [61], layer by layer (LbL) self-assembly chitosan coating [62], thermal-responsive polymer brush coatings [63], and photocatalytic anatase coatings [64, 65].

1.2 Dental implant and peri-implantitis

1.2.1 Ti and dental implant

Since the indispensable milestone discovery that Ti could constitute osseointegration with bone tissue and was firstly applied as an implant by Brånemark in the 1970s [66, 67], the Ti implant started to be widely used in dentistry and craniofacial surgery in the past 20 years [68]. In dentistry, implants are widely used for the replacement of lost teeth in the field of prosthodontics and implantology for supporting crowns, bridges, or prostheses.

The highly polished titanium is used for dental abutments, which is covered by gingival tissue and partly exposed to the oral environment, functioning as a connector between the dental prostheses and the dental artificial tooth root implant.

Ti has been treated as a “gold standard” material among other various materials due to its high survival rate in the application of dental implant [38, 69]. The main available Ti materials applied for dental implants include six types: four types of pure Ti (Grade 1, Grade 2, Grade 3 and Grade 4) and two types of alloys (Ti-6Al-4V (Grade 5) and Ti-6Al-4V-ELI (Grade 23) extra low interstitial) [70]. Ti used for dental implants should reach a sufficient strength against occlusion forces without causing a permanent deformation, combined with corrosion resistance [71].

1.2.2 Prophylaxis and treatment of Peri-implantitis

Peri-implantitis, the inflammation situation of gingival and bone tissue surrounding the inserted implant, which could further progress into the loss of supporting bone and implant failure, standing in the way of achieving the long term functional and esthetic success of the dental implant, is considered as one of the most challenging biological complications [46, 72, 73]. Approximately 20 % of patients and 10 % of implants are involved with peri-implantitis 5 - 10 years after implant placement [74, 75]. The biofilm or plaque formation on dental implant surfaces is one of the main causative reasons for peri-implantitis, which is proved to be of strong evidence according to published human and animal experiments [76-78].

The treatment of peri-implantitis includes surgical and non-surgical therapies [79]. To reach the goal of efficient removal of biofilm on an implant surface, various non-surgical therapies, including a combination of machine driven submucosal mechanical debridement, chemical decontamination, adjunctive antimicrobial treatment, submucosal glycine powder air polishing, and Er:YAG laser treatment has been applied for the treatment of

peri-implantitis [80-83]. The combination of mechanical debridement and chlorhexidine digluconate local application showed great clinical outcomes [83].

Till now, the prophylaxis of peri-implantitis has shown great priority, because of the required extensive resources and additional complex therapy for peri-implantitis treatment [46]. The prophylaxis of peri-implantitis includes the prevention and treatment of peri-implant mucositis, which involves the instruction of self-performed oral hygiene control and the personalized clinical follow up supportive therapy [46, 79, 84]. Before dental implant surgery, preoperative and postoperative mouth rinsing with chlorhexidine (CHX) has been regularly applied for the prophylaxis of peri-implantitis [85].

1.3 Antibacterial agent

In order to prevent and control the occurrence of infection, antibacterial agent application can be used for the control of dental plaque accumulation including: 1) inhibiting the accumulation rate of new plaque; 2) removing the existing plaque; 3) selective suppression towards the pathogenic oral bacterial species; 4) hindering the producing of virulence factors such as proteases and cytotoxins [86].

Based on these mechanisms, various antibacterial agents have been developed and applied in mouthrinses for controlling the biofilm formation. The bis-biguanide such as chlorhexidine has been widely used as a gold standard for the antibacterial agent. The essential oils including thymol, eucalyptol, menthol and methyl salicylate, showing significant clinical inhibition effects toward dental plaque formation and gingivitis, are also functionalized in mouthrinse [87]. The novel compounds of plant extracts (tt-famesol, apigenin) have shown anti-caries activity toward *Streptococcus mutans* [88]. The enzymes, like glucanase, mutanase and amyloglucosidase-glucose oxidase are involved in the mouthrinse, due to its function of disrupting the biofilm structure [89]. Metal ions, e.g. Zn^{2+} and Cu^{2+} , are active against both the

gram-positive and gram-negative bacteria [90]. Cetyl pyridinium chloride (CPC), as a widely used quaternary ammonium compound in mouthrinses with wide antibacterial spectrum and rapid killing effect, provides significant additional plaque and gingival inflammation inhibition effect [91, 92].

Chlorhexidine (1,6-di[4-chlorophenyldiguanido]-hexane) is a broad spectrum cationic bisbiguanide bactericide against both gram-positive and gram-negative bacteria, and some lipophilic viruses, yeasts and dermatophytes [85, 93], which has been widely used for clinical hand and skin disinfection, also applied as a mouthrinse in the field of dentistry [94]. Different formulations of chlorhexidine (CHX), such as gel, mouthwash and spray in concentrations of 0.1 %, 0.12 %, and 0.2 %, have been used in oral cavity for caries prevention, plaque control, gingivitis management, and prophylaxis for peri-implantitis [95, 96]. CHX causes bacterial membrane perforation and forms irreversible complexes with intracellular nucleic acids inducing fatal damage towards bacteria at a lethal concentration [97, 98]. In a sub-lethal concentration, CHX plays a bacteriostatic role of inhibiting and interfering the metabolism of the oral bacteria through hindering: the membrane function of intracellular pH value maintenance through enzymes; cariogenic streptococci's sugar transportation process and acid production process; *Porphyromonas gingivalis*'s major protease function [89].

CHX binds strongly and covalently to the bacterial, oral mucosal, pellicle and dental surface, which could provide a long lasting antibacterial effect in the oral cavity [98]. In contrast, CPC showed diminished activity and less persistence, when it adsorbs to the surface [89, 99]. CPC showed lesser antibacterial efficiency than CHX and essential oils for mouthrinses [100].

1.4 QCM-D and application

1.4.1 Mechanism of QCM-D

Studies of the dynamic interfacial interaction between bulk liquids and solid surfaces are of extreme importance in fundamental research of chemistry,

physics and in the field of biomedicine. In recent decades, the QCM technology has been widely utilized in the analysis of organic and inorganic materials, soft and solvated bio-interface analysis including food processing, implant surfaces, coatings, biosensors and marine technology, which makes a dynamic and even quantitative monitoring of interface changes possible [101].

Quartz crystal microbalance (QCM) is a highly sensitive technique with a detection capability accurate to nanogram. The basic mechanism is the piezoelectricity property of the quartz crystal. The application of alternate electric fields on the quartz will spontaneously contribute to the alternate contraction and expansion of the crystal lattice [102]. The quartz crystal is manufactured through the “AT-cut” process, which generates promising stability with the pure oscillation shear mode together with a low temperature coefficient. The crystal is embeded between two pieces of electrodes. Upon a high enough alternating current (AC) voltage with a frequency close to the resonance frequency (f_0) (or multiple overtones) of the quartz crystal, the standing wave will be generated over the crystal [101]. The thickness of the quartz crystal is in a negative correlation with the resonant frequency (f_0) [102]. And the molecular interacting with the surface will induce changes of the detected frequency. In principle, the rigid adsorption of molecules on the quartz surface will contribute to the decrease of the frequency. Moreover, QCM with dissipation monitoring (QCM-D) is developed through the calculation of dissipation. There are two possibilities to calculate dissipation, one possibility is to calculate based on the duration of oscillatory decay upon intermittently voltage switching off in the “ring down” process [101, 103, 104]; the other possibility is to use the half-bandwidth Γ for calculation, which is half of the value of the frequency bandwidth that extends between the two points where the conductance spectrum is half of the maximum [105].

The data extracted from QCM-D signals can be quantitatively interpreted mass loading in some specific situations according to the Sauerbrey's theory, which declared the linear relationship between the detected frequency change

and mass loading and turning this technology into a mass balance for detecting adsorbed mass accordingly [106]. However, the pre-requisite for this mass loading theory is: a relative small molecular mass and a rigid mass adsorption process with a homogeneous distribution on crystal active surface [102]. Apart from applications in solid/gas interfaces, the QCM-D technology has been further developed in more complicated liquid systems, which involves liquid viscosity and energy decay causing frequency changes [107]. Through QCM-D, the stiffness of an adsorbed film can be interpreted through combination of frequency and dissipation data, which is of great importance in the study of development of viscoelastic structures and contacts in the binding processes. Till now, QCM-D has been applied widely in liquid phase, especially for the pharmaceutical and biomedical fields, and were used there in many cases as biosensors concerning the detection of proteins, DNA, lipids, and cell and bacteria adhesion [108-110].

1.4.2 QCM-D and bacterial adhesion

In recent years, QCM-D has been widely involved in studying mechanisms of bacterial adhesion on different surfaces, bacterial detection, and analyzing antibacterial surfaces [111]. A monoclonal antibody functionalized QCM biosensor has been generated to accomplish the rapid detection of the vegetative cells and *B. anthracis* spores [112]. The combination of beacon immunomagnetic nanoparticles loaded with antibody and gold nanoparticles for mass amplification were applied in QCM systems for the monitoring and detection of *E. coli* activity [113]. For the purpose of investigating the biological adhesion mechanism of infective endocarditis related bacteria, the real-time interaction of *S. gordonii* with platelet rich plasma (PRP) or platelet poor plasma (PPP) covered surfaces are evaluated through QCM gold sensors, which induced both an increase of frequency and dissipation on PPP surface and an increase of frequency but decrease of dissipation on PRP surface [114]. The study of interfacial reactions of oral

primary colonizers on Ti implant surfaces with and without photocatalytic coatings and activation by various wavelengths of ultraviolet light were carried out on Ti QCM-D sensors modified with anatase coatings, which proved the antibacterial function of activated anatase modifications [64]. These studies have proven a number of promising applications of QCM-D in microbiological and biological related investigations.

1.4.3 Combination of QCM-D with online microscopy

Mass-sensitive quartz crystal microbalance with dissipation monitoring (QCM-D) is widely used in sensing bacterial binding [85, 115]. The Sauerbrey equation could be applied when thin and rigid layers of material are attached to the quartz crystal sensor surface [103, 116]. Studies indicate that, the adhesion of bacteria contributes to laterally heterogeneous dissipating film, bacterial mass loading cannot be directly calculated by the classical Sauerbrey equation [101, 114]. Till now there are no efficient calculation methods and models for quantifying the bacterial adhesion. The combination of real-time QCM-D and microscopic observation has been applied in the field of cell/surface interaction [117, 118]. In order to dig out the potential relationship between the change of frequency or dissipation and the adhesion process of bacteria, it is necessary to develop a novel QCM-D microscopic set-up, which could combine the QCM-D signal with real-time microscopic images for a better signal interpretation.

1.5 Aim of the study

The investigation of bacterial interaction on oral implant surfaces with different modifications has arisen great interest of clinicians and researchers. However, interactions at implant/bacteria interfaces and the influence of antibacterial agents are still unclear. Our study aimed at building up a highly sensitive bacterial adhesion detection system on a salivary modified biosensor, to obtain a precise interpretation of the QCM-D signal induced by specific and

unspecific binding of bacteria. Besides, we aimed at seeking for more information for the unsolved problem of the possibility of acoustic sensing the antibacterial agent (ABA) induced bacterial membrane perforation and bacterial cell lysis.

Moreover, due to the dissipating film with viscoelastic properties formed by bacteria adhesion, the induced signal cannot be directly quantified through the limited Sauerbrey equation. Thus, we developed a new design trying to correlate the QCM-D signals with the number of adhered bacteria by the development of a novel set-up of a QCM-D flow chamber combined with fluorescent microscopy to allow real-time monitoring of bacterial interactions.

2. Materials and Methods

2.1 Surface characterization of sensor surface

2.1.1 Contact angle and wettability analysis

The DSA 10-Mk2 drop shape analysis system (Kruess, Hamburg, Germany) was utilized to measure the surfaces wettability of the applied quartz crystals (**Figure 1**). For each measurement, a 2 μL water droplet was automatically deposited on the Ti coated sensor surface through the automated dosing system. The process of droplet deposition and developing to an equilibrated droplet on the surface was recorded by a video camera, which was in line with the dosing needle and the lamp. The needle diameter has been 0.5 mm. Based on the video analysis, the 20th second contact angle (20 s after the initial surface contact) was calculated by the circle fit method (DSA software version 1.91.0.2).

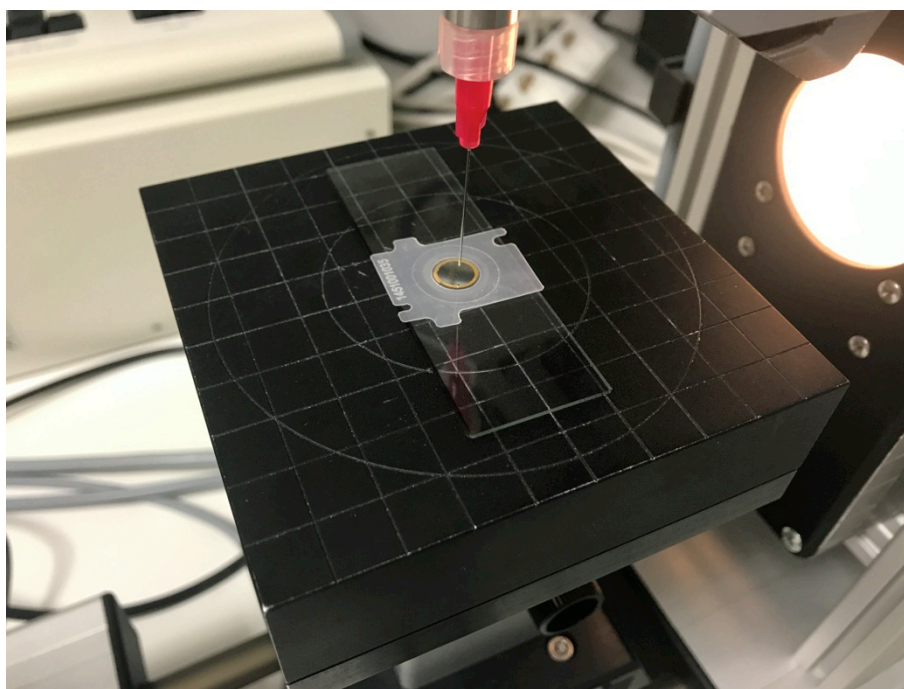


Figure 1: Contact angle measurement through the DSA 10-Mk2 drop shape analysis system (Kruess, Hamburg, Germany). The Ti-coated quartz crystal was laid on the measurement platform. A water droplet was deposited in the center of the sensor surface.

2.1.2 Surface roughness analysis

For the surface roughness analysis of the Ti coated quartz crystal sensors, measurements at different positions and in several scan areas were done by white light interferometry (WLI) and by atomic force microscopy (AFM), in which the NewView 7300 from Zygo (Weiterstadt, Germany) and the Dimension Icon in the tapping mode from Bruker (Karlsruhe, Germany) were utilized. “The root mean square roughness (Sq), the average roughness (Sa), as well as the Power Spectral Density (PSD) function were calculated from the topographical data $z(x,y)$ within a certain scan range L to receive quantitative information about the surface roughness. The PSD is defined by the absolute square of the surface profile’s fourier spectrum (in case of isotropic surfaces) equation (1): [85]”

$$\text{PSD}(f_x + f_y) = \lim_{L \rightarrow \infty} \frac{1}{L^2} |\text{FT}\{z(x,y)\}|^2 \quad \text{equation (1)}$$

“The PSD function provides the advantages of (i) determining the vertical as well as the lateral distribution of surface heights, and of (ii) combining information resulting from different measurement systems to analyze the roughness within a wide spatial frequency range [119], and of (iii) enabling a direct link between roughness and functional surface properties such as wetting or optical characteristics of a sample [120].” [85]

2.2 Online sensor system-quartz crystal microbalance

In this study, a commercial QCM-D device (qCell T; 3T analytik, Tuttlingen, Germany) was used for real-time monitoring of dynamic interfacial interactions among bacteria-surface, macromolecule-surface and macromolecule-bacteria [121]. The resonance frequency f_0 of the AT-cut quartz crystal sensors (3T analytik, Tuttlingen, Germany) is 10 MHz. The Ti coating on the sensor surface

2. Materials and Methods

was produced by sputtering on basic Au quartz crystal sensors [121]. Before each experiment, the sensors were ultrasonically cleaned in an order of 5 min of 70 % ethanol, 5 min of 2 % Hellmanex III (Hellma, Müllheim, Germany), and 5 min of Millipore water, respectively, and eventually were dried through N₂ before experimental runs. Notionally, in the situation of a rigid mass adsorption, a homogenous surface mass distribution, and the mass loading caused frequency change Δf below 0.2 % of the resonant frequency, the surface mass loading can be quantitatively calculated through the Sauerbrey equation (2):[106]

$$\Delta m = -\frac{A\sqrt{\rho_q\mu_q}}{2nf_0^2}\Delta f = -\frac{AC}{n}\Delta f \quad \text{equation (2)}$$

The mass loading Δm can be calculated relying on the following parameters: A represents the piezoelectrically active quartz crystal area (19.6 mm²), ρ_q denotes the density of the quartz (2.648 g cm⁻³), μ_q implies the shear modulus of the AT-cut quartz crystal (2.947×10^{11} g cm⁻¹ s⁻²), n denotes the harmonic number ($n = 1$ for a 10-MHz quartz crystal driven at 10 MHz), and C implies the Sauerbrey factor of the quartz crystal (here $C = 4.42$ ng cm⁻² Hz⁻¹). The theoretical sensitivity of the applied qCell T system is 0.87 ng Hz⁻¹ [85]. The quartz crystal was fixed in a flexible, thin polymer sheet for better handling and preventing of quartz damage induced by experimental operations. The diameter of the sensor working area exposed to liquid, which constitute the bottom of the QCM-D chamber, is 8 mm (**Figure 2**) [85]. All the experiments are running at a temperature setting of 23 °C.

A digital peristaltic pump (Reglo Digital MS-4/12, Ismatec, Wertheim, Germany) with adjustable flow rate was used for generating a constant flow of different liquids through the chamber of the flow cell. The inner volume of the flow chamber was 30 μ L. On top of the chamber, there was a window right above the sensor, enabling an optical control, e.g., in the process of liquid filling into the chamber (**Figure 3**).

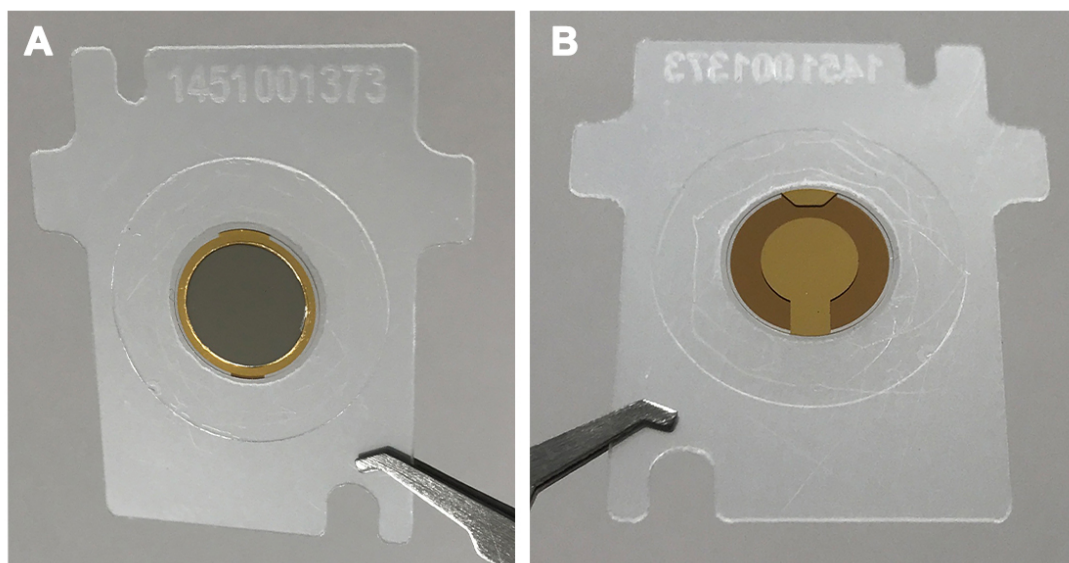


Figure 2: Overview of QCM-D Ti coated quartz crystal sensor surface. **A.** Ti coated smooth sensor surface; **B.** Backside of the sensor surface with the electrode part.

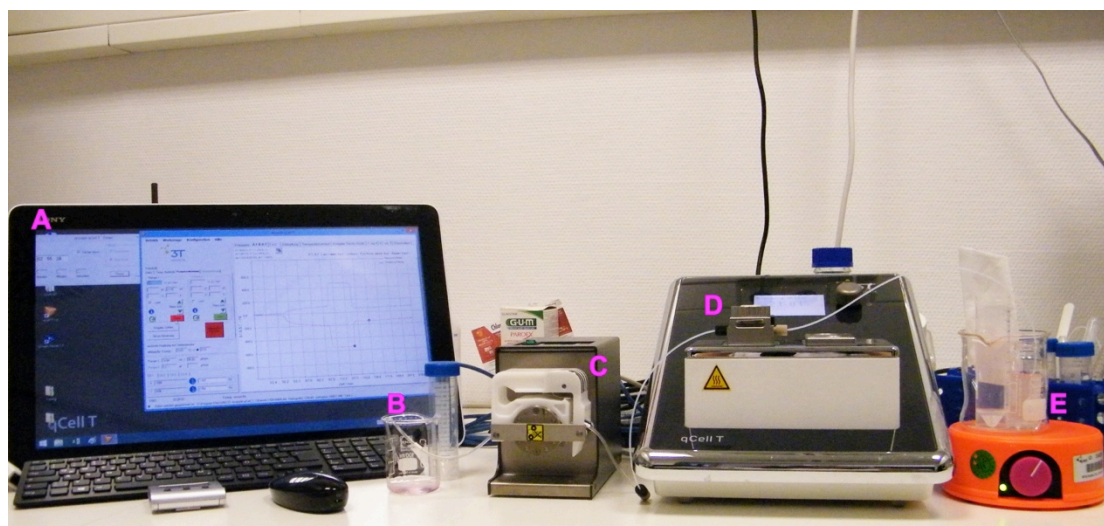


Figure 3: QCM-D device setup (qCell T, 3T analytik, Tuttlingen, Germany): **A.** Computer for QCM-D software; **B.** Waste collector; **C.** Peristaltic pump for flow rate control; **D:** QCM-D device with a flow chamber and a temperature control unit; **E:** Bacterial solution stirring with a magnetic stirrer.

2.3 QCM-D runs

2.3.1 Online assembling of the biosensor by human saliva

As previously described, for the complete study, human saliva was collected once from a healthy volunteer, for purpose of preventing the interpersonal and time-related deviation [85, 114]. Before saliva donation,

informed consent was acquired from the donor. In general, the primarily collected saliva was filtered through several steps to remove food sediments and bacteria from the donor's oral cavity. Firstly, the collected saliva was filtered through a cell strainer (BD Falcon, BD Biosciences, Durham, NC, USA) and then centrifuged at a speed of 14000 g at 4 °C for 30 min. Secondly, the supernatant was subsequently sterile-filtered through a series of low protein binding syringe filters (Acrodisc Syringe Filters with Supor PES membrane; Pall, St Columb, UK) with decreasing pore diameters of 5 µm, 1.2 µm and 0.45 µm. Finally, after being 1 to 5 diluted by phosphate-buffered saline (PBS; DPBS, Gibco®, Life Technologies, Darmstadt, Germany), the obtained saliva was distributed into 5 mL tubes and stored at -18 °C. Before infiltrating the salivary solution into the QCM-D chamber, the frozen saliva samples were thawed in a 37 °C water bath and went through sonication to obtain a homogenized solution. In order to form the saliva coated biosensors, saliva flow was realized for 30 min with controlled flow rate of 60 µL/min over the Ti sensor surface. By this, the so-called pellicle film was formed through salivary macromolecule adsorption to the Ti surface.

2.3.2 Bacterial suspension and antibacterial agent (ABA)

S. gordonii strain DL1 was grown in Schaedler medium (Becton Dickinson GmbH, Heidelberg, Germany) by incubating at 37 °C overnight, and was harvested through centrifugation at 1560 g for 5 min [85]. After discarding the supernatant, the pellet was resuspended in PBS and diluted into the concentration of 1×10^8 CFU ml⁻¹ (OD_{620 nm} = 0.54).

For experiments where *S. gordonii* and ABA are initially mixed before starting the flow, 20 ml of harvested *S. gordonii* suspension were mixed with 5 ml commercial ABA mouth rinse (GUM®, PAROEX®, Schönau, Germany) consisting of 0.05 % cetylpyridinium chloride (CPC) and 0.12 % chlorhexidine digluconate (CHX), which was used to simulate the clinical situation in the oral cavity. The mixture was constantly stirred with a magnetic stirrer during the

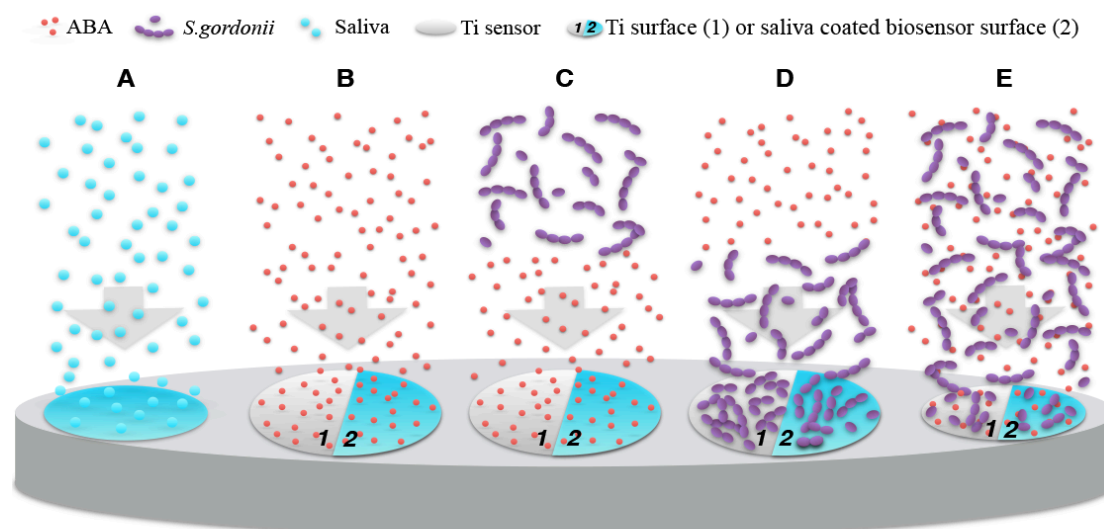
whole process of flowing.

2.3.3 QCM-D and running sequences

The cleaned Ti-coated quartz crystal was inserted into the QCM-D flow chamber (qCell T, 3T analytik, Tuttlingen, Germany). The backside of the sensor is connected with the electronic unit of the machine and the upper side is exposed in the flow chamber monitoring the contact and interfacial interaction with the molecules in the flowing liquid. For starting an experimental run, obtaining stable signal baselines during buffer rinsing with phosphate buffered solution (PBS) is a prerequisite, which implies a frequency drift lower than ± 2 Hz/min and a dissipation change below ± 5 Hz/min at a basic flow rate of 60 μ L /min [85]. To simulate different interfacial interactions as in different clinical situations, various protocols were designed with different sequences of the different analyte solutions (**Figure 4**).

The flowing time of saliva, PBS, and ABA was 30 min, respectively. For *S. gordonii* suspension, the flowing duration was prolonged to 120 min under constant magnetic stirring. For example, in protocol D2 (**Figure 4**), after reaching a stable baseline with PBS, the sterile saliva was flown over the Ti-coated sensor surface for 30 min to form the saliva-coated biosensor followed by 30 min PBS flow. Subsequently, a 120 min of *S. gordonii* flow was conducted to form the bacterial film, followed by a 30 min PBS flow. Eventually, 30 min of ABA flow was applied to simulate the situation of mouth rinse application on implant surfaces with potential plaque formation in the oral cavity, and this experiment was finalized with 30 min of PBS flow. For protocol E (**Figure 4**), which aimed at exploring the clinical mouth rinse situation of the interaction between a mixture of *S. gordonii* and ABA and the sensor surface with or without saliva coating, 5 ml of ABA suspension was initially mixed together with 20 ml of *S. gordonii* solution and applied under constant magnetic stirring. Between each run of the different solutions, a rinsing step with PBS was applied to remove loosely attached microbial mass or loosely

bound molecules.



A: Online formation of saliva-coated Ti-based biosensors

B: ABA interacting with Ti sensors or with saliva-coated biosensors

B1: (ABA) PBS→ABA→PBS

B2: (Sal-ABA) PBS→Sal→PBS→ABA→PBS

C: *S. gordonii* interacting with Ti sensors or with saliva-coated biosensors, both pre-conditioned with ABA

C1: (ABA-*S.g.*) PBS→ABA→PBS→*S.g.*→PBS

C2: (Sal-ABA-*S.g.*) PBS→Sal→PBS→ABA→PBS→*S.g.*→PBS

D: ABA interacting with *S. gordonii* attached to Ti sensors or to saliva-coated biosensors

D1: (*S.g.*-ABA) PBS→*S.g.*→PBS→ABA→PBS

D2: (Sal-*S.g.*-ABA) PBS→Sal→PBS→*S.g.*→PBS→ABA→PBS

E: Mixture of ABA and *S. gordonii* interacting with Ti sensors or with saliva-coated biosensors

E1: (mixed ABA+*S.g.*) PBS→mixed ABA+*S.g.*→PBS

E2: (Sal-mixed ABA+*S.g.*) PBS→Sal→PBS→mixed ABA+*S.g.*→PBS

ABA (antibacterial agent), *S.g.* (*S. gordonii*), Sal (saliva), Ti (titanium).

Figure 4: Schematic protocols A-E showing the different experimental sequences of analytes perfused over the titanium quartz crystal sensors in the QCM-D runs. ABA (antibacterial agent), *S.g.* (*S. gordonii*), Sal (saliva), Ti (titanium). [85]

2.4 Live/Dead staining and microscopic analysis

At the end of the QCM-D runs with bacteria, the chamber was emptied by a flow rate of 300 $\mu\text{l}/\text{min}$. The quartz sensors were demounted and stained with Live/Dead BacLight™ Viability kit (Molecular Probes®, Life Technologies) for 15 min. Subsequently, the sensors with the attached stained bacterial film were investigated with the fluorescence microscope (Optiphot-2, Nikon, Tokyo, Japan) combining with a remote control DSLR (Nikon 550D). The filters used for visualizing the stained *S. gordonii* were a 520 nm high-pass emission filter

and a 450–490 nm excitation band-pass filter (Nikon B2 Filtercube).

2.5 SEM and FE-SEM analysis

After QCM-runs, the sensors were demounted from the flow chamber. The demounted sensors with attached bacterial films from protocol D were gently rinsed with PBS and then fixed in 2 % glutaraldehyde solution (dissolved in PBS, pH 7.4) at 4 °C for around 20 h over night. After rinsing with PBS, the glutaraldehyde solution fixed bacteria were dehydrated through an ascending series of ethanol concentrations (30 %, 40 %, 50 %, 60 %, 70 %, 80 %, 90 %, 96 %, 100 %). The dehydrated samples were stored in 100 % ethanol and further substituted by liquid CO₂ through a critical-point-drying process with the Critical Point Dryer (E 3100, Quorum Technologies, Laughton, UK, **Figure 5**) connected with a temperature control system. Before surface analysis, the sensors were sputtered with a thin layer of Au–Pd by the Sputter Coater (SCD 050, Baltec, Germany) (**Figure 6**). Later on, the specimens were investigated by the scanning electron microscope (Leo 1430 SEM, Zeiss, Oberkochen, Germany, **Figure 7**) and the high-resolution field emission scanning electron microscope FE-SEM (JSM-6500F, Jeol, Japan, cooperation with Core Facility LISA+, Eberhard Karls University Tübingen **Figure 8**).

2. Materials and Methods



Figure 5: E 3100 Critical Point Dryer (Quorum Technologies, Laughton, UK).



Figure 6: Sputter Coater (SCD 050, Baltec, Germany).



Figure 7: Scanning electron microscope (Leo 1430 SEM, Zeiss, Oberkochen, Germany).



Figure 8: Field emission scanning electron microscope (Fe-SEM, JSM-6500F, Jeol, Japan) [122].

2.6 Helium Ion Microscope (HIM) analysis

The helium ion microscope (HIM) is a technology based on the scanning helium ion beam providing excellent high imaging resolution coupled with a tremendous depth of field [123]. The Orion Nanofab HIM (Carl Zeiss Microscopy GmbH, Oberkochen, Germany, **Figure 9**) utilized in this study allows a maximum resolution of 0.4 nm with a 5-10 times greater depth of field than with the modern SEM and FE-SEM [124]. The helium ions are generated

2. Materials and Methods

most efficiently at the apex of the tip, consisting of only three individual atoms. Each of these atoms contributes to the generation of helium ions but only the most intense is selected for imaging. The helium ions originating from this atom are directed specifically into the optics of the microscope and focused through the column to the sample. Helium ions can penetrate significantly further into the substrate at the same acceleration voltage as the electrons, resulting in the emission of secondary electrons from a smaller interaction area at the surface of the substrate. Thus, even better resolution can be obtained than with an electron microscope. Besides, substrates are always positively charged by bombardment with helium ions, they can be neutralized in the HIM with an electron gun. The HIM is therefore particularly well suited to imaging insulating substrates, which means the sputtering process is no longer indispensable [122]. All in all, the HIM induces a minimized sample destruction and obtains high surface contrast and resolution of 5 angstrom images without metal surface coating [124]

After going through the critical point drying process, the bacteria bound to the sensors both with and without Au-Pd sputtering were analyzed through the HIM, to investigate possible changes of the bacterial surfaces after the interaction with ABA and simultaneously to figure out any difference of the bacterial structure caused by sputtering.

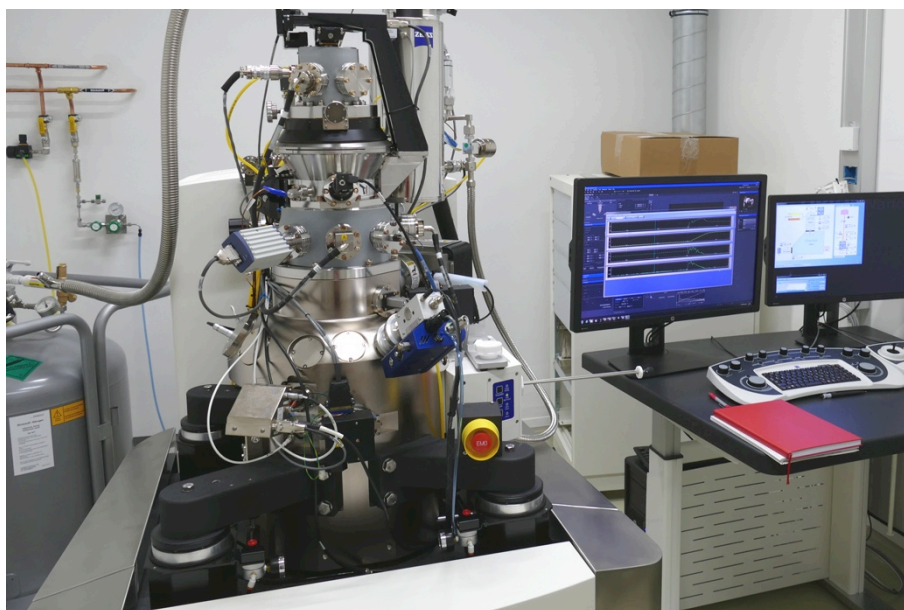


Figure 9: Zeiss ORION NanoFab HIM (Carl Zeiss Microscopy GmbH, Oberkochen, Germany) [122].

2.7 Dissipation-frequency (ΔD - Δf) plots

Correlations between frequency and dissipation were investigated based on D (y-axis)- f (x-axis) plots. Previous studies have shown that the rigidity or viscosity of adsorbed films can be deduced from the quotient of ΔD and Δf ($\Delta D/\Delta f$) [85, 125]. For example, a changing frequency during an adsorption process combined with an unchanged, constant dissipation could be interpreted as a complete rigid and homogeneous layer of loaded mass on the sensor surface. An increase of the softness and water content of the surface bound film would induce an increase of dissipation and a decrease of frequency [85]. “If the ΔD - Δf plot points to a dissipation decreasing direction, the film tends to become more rigid, and vice versa. Concurrently, if the ΔD - Δf plot points to a frequency decreasing direction, this represents mass loading on the film, and vice versa [126]”. [85]

2.8 Real-time combination with QCM-Microscopy setup

In order to correlate in real-time the QCM signal to the number of the bacteria adhered to the sensor surface, a newly developed QCM-D flow chamber (qCell μ Opto; 3T analytik, Tuttlingen, Germany) with a modified

2. Materials and Methods

optical window, which can be combined with a fluorescent microscope, was developed by 3T analytic and tested and evaluated in our research group (**Figure 10**). Concerning the focusing issue that a standard microscopic lens with limited field depth is not able to easily focus on the sensor surface through a certain thickness of liquid in the chamber above the sensor surface, various lenses with different magnification and depth of field were tested and compared before starting the experiment.

The sensors were ultrasonically cleaned in an order of 5 min of 70 % ethanol, 5 min of 2 % Hellmanex III (Hellma, Müllheim, Germany), and 5 min of Millipore water, respectively, then went through a 15 min of O₂ plasma cleaning.

The early oral colonizer *S. gordonii* was cultured in Schaedler medium, harvested by centrifugation, stained with SYTO[®]9 and diluted with PBS to OD_{620 nm} = 0.54 and 0.1 with and without washing procedure for the residual fluorescent staining molecules (**Figure 11**). Different staining and dilution procedures were compared, to reach the goal of a better focusing situation with clearly visible stained bacteria and low background disturbance. After reaching stable signal baselines with PBS, the stained bacteria were pumped with 60 µL/min through the system for 3 hours, followed by 30 min PBS rinsing. Fluorescent microscopic images were made every 5 min. The bacterial number was counted by image evaluation (Image J) and then correlated with the frequency and dissipation signals through qGraph Viewer.

This QCM-D microscopy set-up was also utilized in the real-time monitoring of interaction of the ABA on Ti surface bound *S. gordonii*. The glass slide test, which is putting a droplet of Live/Dead stained bacteria solution on a glass slide, covering with a cover glass and observing under the fluorescent microscope, was primarily used to investigate the possible staining methods for indicating the dynamic process of bacterial death. The different *S. gordonii* solution (200 µL) staining procedures included: 1) directly adding Live/Dead staining (200 µL) for 15 min; 2) adding Live/Dead staining (200 µL) for 15 min

2. Materials and Methods

followed by PBS washing combined with centrifugation and then adding ABA solution (100 μ L); 3) Adding ABA (100 μ L) and Live (SYTO 9) (100 μ L) staining for 15 min, followed by washing with PBS combined with centrifugation, then adding Dead (100 μ L, PI: propidium iodide) staining for 15 min; 4) Live (100 μ L, SYTO 9) staining for 15 min, wash with PBS combined with centrifugation, then adding a mixture of ABA and PI (100 μ L ABA+ 100 μ L PI) staining.

In the real-time microscopic monitoring of ABA interaction, the Live/Dead staining procedure was based on the primary test: the *S. gordonii* ($OD_{620\text{ nm}} = 0.74$) solution stained with SYTO 9 for 15 min was flown into the chamber for 30 min. During the 15 min PBS rinsing stage, fluorescent pictures were taken every 5 min. Later on, the mixed 200 μ L ABA + 200 μ L PI was flown over the sensor surface bound *S. gordonii* for 5 min and the pump was stopped for 5 min incubation. At this color switching stage, the photos were taken every 60s. In the following PBS rinsing stage, the photos were taken with every 3 min.

Another attempt was made through staining bacteria with FDA/EB. A 1 h flow of FDA (fluorescein diacetate, green) stained *S. gordonii* ($OD_{620\text{ nm}} = 1.4$) was applied to form a thick green stained bacterial film followed by 30 min of PBS rinsing. Then the mixed 500 μ L ABA and 500 μ L EB (ethidium bromide, red) solution was flown for 16 min combined with a PBS rinsing process. In the period of application of a mixture of ABA and EB over the FDA stained bacteria, pictures were taken every 60 s. In the PBS rinsing stage, photos were taken every 5 min.

2. Materials and Methods

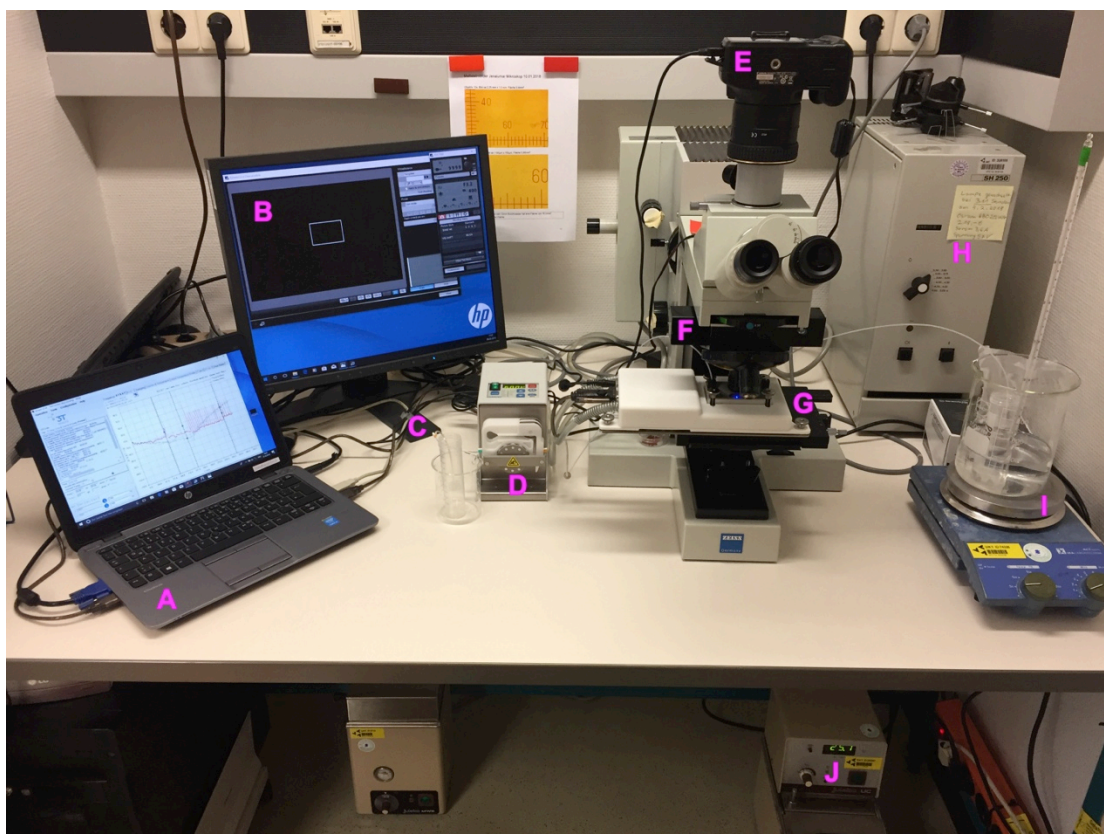


Figure 10: QCM-fluorescent microscope dynamic observation. The whole QCM-flow chamber system consists of the following parts: **A.** Computer for signal observation in QCM-D software; **B.** Screen for fluorescent microscopy observation and photograph taking; **C.** Waste collector; **D.** Pump for flow rate control; **E.** Camera connected to the fluorescent microscope; **F.** Fluorescent microscope; **G.** QCM-D measurement platform with a flow chamber; **H.** Power for the fluorescent lamp box; **I.** Water bath and magnetic stirrer for bacterial solution; **J.** Water bath for flow chamber temperature control.

2. Materials and Methods

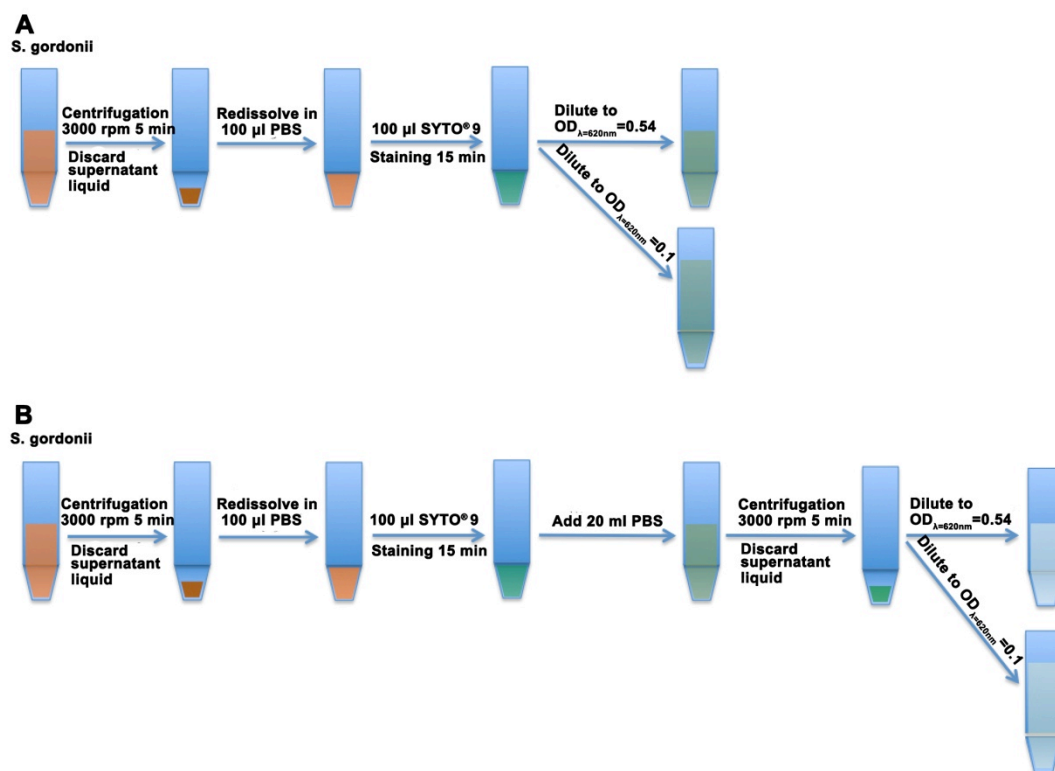


Figure 11: Bacterial staining protocols for continuous flow measurements in the QCM-fluorescent microscope dynamic observation flow chamber setup, to select the best staining method for low background disturbance and clear focusing. **A.** After harvesting, *S. gordonii* was stained with SYTO 9 and adjusted to $OD_{620\text{ nm}} = 0.54$ and 0.1; **B.** After harvesting, the *S. gordonii* stained with SYTO 9 was washed by PBS and centrifuged to remove the residual free SYTO 9 molecules in solution, and finally diluted into $OD_{620\text{ nm}} = 0.54$ and 0.1.

2.9 Statistical analysis

All QCM-D experiments utilizing the qCell T machine were repeated for at least 5 times, with the exception of the experiments in protocol E with the mixture of ABA and *S. gordonii* suspension, which were only repeated 3 times. Data were mainly presented as means and standard deviations. The differences between mean values of frequency and dissipation in different groups, respectively, were compared and statistically analyzed through one-way analysis of variance (ANOVA) and post-hoc test (Tukey analysis). Differences were regarded being of statistical significance when $p < 0.05$.

3. Results

3.1 Sensor surface characterization

Before the QCM-D experiments, exemplary Ti-coated sensors went through wettability and roughness analysis. In the contact angle measurement, upon the 20th second, the 2 μL water droplets deposited on the sensor surface reached the equilibrium status with a contact angle of $47^\circ \pm 2.5^\circ$, which indicates a moderate hydrophilicity of the Ti sputtered sensor surface (**Figure 12**).

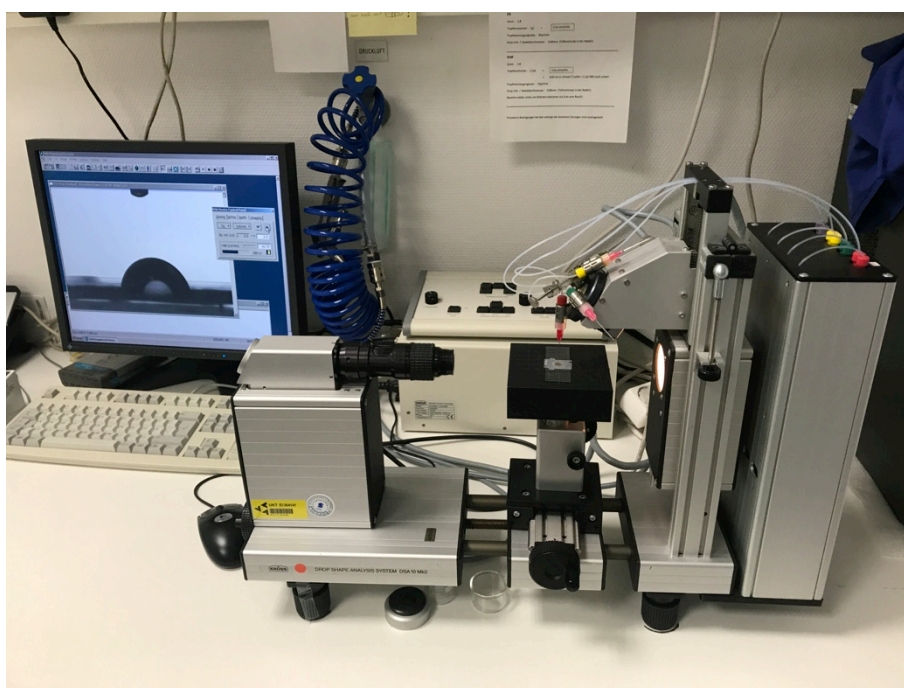


Figure 12: Contact angle measurement through DSA 10-Mk2 drop shape analysis system (Krüss, Hamburg, Germany).

“The topographic images (**Figure 13**) in the small scan areas ($\leq 50 \mu\text{m} \times 50 \mu\text{m}$) show a morphology, which is characteristic for Ti coatings. For the scan areas received from the WLI measurements, this fine coating structure is not solvable, but the long-wave information from the quartz crystal can be achieved. Both sputtered quartz crystals exhibit the same moderate surface roughness, e.g. $S_a = 0.84 \text{ nm}$ and $S_q = 1.1 \text{ nm}$ in a scan area of $3 \mu\text{m} \times 3 \mu\text{m}$. The PSD function (**Figure 14**) calculated from all measurements of both sensors confirm the observed roughness

3. Results

characteristic: The Ti coating leads to a bump in the PSD function around a spatial frequency of approx. $6 \mu\text{m}^{-1}$. This is typical for coatings and enables an estimation of its intrinsic thin film roughness. In the lower spatial frequency range, the function is dominated by the quartz crystal surface characteristic.” [85]

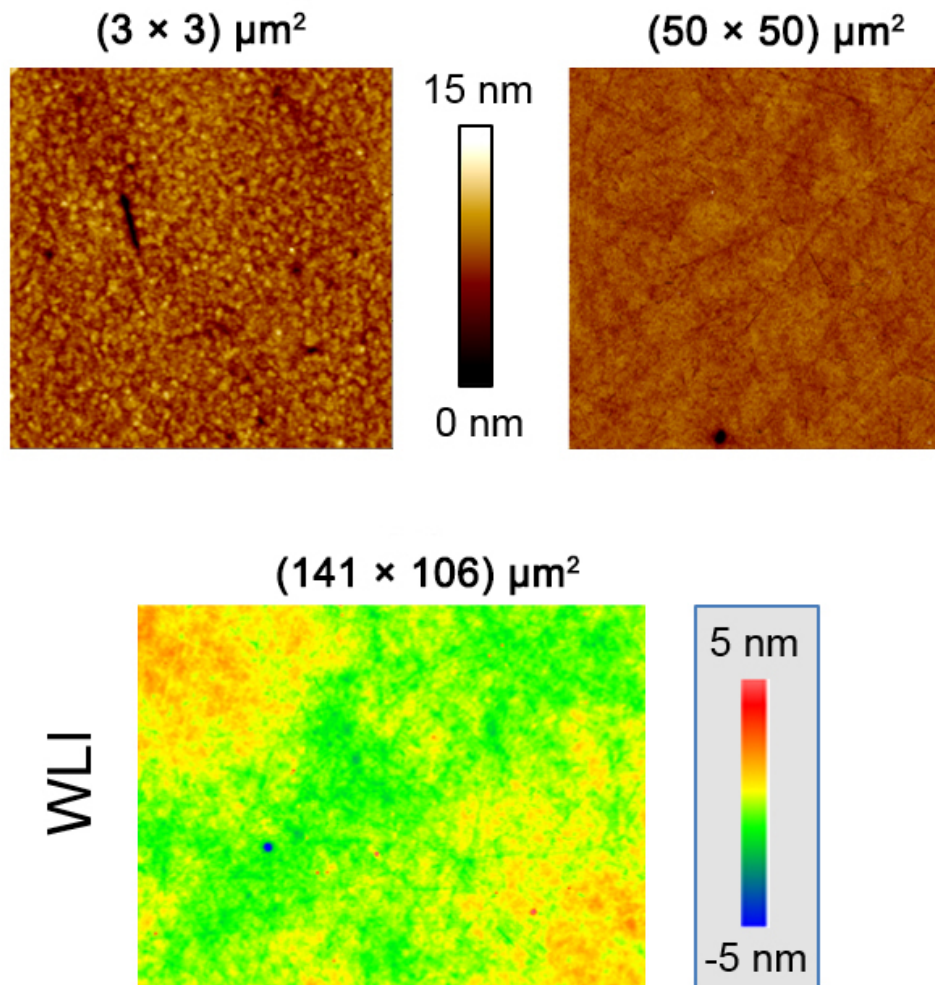


Figure 13: AFM and WLI outcomes of the Ti-coated quartz crystal sensor surfaces. [85]

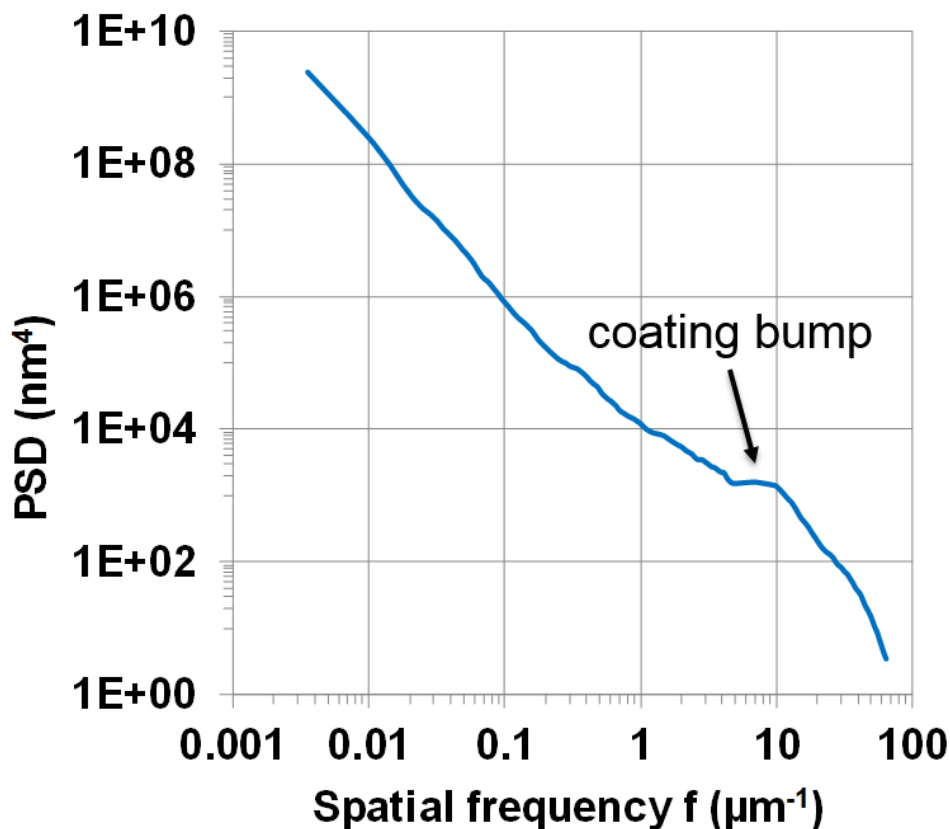


Figure 14: PSD function of the Ti-coated quartz crystal sensor surface. [85]

3.2 QCM-D online experiments and Live/Dead staining

3.2.1 Online formation of saliva-coated Ti-based biosensors

As shown in **Figure 15**, after reaching the baseline with PBS, the prepared saliva solution was infiltrated into the chamber for 30 min, then, a final rinsing step with PBS was carried out for another 30 min. The salivary proteins interacting with the sensor surface induced an irreversible decrease of the frequency and increase of the dissipation, even upon the PBS rinsing step, which represented the irreversible formation of salivary pellicle on the Ti coated sensor surface. The signal reached equilibrium at a mean value of frequency decrease of $\Delta f_{\text{mean}} = -122$ Hz and dissipation increase of $\Delta D_{\text{mean}} = +42$ Hz (first 60 min of reaction time in **Figure 16**). The retained saliva-mass adhering to the Ti surface was on average 537 ng/cm². The saliva coating process on the Ti-coated sensors aimed at forming the salivary conditioned biosensors, which were used in the later process of detecting the

pellicle-mediated specific interactions with ABA and bacteria.

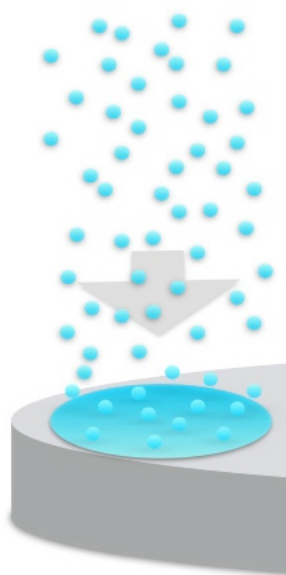


Figure 15: QCM-D running sequence protocol A: online formation of saliva-coated Ti-based biosensors. [85]

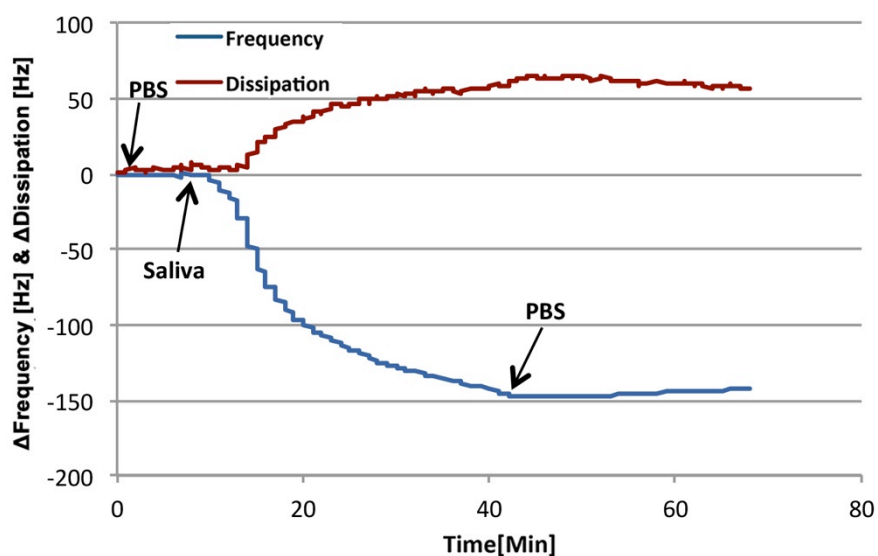


Figure 16: Exemplary QCM-D curves: online formation of saliva-coated Ti-based biosensors (protocol A in **Figure 4**). [85]

3.2.2 ABA interacting with Ti sensors

After application of the running sequence in **Figure 17** (1), the interaction of ABA with the Ti surface showed a typical “U”-shaped signal with a particular reversible frequency change, with a rapid decrease and a rapid increase upon PBS rinsing (**Figure 18**). The average frequency decrease (Δf_{mean}) was -361

3. Results

Hz with fast kinetics and reached an equilibrium state that was maintained for the remaining flow time. Upon PBS rinsing, within about 5 minutes, the frequency increased sharply ($\Delta f_{\text{mean}} = +332$ Hz) reaching nearly the primary baseline level. On the contrary, within about 5 minutes, the dissipation signal increased fast ($\Delta D_{\text{mean}} = +270$ Hz) and reached equilibrium, then, upon PBS it decreased fast ($\Delta D_{\text{mean}} = -278$ Hz) to the level of the baseline [85]. After decrease and increase of frequency, the total change of frequency was on average -29 Hz. Calculation according to the Sauerbrey equation yields a small amount of residual ABA of 127.3 ng/cm^2 on the Ti surface after PBS rinsing.

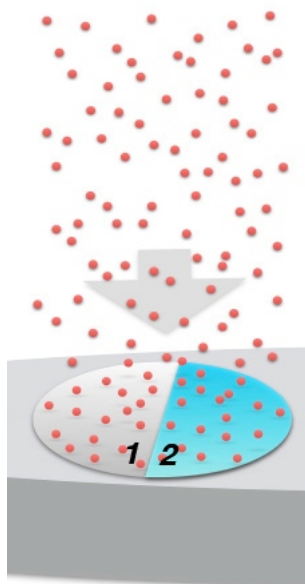


Figure 17: QCM-D running sequence protocol B: online interaction of ABA and Ti-based biosensors surface with (2) and without (1) saliva coating. [85]

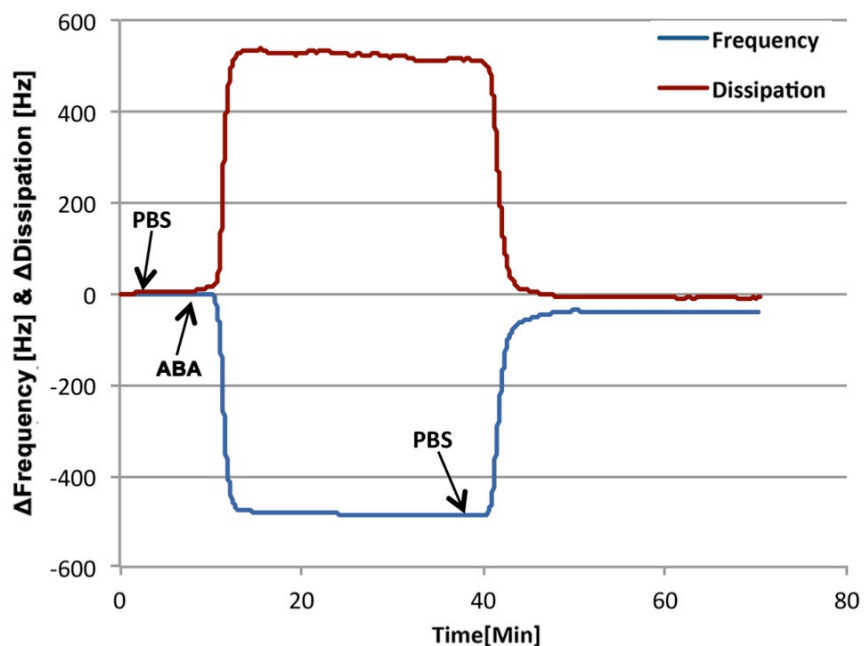


Figure 18: Exemplary QCM-D curve: interaction of ABA and Ti-based biosensors surface (protocol B1 in **Figure 4**). [85]

3.2.3 ABA interacting with saliva-coated biosensors

ABA interacting with a saliva coated biosensor surface (**Figure 17 (2)**) is shown in **Figure 19**. ABA caused a fast decrease of frequency ($\Delta f_{\text{mean}} = -302$ Hz) and a fast increase of dissipation ($\Delta D_{\text{mean}} = +251$ Hz), then both the frequency and dissipation came to equilibrium. When the PBS flow started, a sharp increase of frequency ($\Delta f_{\text{mean}} = +338$ Hz) and sharp decrease of dissipation ($\Delta D_{\text{mean}} = -273$ Hz) occurred (**Figure 19**). After rinsing on the pre-conditioned Ti surface, the total ABA-induced frequency change is +36 Hz, which theoretically equals a mass-loss of 159 ng/cm^2 .

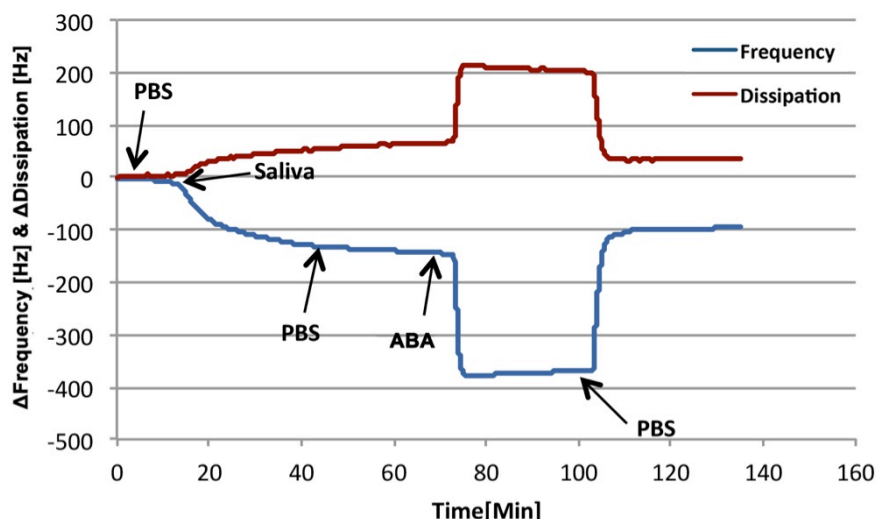


Figure 19: Exemplary QCM-D curves: interaction of ABA and Ti-based biosensors surface coated with saliva (protocol B2 in **Figure 4**). [85]

3.2.4 Influence of salivary pellicle on *S. gordonii* adhesion

1) *S. gordonii* interacting with Ti sensors

According to the running sequence in **Figure 20** (1), after 120 min flow of bacterial solution, *S. gordonii* (*S.g.*) caused a gradual frequency decrease of $\Delta f_{\text{mean}} = -226$ Hz and an increase of dissipation of $\Delta D_{\text{mean}} = +398$ Hz, both reached an equilibrium state (**Figure 21**). The frequency decrease indicated a mass loading process due to the *S. gordonii* attachment. The frequency and dissipation kept unchanged upon PBS rinsing, which implied none obvious desorption being induced by PBS. As shown in **Figure 22**, dense and green bacterial films were visible on the sensor surface after Live/Dead staining.

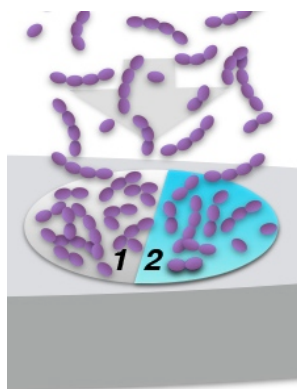


Figure 20: First part of QCM-D running sequence of protocol D: *S. gordonii*

interacting with Ti-based biosensors surface with (2) and without (1) saliva coating. [85]

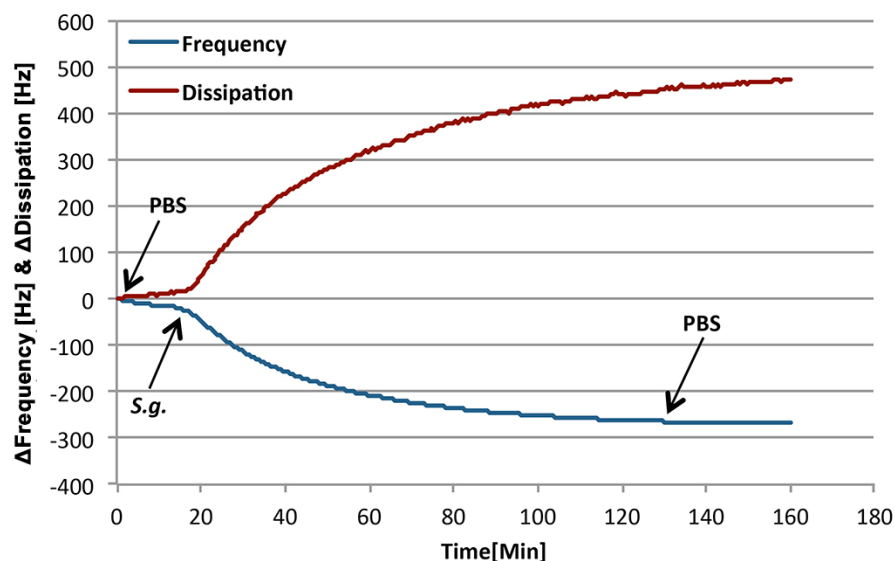


Figure 21: Exemplary QCM-D curves: *S. gordonii* interaction with Ti-coated sensor surface (first part of protocol D1 in **Figure 4**). [85]

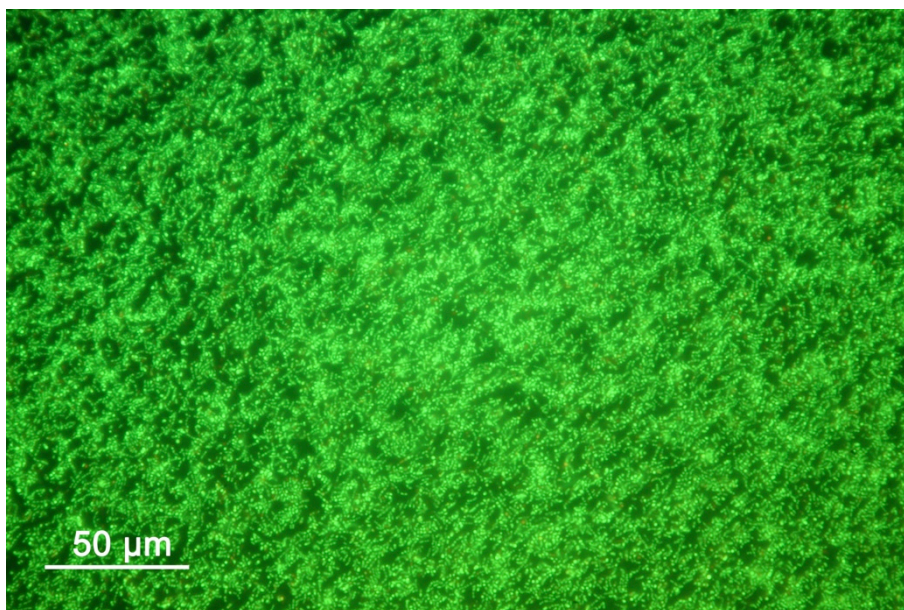


Figure 22: Exemplary image of Live/Dead stained *S. gordonii* after 120 min flowing over Ti-coated sensor surface (first part of protocol D1 in **Figure 4**). [85]

2) *S. gordonii* interacting with saliva-coated biosensors

According to the running sequence in **Figure 20** (2), completely different results were found. When applying *S. gordonii* now on the saliva coated biosensor surface for 120 min, the dissipation increased for $\Delta D_{\text{mean}} = +28$ Hz, nevertheless, the frequency increased similarly for $\Delta f_{\text{mean}} = +39$ Hz, which

3. Results

abnormally indicated a mass-loss effect rather than the typical mass loading effect (**Figure 23**). However, green stained and thus alive bacteria were found on the biosensor surface after Live/Dead staining, exhibiting a relatively lower density compared with the bacteria on the unconditioned Ti (**Figure 24**).

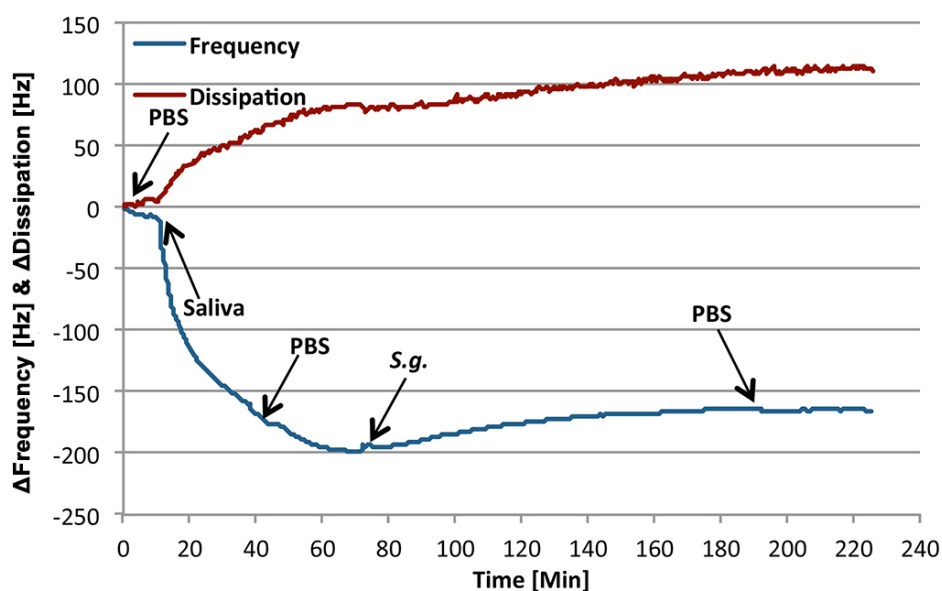


Figure 23: Exemplary QCM-D curves: *S. gordonii* interacting with saliva coated biosensor surface (first part of protocol D2 in **Figure 4**). [85]

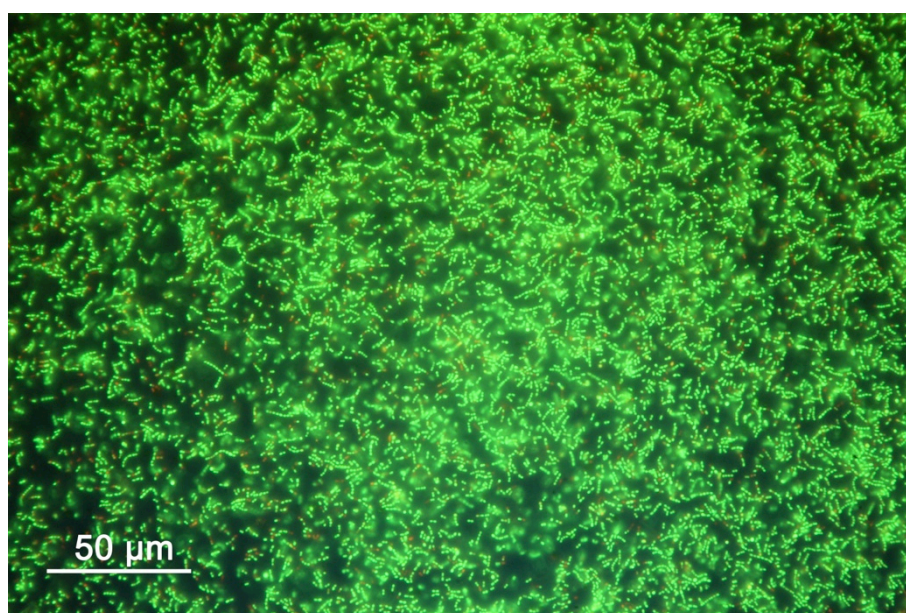


Figure 24: Exemplary image of Live/Dead stained *S. gordonii* after 120 min flowing on saliva coated biosensor surface (first part of protocol D2 in **Figure 4**). [85]

3.2.5 Impact of ABA application on *S. gordonii* adhesion

1) *S. gordonii* interacting with Ti sensors, pre-conditioned with ABA

On the titanium surface pre-conditioned with ABA mouth rinse solution for 30 min (**Figure 25** (1)), a frequency decrease of $\Delta f_{\text{mean}} = -121$ Hz and a dissipation increase of $\Delta D_{\text{mean}} = +246$ Hz (**Figure 26**) was induced by the adhesion of *S. gordonii*. After Live/Dead staining, the adhered *S. gordonii* on the ABA pre-conditioned sensor surface are still dense and green colored, which is similar to the bacteria on the Ti sensor surface without ABA conditioning: almost all bacteria bound on the ABA pretreated surface were kept alive (**Figure 27**).

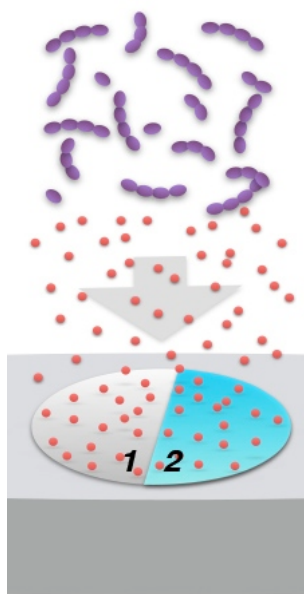


Figure 25: QCM-D running sequence of protocol C: impact of ABA on *S. gordonii* adhesion toward Ti-coated biosensors surface with (2) and without (1) saliva coating. [85]

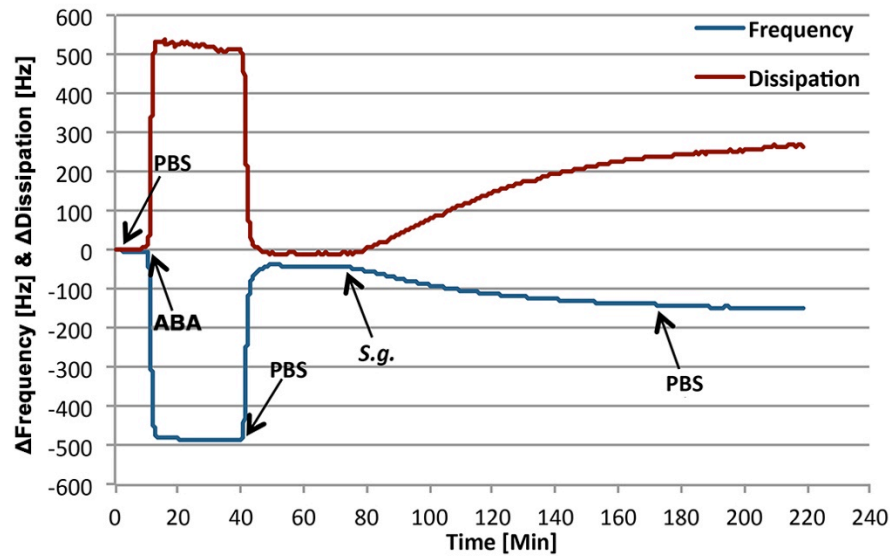


Figure 26: Exemplary QCM-D curves: *S. gordonii* interacting with Ti-coated sensor surface preconditioned with ABA (protocol C1 in **Figure 4**). [85]

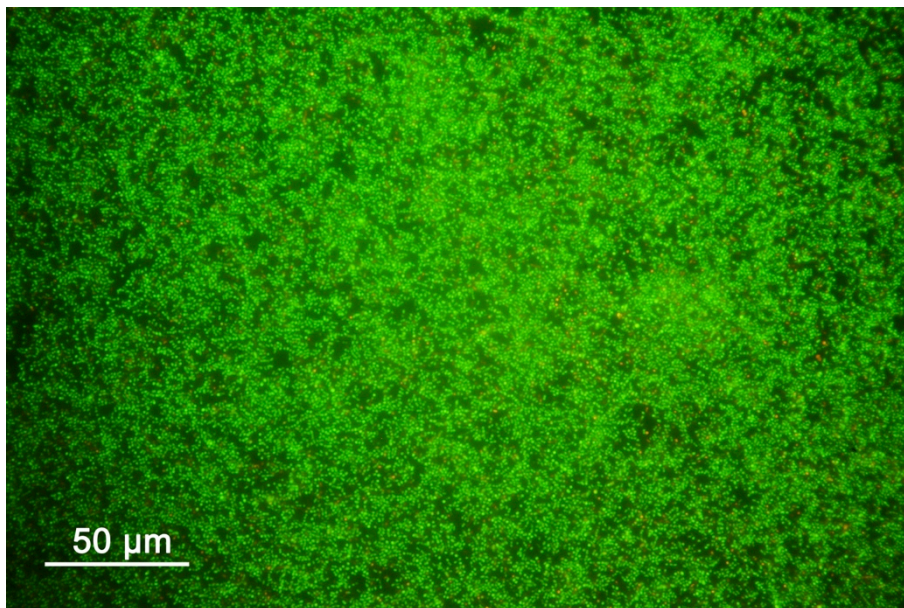


Figure 27: Exemplary image of Live/Dead stained *S. gordonii* after 120 min flowing over Ti-coated sensor surface preconditioned with ABA (protocol C1 in **Figure 4**). [85]

2) *S. gordonii* interacting with saliva-coated biosensors, pre-conditioned with ABA

To figure out the influence of pellicle toward the ABA binding and the interaction with bacterial adhesion, 30 min of ABA solution was flown over the salivary preconditioned biosensor surface, followed with another 120 min of *S. gordonii* run (**Figure 25** (2)). Similar to the interaction of *S. gordonii* on the

3. Results

pellicle surface, *S. gordonii* also induced an increase of both frequency ($\Delta f_{\text{mean}} = 20$ Hz) and dissipation ($\Delta D_{\text{mean}} = 35$ Hz) (**Figure 28**). The fluorescent microscopy outcomes disclosed a dense and predominantly green layer of *S. gordonii* on the biosensor surface (**Figure 29**).

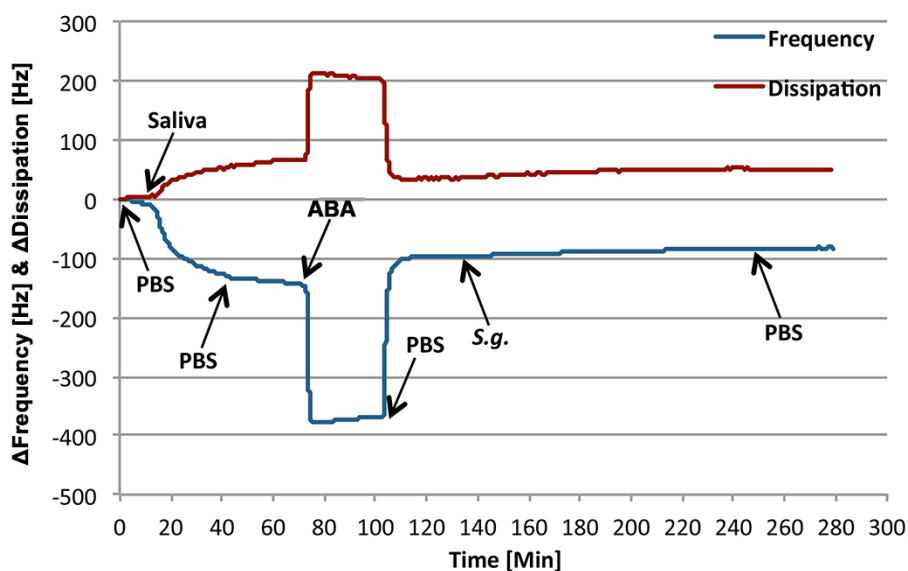


Figure 28: Exemplary QCM-D curves: *S. gordonii* interacting with saliva-coated biosensor surface preconditioned with ABA (protocol C2 in **Figure 4**). [85]

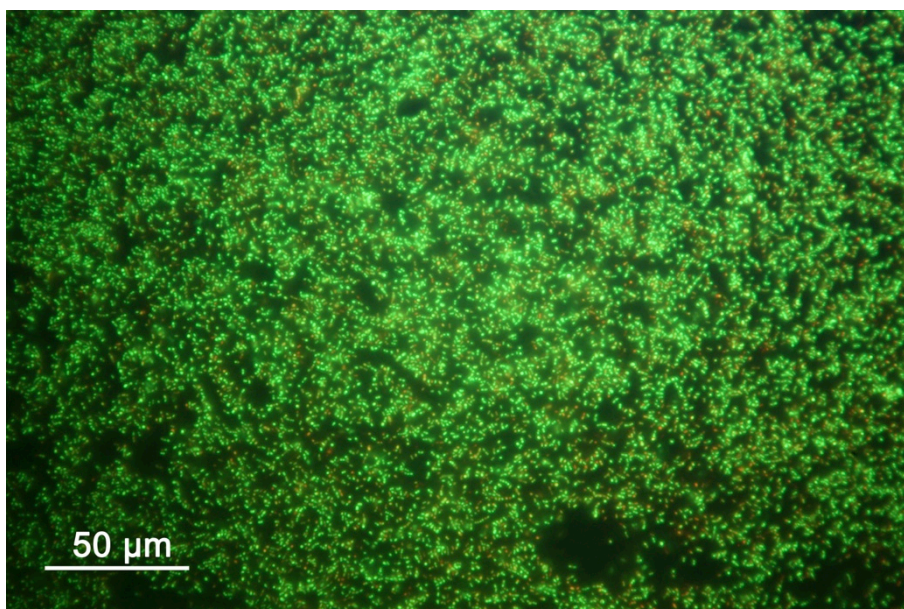


Figure 29: Exemplary image of Live/Dead stained *S. gordonii* after 120 min flowing over saliva-coated biosensor surface preconditioned with ABA (protocol C2 in **Figure 4**). [85]

3) ABA interacting with *S. gordonii*, pre-adhered to Ti sensors

For the investigation of ABA solution interacting with *S. gordonii* adhered on Ti surface, 30 min of ABA solution was flown over the *S. gordonii* film formed for 120 min on the Ti coated sensor surface (**Figure 30(1)**). As depicted in **Figure 31**, a typical signal of dissipation increase and frequency decrease was developed during the 120 min process of *S. gordonii* adhesion. Subsequently, a rapid decrease of frequency ($\Delta f_{\text{mean}} = -985$ Hz) together with a fast increase of dissipation ($\Delta D_{\text{mean}} = +1050$ Hz) was induced by the ABA solution. Upon PBS rinsing, a sharp decrease of dissipation ($\Delta D_{\text{mean}} = -899$ Hz) and a sharp increase of frequency ($\Delta f_{\text{mean}} = +818$ Hz) occurred [85]. The final total frequency change upon ABA is -167 Hz, which represents a final mass increase of the adsorbed film due to ABA interaction of 740 ng/cm^2 (**Figure 31**). Fluorescence microscopy revealed a dense red stained *S. gordonii* biofilm, representing the killed bacteria on the sensor surface (**Figure 32**).

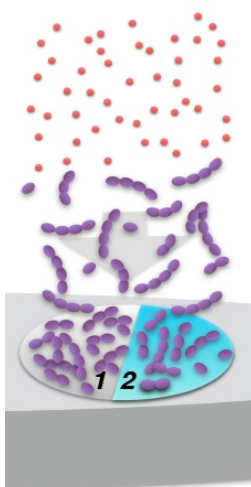


Figure 30: QCM-D running sequence of protocol D: ABA interacting with *S. gordonii* pre-adhered to Ti sensors with (2) and without (1) saliva coating. [85]

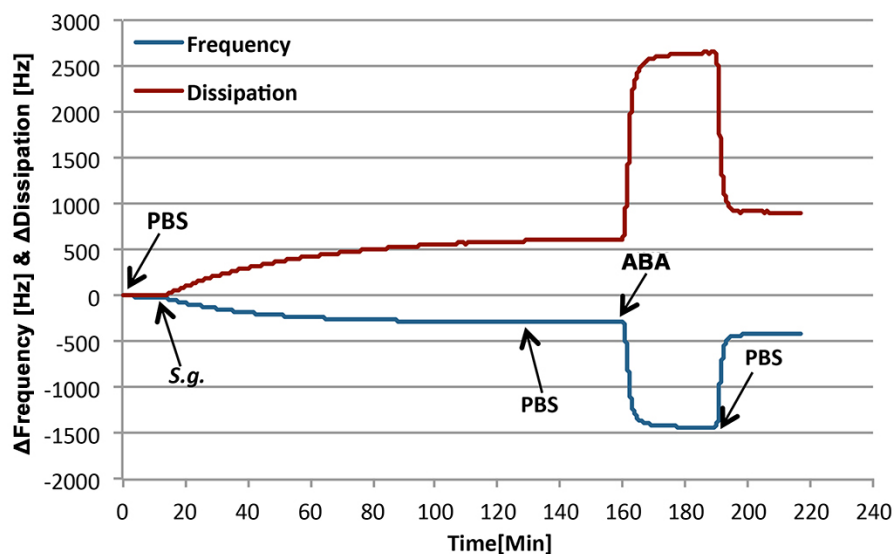


Figure 31: Exemplary QCM-D curves: ABA interacting with *S. gordonii* attached to Ti-coated sensor surface (protocol D1 in **Figure 4**). [85]

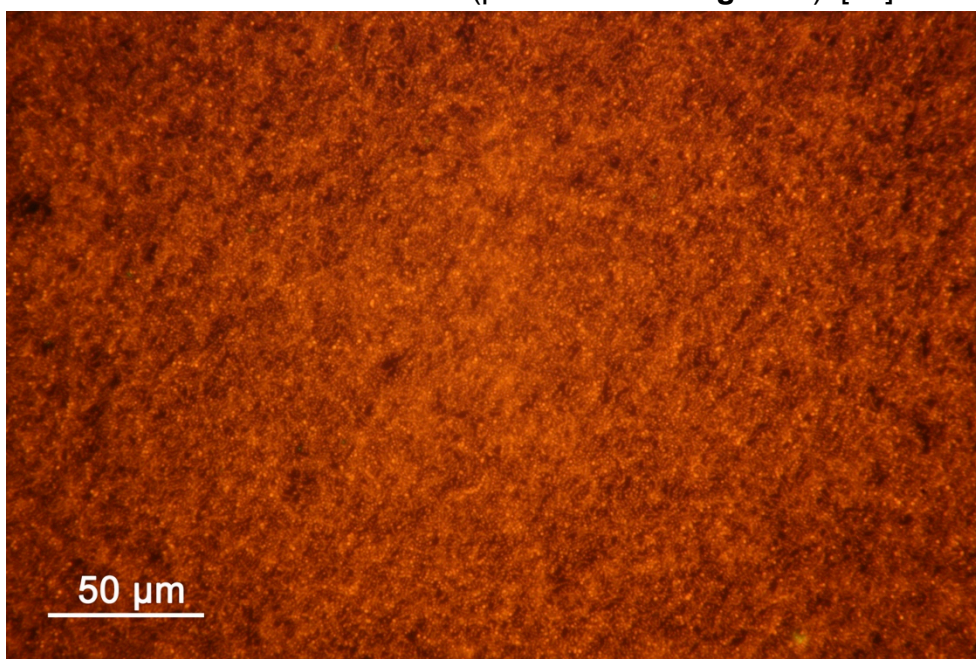


Figure 32: Exemplary image of Live/Dead staining of ABA applying to Ti-coated sensor surface attached *S. gordonii* (protocol D1 in **Figure 4**). [85]

4) ABA interacting with *S. gordonii*, pre-adhered to saliva-coated biosensors

According to the sequence in **Figure 30** (2), after the attachment of *S. gordonii* on the saliva-coated biosensor, ABA caused similarly significant signal changes ($\Delta f_{\text{mean}} = -753$ Hz, $\Delta D_{\text{mean}} = +779$ Hz), also followed by fast reversibility ($\Delta f_{\text{mean}} = +586$ Hz, $\Delta D_{\text{mean}} = -513$ Hz,) upon the starting of PBS

3. Results

flow. The total residual mass drop caused by ABA interaction on this surface was on average 737 ng/cm² (**Figure 33**). Microscopic results revealed a red and dense *S. gordonii* film (**Figure 34**), which implied that all these surface bound bacteria were killed after ABA rinsing.

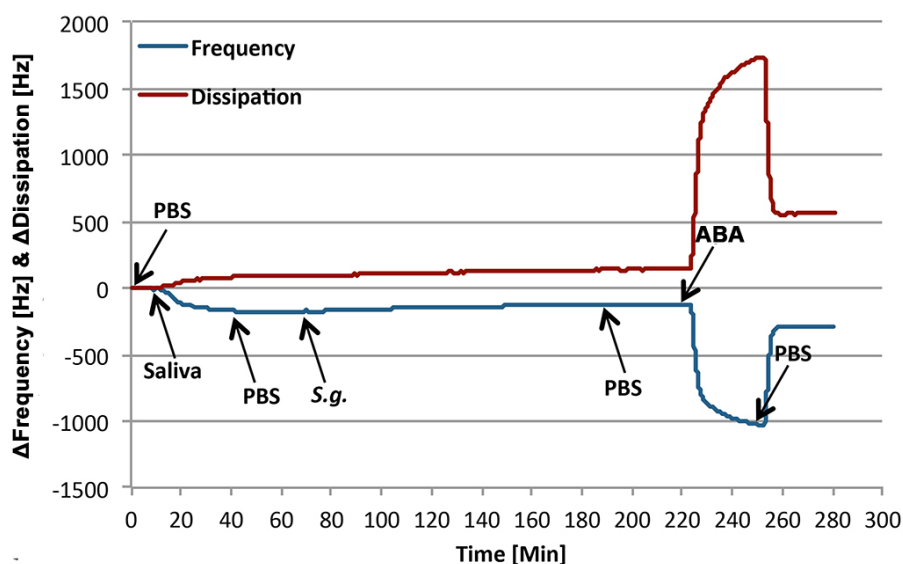


Figure 33: Exemplary QCM-D curves: ABA interacting with *S. gordonii* attached to saliva-coated biosensor surface (protocol D2 in **Figure 4**). [85]

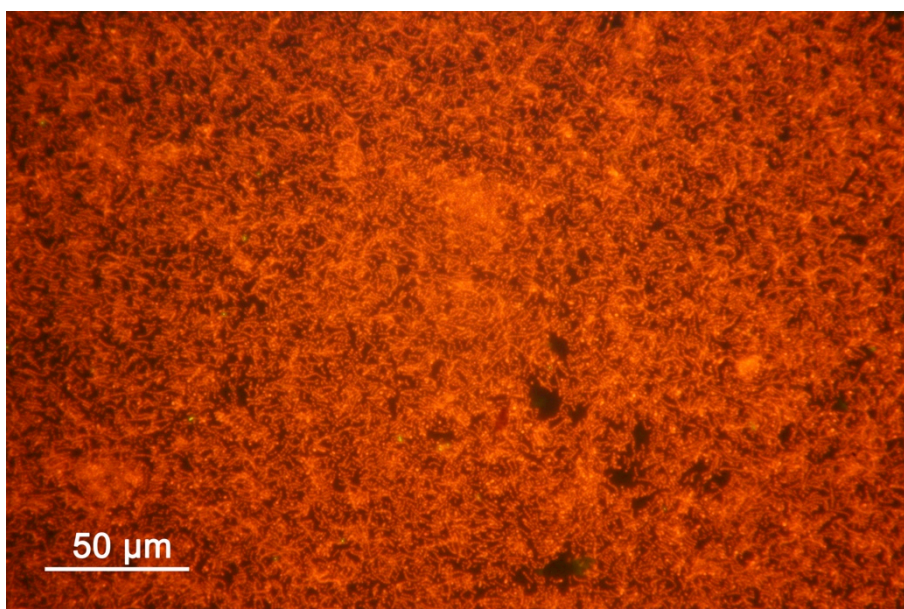


Figure 34: Exemplary image of Live/Dead staining of ABA acting on *S. gordonii* attached to saliva-coated biosensor surface (protocol D2 in **Figure 4**). [85]

5) Mixture of ABA and *S. gordonii* interacting with Ti sensors

As shown in **Figure 35** (1), the mixture of ABA and *S. gordonii* was

3. Results

applied on the Ti coated sensor surface for 120 min. After the sharp decrease of frequency ($\Delta f_{\text{mean}} = -92$ Hz) in almost 5 min, and a sharp dissipation increase ($\Delta D_{\text{mean}} = +39$ Hz), both the frequency and dissipation reached equilibrium. The equilibrated signals were partially reversible, with a fast frequency increase ($\Delta f_{\text{mean}} = +56$ Hz), and a fast decrease of dissipation ($\Delta D_{\text{mean}} = -36$ Hz) after PBS rinsing (**Figure 36**). The Live/Dead staining outcomes indicated that the *S. gordonii* attached on the sensor surface formed a film of relatively low density (**Figure 37**).

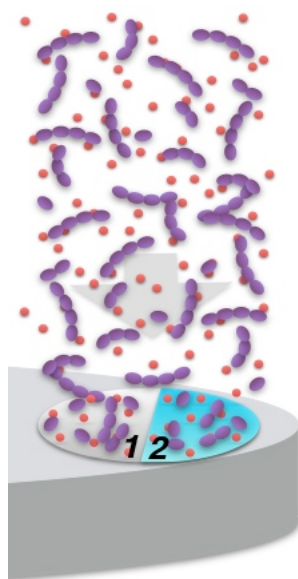


Figure 35: QCM-D running sequence of protocol E: mixture of ABA and *S. gordonii* interacting with Ti sensors with (2) and without (1) saliva coating. [85]

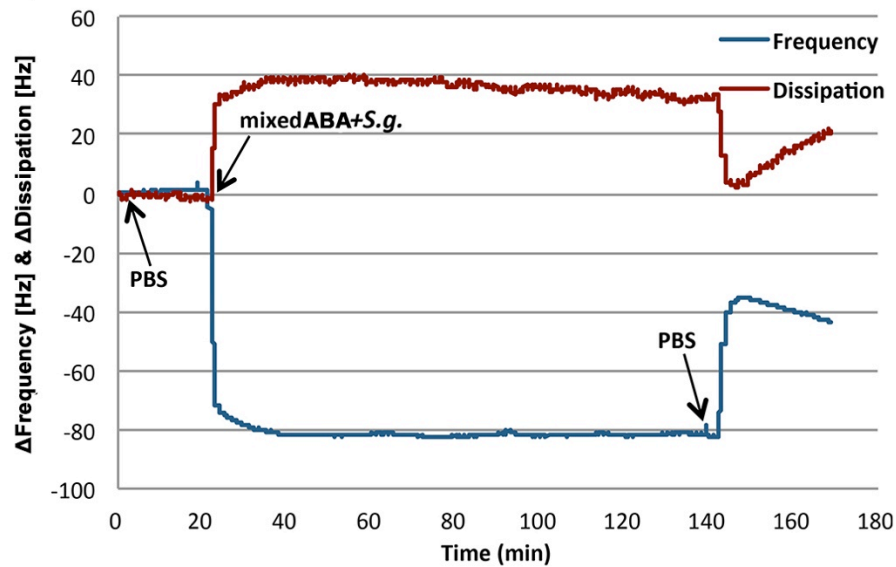


Figure 36: Exemplary QCM-D curves: mixture of ABA and *S. gordonii* interacting with Ti-coated sensor surface (protocol E1 in **Figure 4**). [85]

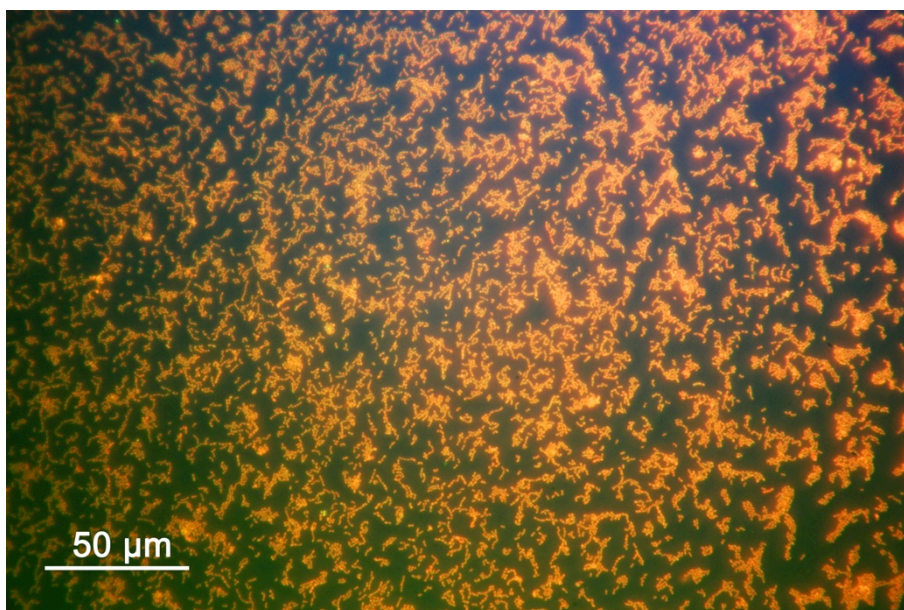


Figure 37: Exemplary image of Live/Dead staining of mixture of ABA and *S. gordonii* interacting with Ti-coated sensor surface (protocol E1 in **Figure 4**). [85]

6) Mixture of ABA and *S. gordonii* interacting with saliva-coated biosensors

In order to simulate the clinical situation of applying ABA mouth rinse, which is mixed with the bacteria in the oral cavity, on the Ti implant surface covered with pellicle, a mixture of ABA and *S. gordonii* was flown over the

3. Results

salivary biosensor surface for 120 min (**Figure 35** (2)). After an initial rapid decrease of frequency and an increase of dissipation, both the frequency and dissipation exhibited a simultaneous positive signal drift in the 120 min flow process, ending with a final change of $\Delta f_{\text{mean}} = +14$ Hz and $\Delta D_{\text{mean}} = +44$ Hz [85]. Inconspicuous reversibility occurred upon PBS rinsing accompanied with a minor increase in frequency ($\Delta f_{\text{mean}} = +39$ Hz) and a minor drop in dissipation $\Delta D_{\text{mean}} = -22$ Hz (**Figure 38**). The fluorescence microscopic results showed completely red stained bacteria and medium density of the *S. gordonii* film (**Figure 39**).

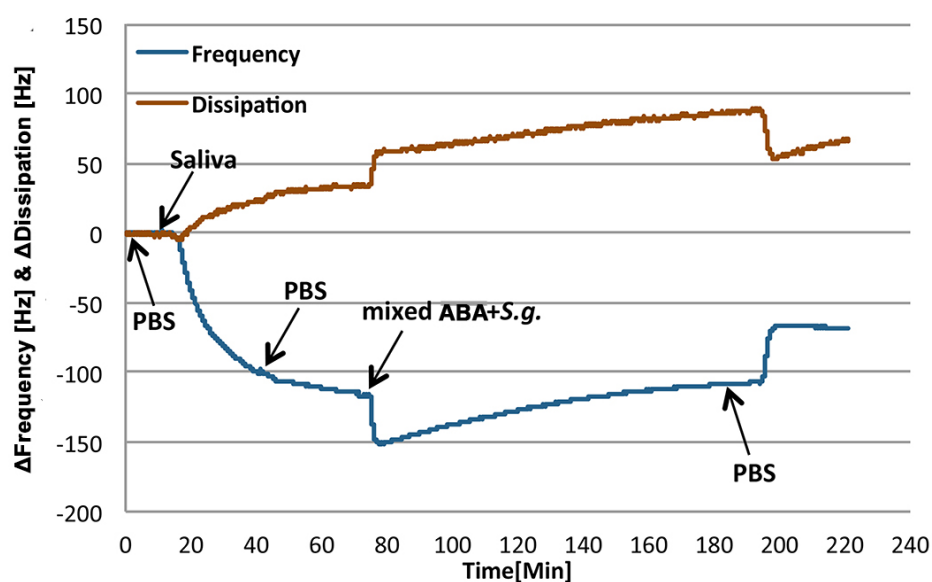


Figure 38: Exemplary QCM-D curves: mixture of ABA and *S. gordonii* interacting with saliva-coated biosensor surface (protocol E2 in **Figure 4**). [85]

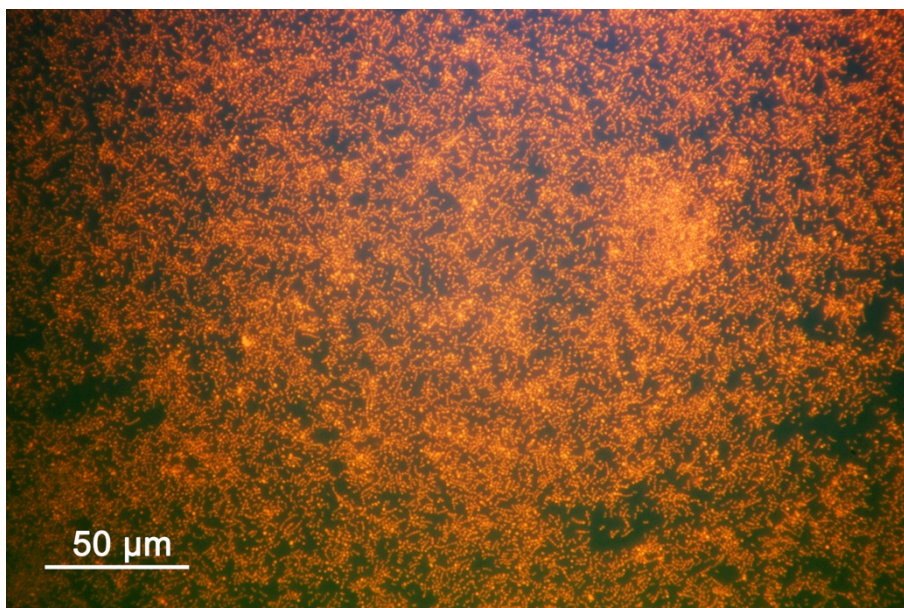


Figure 39: Exemplary image of Live/Dead staining of mixture of ABA and *S. gordonii* interacting with saliva-coated biosensor surface (protocol E2 in **Figure 4**). [85]

3.2.6 Summarized results of ABA and bacteria caused f and D shifts

To sum up the results of the different QCM-D runs, and to simultaneously compare the frequency shifts induced by the different analyte solutions, the mean values of final frequency shifts induced by ABA interacting with different interfaces, and frequency changes caused by bacterial attachment toward differently conditioned Ti-coated sensor surfaces, and the bacterial viability were calculated and summarized in **Table 1**. “ABA showed distinct frequency shifts when flown over pre-adhered *S. gordonii*, indicating a strong interaction of ABA molecule and bacterial surface (**Figure 40**). After rinsing with PBS, the final ABA caused frequency shifts were largest on the bacteria compared to that on saliva or pure Ti surfaces (**Figure 41**). All the *S. gordonii* adhesion on different modified surfaces involving saliva coated biosensor showed positive change of frequency. ” [85]

3. Results

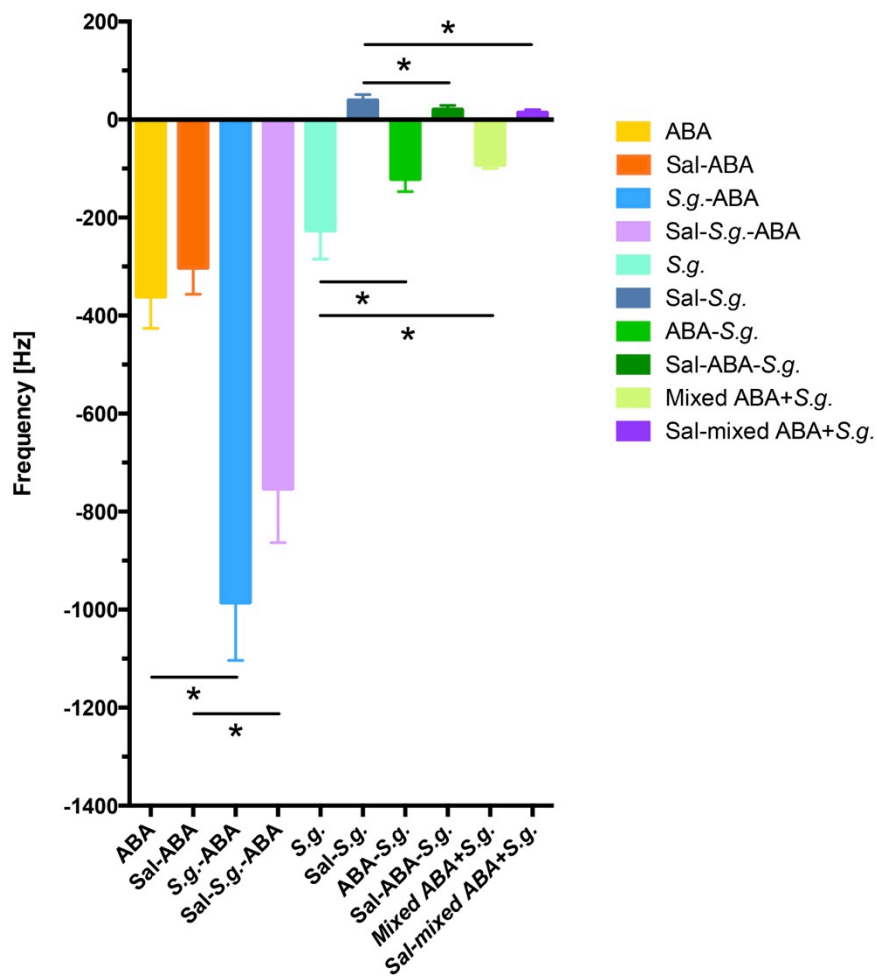


Figure 40: “*S. gordonii* (left part) and ABA (right part) caused frequency changes in different flowing sequence groups including on the saliva-coated biosensor and Ti-coated sensor surface. The data shown above are mean \pm SD, n = 5; Asterisks (*) represented the statistically significant differences between the means of different groups (P<0.05). ABA (antibacterial agent), *S.g.* (*S. gordonii*), Sal (saliva), Ti (titanium).” [85]

3. Results

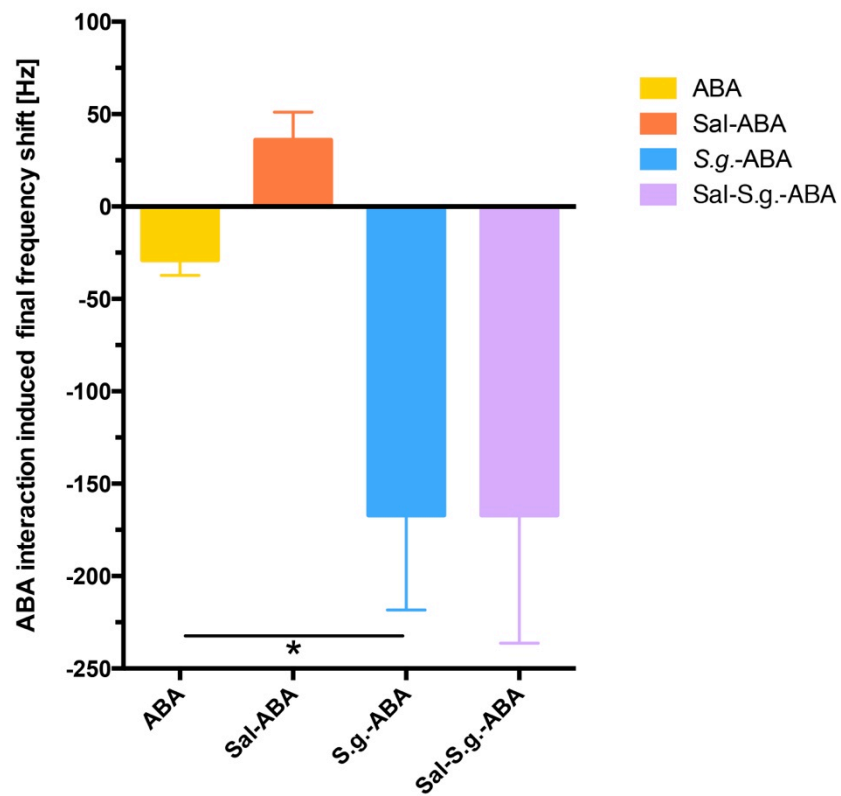


Figure 41: “After PBS flowing, ABA interaction caused final frequency change on different surface situation in different flowing sequences groups. The data shown above are mean \pm SD, n = 5; Asterisks (*) represented the statistically significant differences between the means of different groups (P < 0.05). ABA (antibacterial agent), S.g. (*S. gordonii*), Sal (saliva), Ti (titanium).” [85]

3. Results

Table 1: Summary of QCM-D frequency and dissipation shifts and Sauerbrey calculations of adsorbed mass upon different interaction sequences of ABA and *S. gordonii*, and the bacterial viability based on Live/Dead staining. The blue colored numbers indicate the decrease of frequency and the red color represents the observed death of bacteria.

		Δf_{mean} (Hz) Before PBS	ΔD_{mean} (Hz) Before PBS	Δf_{mean} (Hz) After PBS	ΔD_{mean} (Hz) After PBS	Δf_{mean} (Hz)	ΔD_{mean} (Hz)	Mass loading (ng/cm ²)	Viability
Saliva-surface and ABA surface molecular interactions	Saliva coating on Ti sensor (A)	-	-	-	-	-122	+42	+537	-
	ABA interacting with Ti sensors (B1)	-361	+270	+332	-278	-29	-8	+127	-
Influence of salivary pellicle on <i>S. gordonii</i> adhesion	ABA interacting with saliva-coated biosensors (B2)	-302	+251	+338	-273	+36	-22	-159	-
	<i>S. gordonii</i> interacting with Ti sensors (D1)	-	-	-	-	-226	+398	-	Live
	<i>S. gordonii</i> interacting with saliva-coated biosensors (D2)	-	-	-	-	+39	+28	-	Live
	<i>S. gordonii</i> interacting with ABA coated Ti sensors (C1)	-	-	-	-	-121	+246	-	Live
Impact of ABA application on <i>S. gordonii</i> adhesion	<i>S. gordonii</i> interacting with ABA pre-conditioned saliva-coated biosensors (C2)	-	-	-	-	+20	+35	-	Live
	ABA interacting with <i>S. gordonii</i> pre-adhered on Ti sensors (D1)	-985	+1050	+818	-899	-167	+151	+740	Dead
	ABA interacting with <i>S. gordonii</i> pre-adhered on saliva-coated Ti sensors (D2)	-753	+779	+586	-513	-167	+266	+737	Dead
	Mixture of ABA and <i>S. gordonii</i> interacting with Ti sensors (E1)	-92	+39	+56	-36	-36	+3	-	Dead
	Mixture of ABA and <i>S. gordonii</i> interacting with saliva-coated biosensors (E2)	+14	+44	+39	-22	+53	+22	-	Dead

3.3 SEM, FE-SEM and HIM analysis after QCM-D run

As shown in Live/Dead staining results above, after rinsing with the ABA, all surface-adhered bacteria were killed [85]. For the purpose of analyzing possible ABA induced bacterial surface structure changes, the samples were investigated through SEM, FE-SEM and HIM. As control group, the *S. gordonii* adhered on pellicle surface are analyzed under SEM and FE-SEM. At the magnification of 5000x, a single layer of *S. gordonii* chains was found dispersed irregularly on the pellicle surface (**Figure 42**). At the magnification of 40000x and 120000x through high resolution FE-SEM, the *S. gordonii* arranged in chain was found laying on the pellicle surface and was characterized with granular surface, which might be due to the sputtering Au-Pd particles covering the bacterial surface (**Figure 43, Figure 44**). In the ABA treatment group, at the magnification of 5000x and 10000x, *S. gordonii* chains laying on the pellicle showed almost no difference compared to the control group (**Figure 45, Figure 46**). At a higher magnification of 43000x and 150000x, no obvious membrane perforation could be observed on the granular bacterial surface after interacting with ABA (**Figure 47, Figure 48**).

After being treated by ABA solution, no significant membrane perforation of *S. gordonii* could be detected through SEM and FE-SEM. This might be due to the Au-Pd sputtering on the bacterial surface, which might cover the potential perforation of the bacterial membrane to prevent it from being detected. According to the cross sectional HIM image of Au-Pd sputtered *S. gordonii*, an approximately 20 nm thick Au-Pd layer could be seen (**Figure 49, Figure 50**). The small holes on the cross-section surface near to the membrane layer might represent perforations within the membrane. Thus, a further attempt of using HIM to analyze the non-sputtered *S. gordonii* was made (**Figure 51**). At a relative low magnification, the HIM showed smooth bacterial surfaces, which is quite different from the granular surface characteristic of the sputtered bacterial surface (**Figure 51 A.B**). However,

3. Results

when the un-sputtered bacteria were exposed under the HIM beam continuously, the *S. gordonii* experienced a distinct shrinkage (**Figure 51 C.D**). Due to the issue of shrinkage, checking the surface perforation of the bacterial membrane under HIM with current parameter settings was not feasible. Other parameter settings will be tested in the future to avoid the bacterial shrinkage problem. Till now, no distinct bacterial membrane damage on the samples could be detected through SEM, FE-SEM, and HIM.

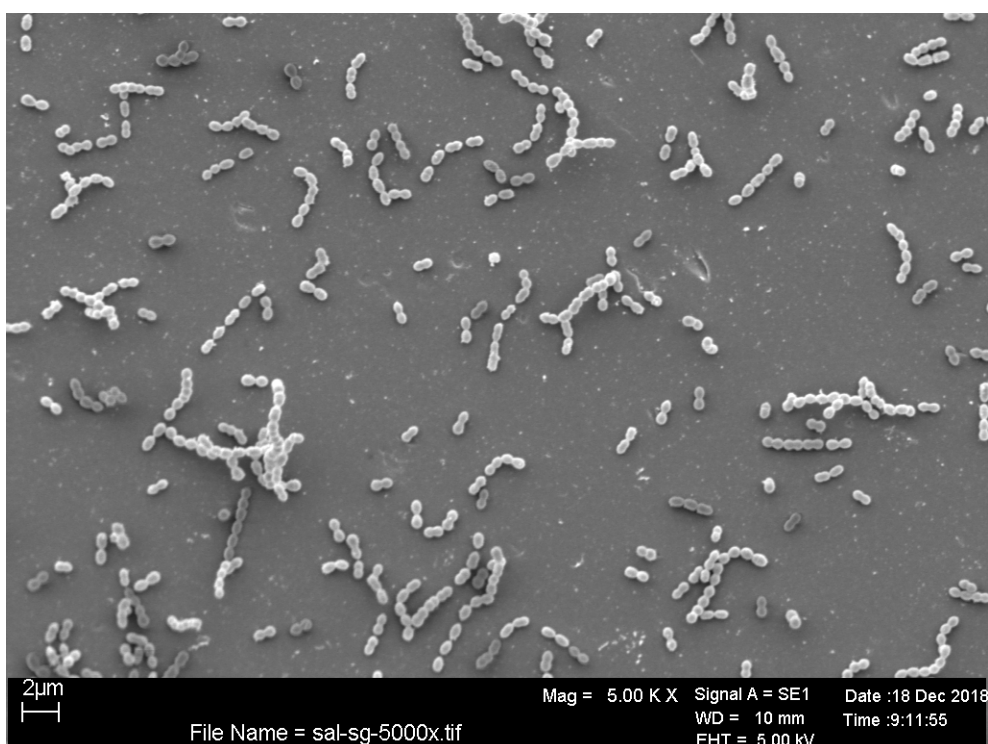


Figure 42: SEM image after 120 min flow of *S. gordonii* adhered on saliva coated biosensor at the magnification of 5000x.

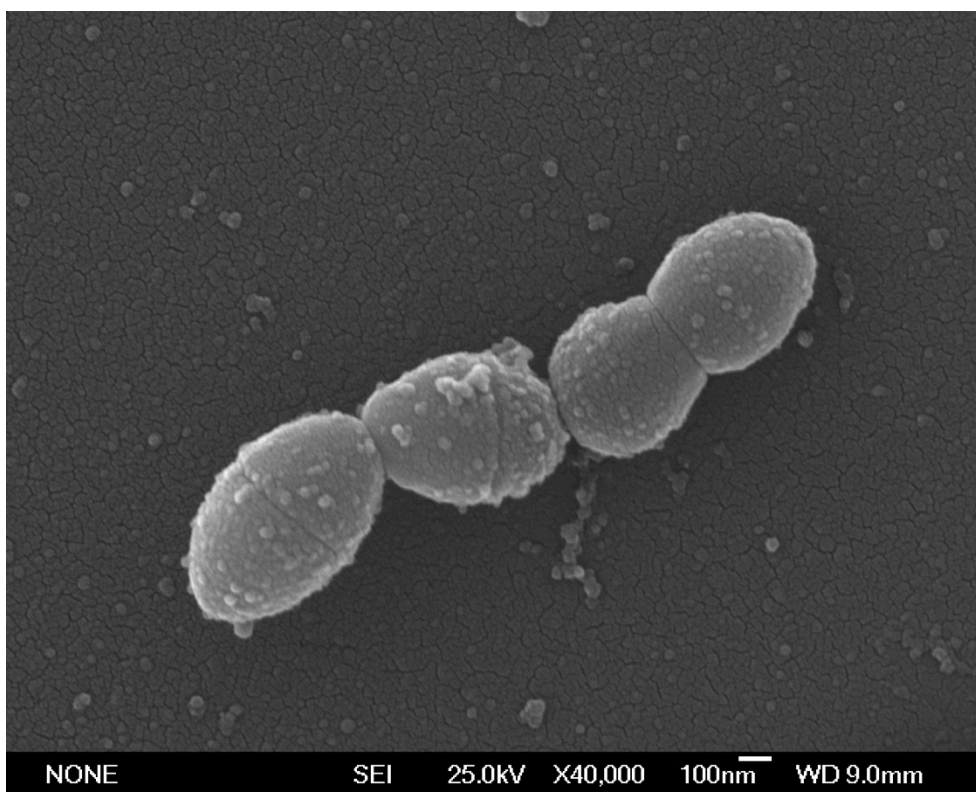


Figure 43: FE-SEM image after 120 min flow of *S. gordonii* adhered on saliva coated biosensor at the magnification of 40000x. [85]

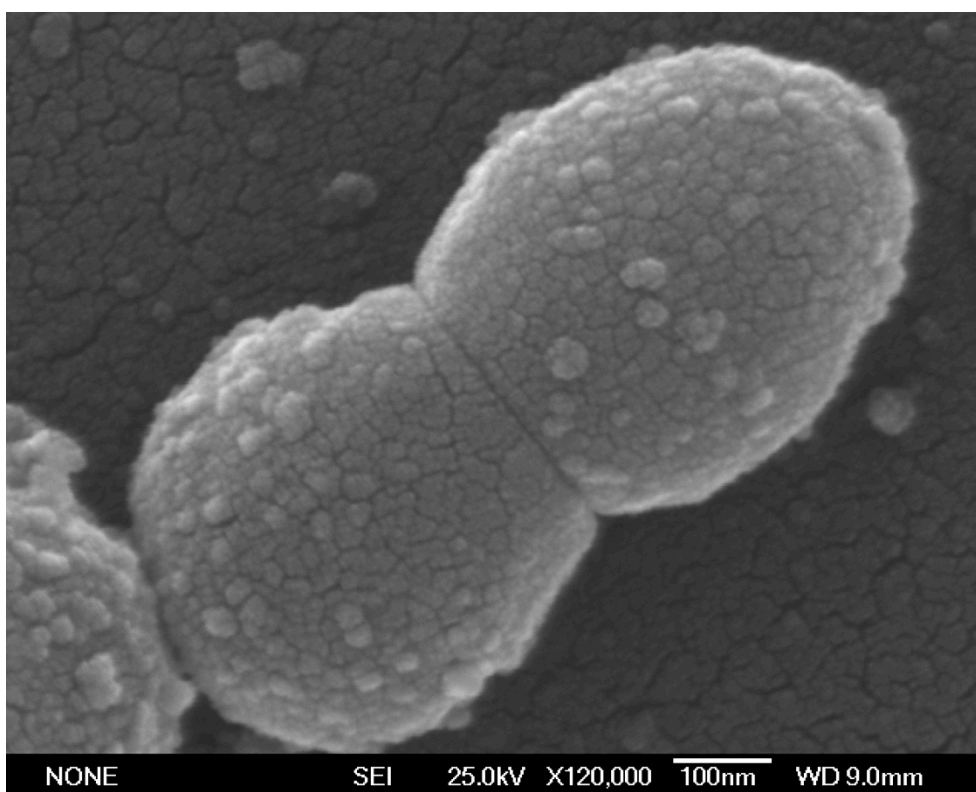


Figure 44: FE-SEM image after 120 min flow of *S. gordonii* adhered on saliva coated biosensor at the magnification of 120000x. [85]

3. Results

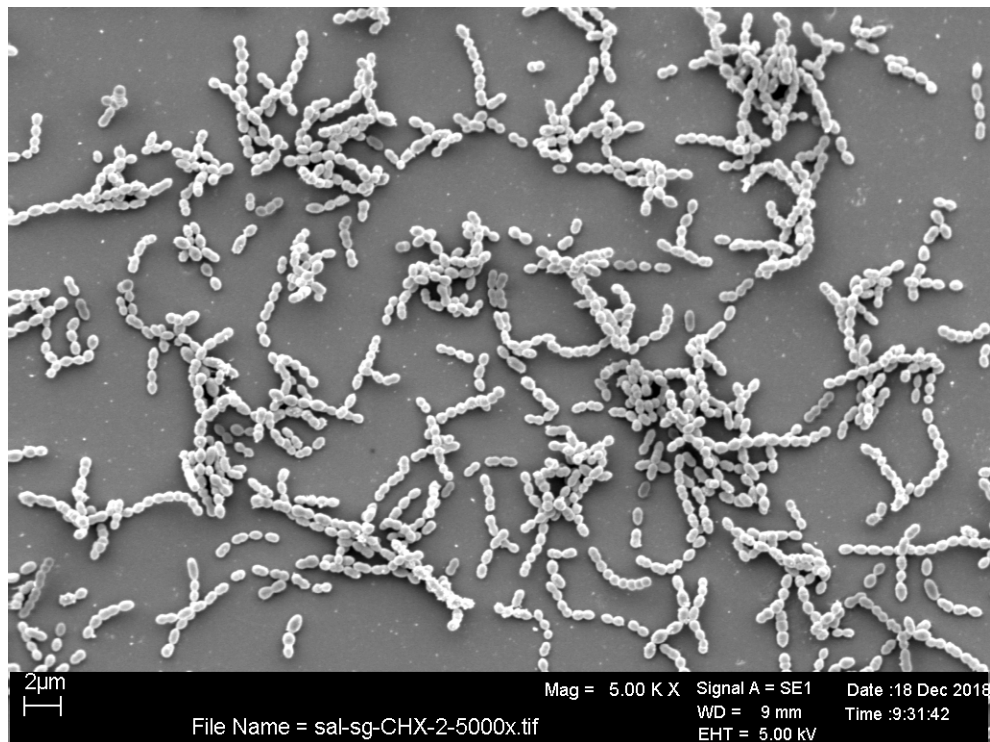


Figure 45: SEM image after 120 min flow of *S. gordonii* treated by ABA for 30 min on saliva coated biosensor at the magnification of 5000x SEM. [85]

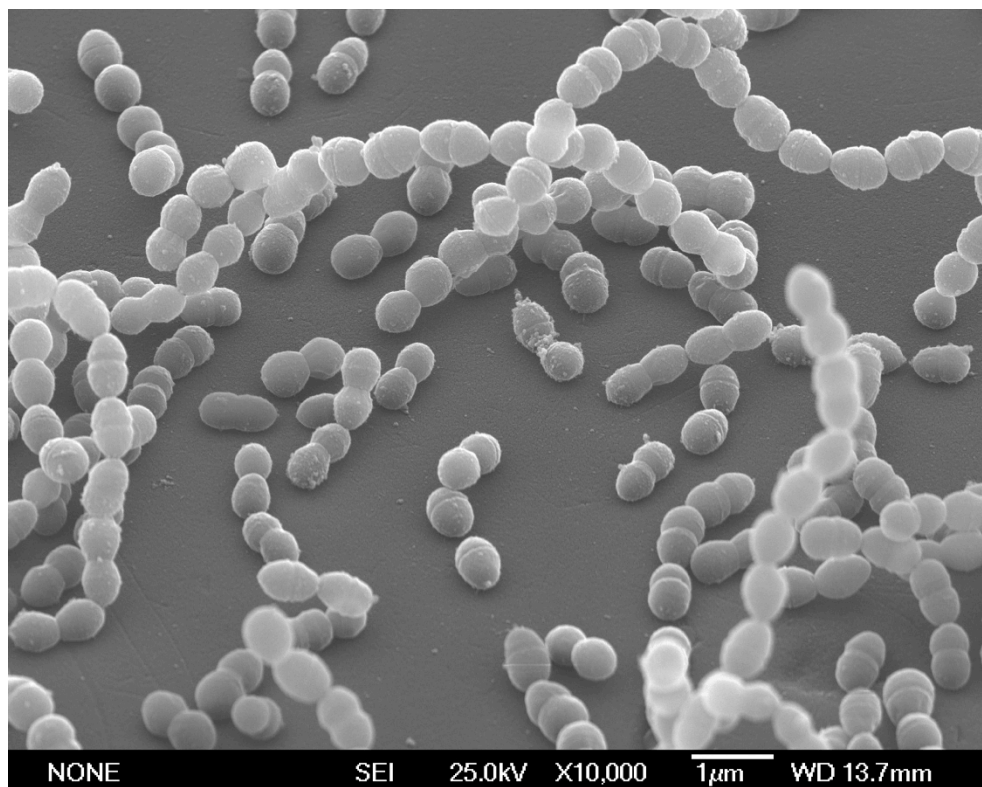


Figure 46: FE-SEM image after 120 min flow of *S. gordonii* treated by ABA for 30 min on saliva coated biosensor at the magnification of 10000x. [85]

3. Results

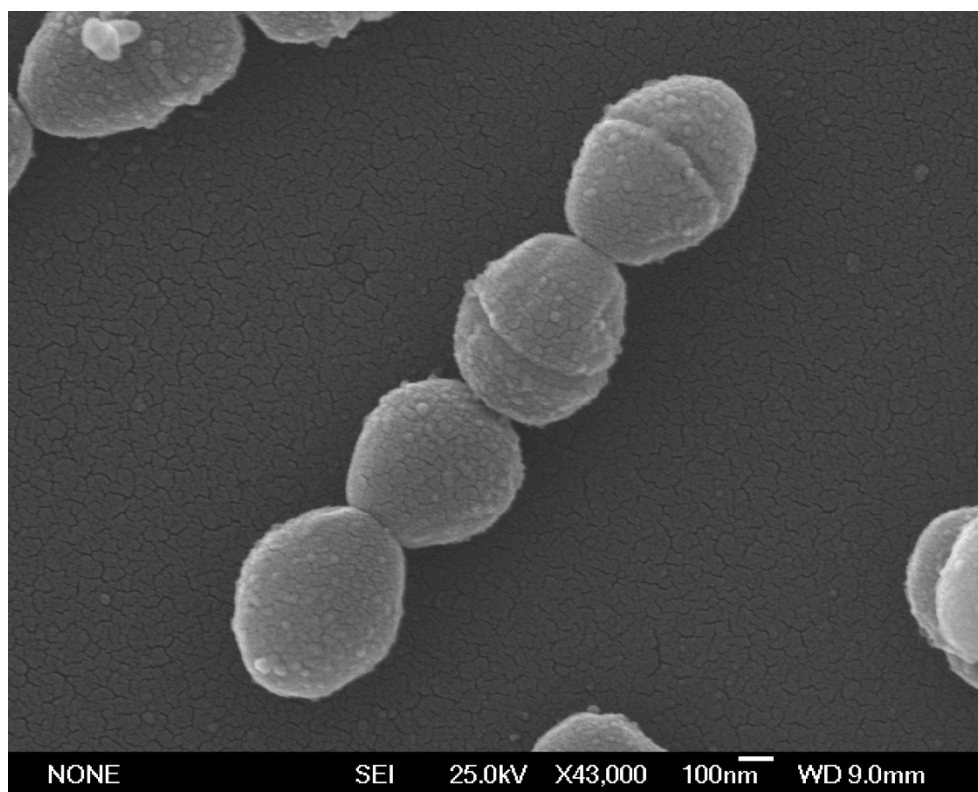


Figure 47: FE-SEM image after 120 min flow of *S. gordonii* treated by ABA for 30 min on saliva coated biosensor at the magnification of 43000x. [85]

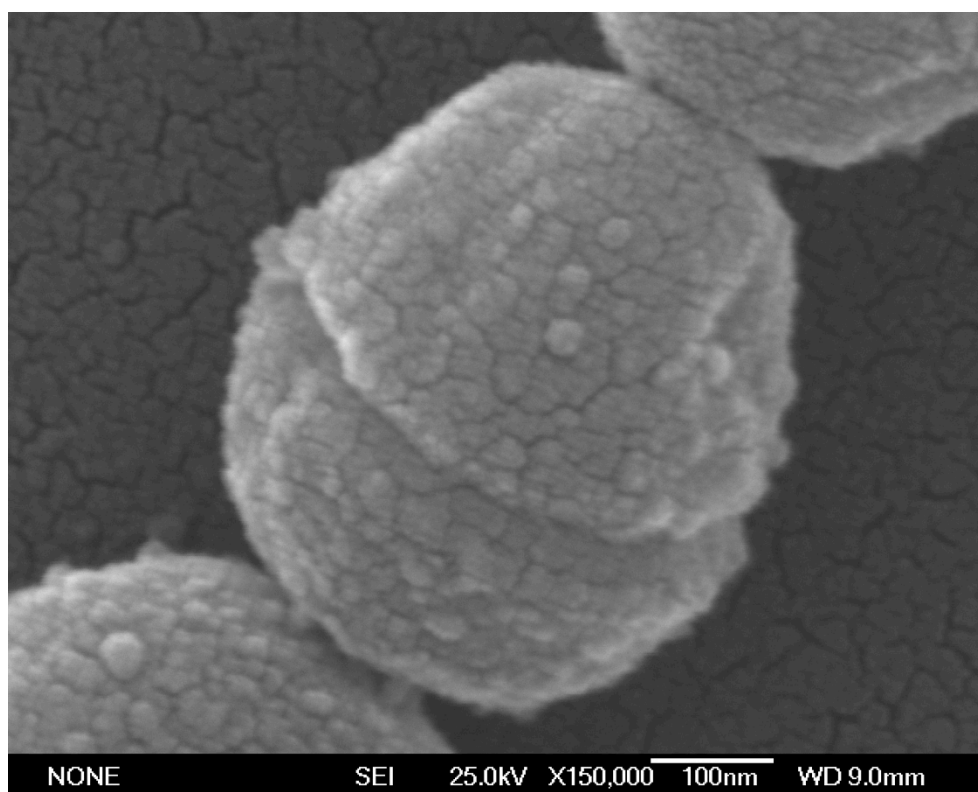


Figure 48: FE-SEM image after 120 min flow of *S. gordonii* treated by ABA for 30 min on saliva coated biosensor at the magnification of 150000x. [85]

3. Results

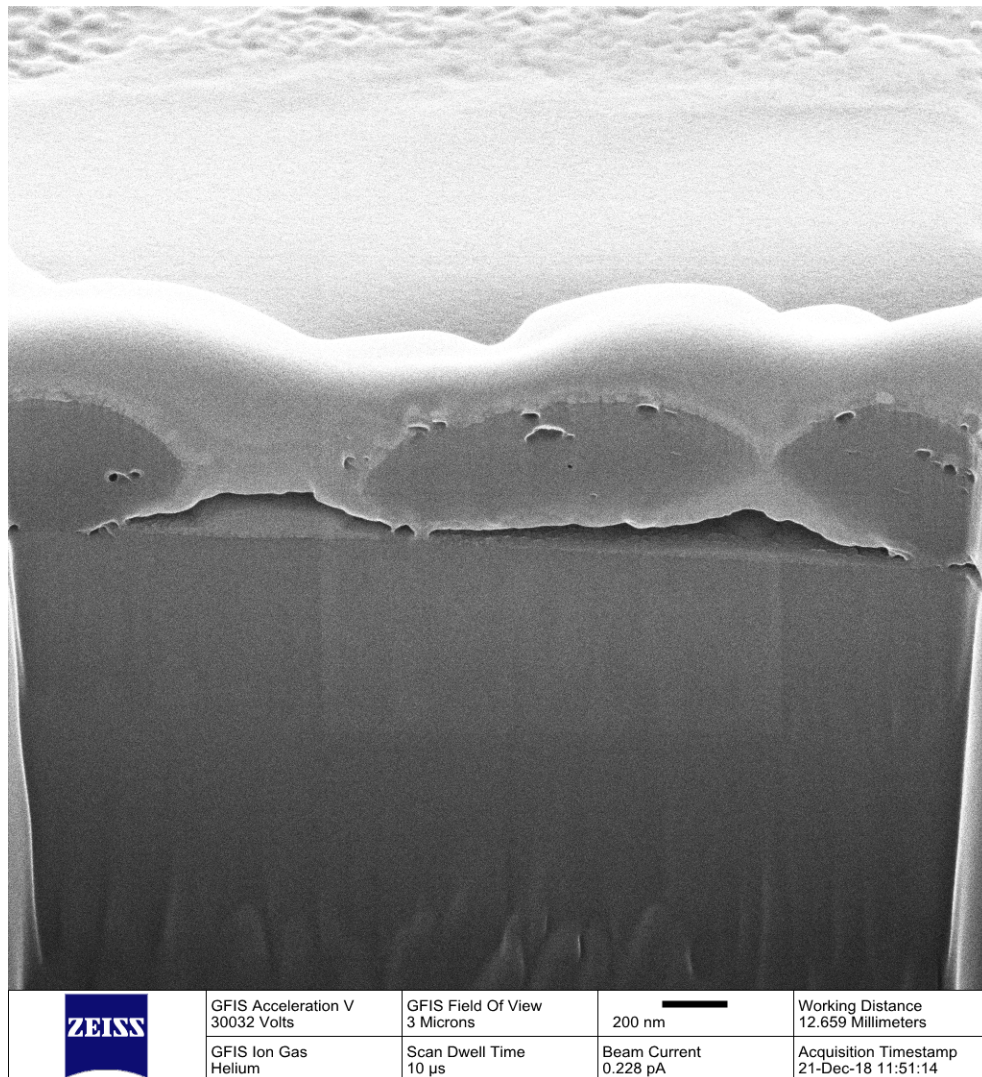


Figure 49: HIM cross-section image of ABA treated *S. gordonii* adhered on saliva coated biosensor surface (details show below). The bacterial cells are sputtered with a layer of Au-Pd and an additional layer of Pt to protect the bacteria in the cutting cross section process.

3. Results

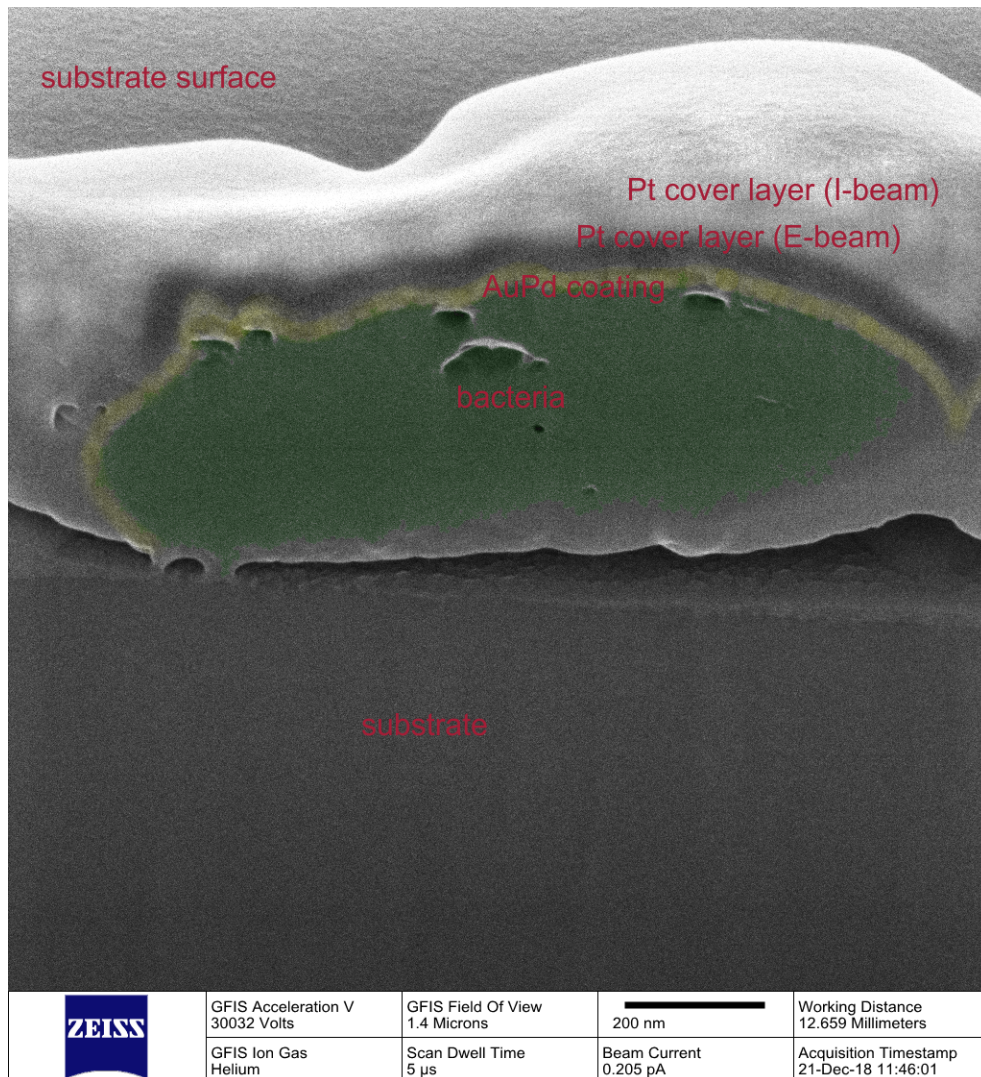


Figure 50: HIM cross-section image of the single *S. gordonii* treated with ABA adhered on saliva coated biosensor surface. The bacterial cells were sputtered with a layer of Au-Pd and an additional layer of Pt before the cross section process. The green color represents the bacteria cell; The yellow color represents the sputtered Au-Pd layer; The black layer is the Pt cover layer for E-beam; The outmost layer is the Pt cover layer for I-beam.

3. Results

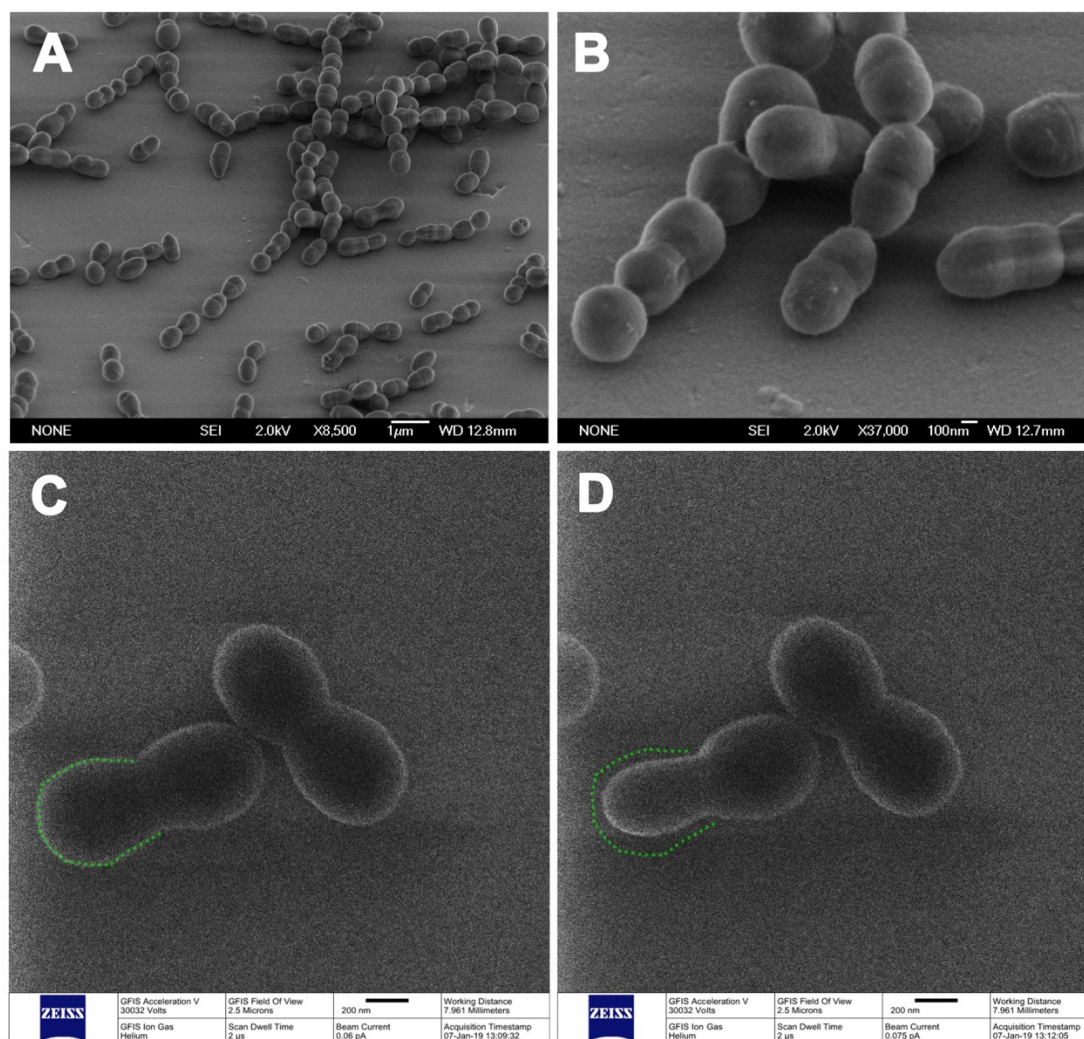


Figure 51: HIM images of un-sputtered (no Au-Pd coating) ABA treated *S. gordonii* adhered on the saliva coated biosensor surface. **A:** HIM 8500x; **B:** HIM 37000x; **C & D:** The shrinkage of the uncoated bacterial cell (marked with the green dot line) after being continuously exposed to the beam.

3.4 Dissipation-frequency (ΔD - Δf) plots and their interpretation

Figure 52 shows the ΔD - Δf plot of *S. gordonii* solution flowing over the ABA preconditioned Ti coated sensor surface. Upon PBS rinsing, the $\Delta D/\Delta f$ curve of ABA with a negative slope headed back exactly coinciding with the original ABA curve to the start point of ABA, and changed to a steeper negative slope upon *S. gordonii*. When applying *S. gordonii* over the ABA treated saliva coated sensor surface (**Figure 53**), the negative gradual slope caused by saliva turned steeper upon ABA. When rinsing with PBS, the curve returned with exactly the same slope as ABA to the ABA start point and then headed to

a positive slope upon *S. gordonii*. In the sequence of flowing ABA solution over *S. gordonii* pre-adhered to the Ti-coated sensor surface (**Figure 54**), the steep negative slope caused by *S. gordonii* became less steep upon ABA and was partly reversible upon PBS rinsing, which means the ABA induced advancing curve and the PBS induced return curve being of a general mirror symmetry but appeared with inconsistent starting point and ending point. As depicted in **Figure 55**, during the process of applying ABA on the *S. gordonii* bound saliva-coated biosensor, the $\Delta D/\Delta f$ curve started with a saliva induced flat negative slope and a positive slope due to *S. gordonii*, followed by an ABA induced steep negative slope, and finally showed a similar partial reversibility as described above. A multi-comparison between the different $\Delta D-\Delta f$ plots were carried out and described below:

“The $\Delta D/\Delta f$ slopes of ABA, saliva, and *S. gordonii* interacting with pure Ti are all negative, characterized by decreasing frequencies and increasing dissipations during interaction. A significant exception from this D/f signal pattern that reflects mass loading has been found in the interaction of *S. gordonii* with the saliva-coated biosensor, where the frequency slightly increased during adhesion indicating mass-loss (**Figure 53, Figure 55**).” [85]

“Comparing the impact of antibacterial agent on the rigidity of bacterial films, the slopes indicate a slightly higher film rigidity on pure Ti (**Figure 54**) compared to a film formed on Ti that was pre-conditioned by ABA (**Figure 52**). The agent further increases the rigidity of bacterial films if applied onto an already formed film (**Figure 54**). In cases it acts on a film with bacteria bound to pure Ti as shown in **Figure 54** compared to bacteria specifically bound to a pre-adsorbed salivary film (**Figure 55**), the latter appears slightly more dissipative [85]. Furthermore, the interaction of bactericide in both cases is not fully reversible as observed on pure Ti (**Figure 52**) and on the biosensor, where it increased the softness of the pellicle film to a low extent (**Figure 53**). This irreversibility observed in

Figure 54 and Figure 55 indicates at the end of the interaction with *S. gordonii* that the antibacterial agent has caused a significant increase of adsorbed, dissipative mass.” [85]

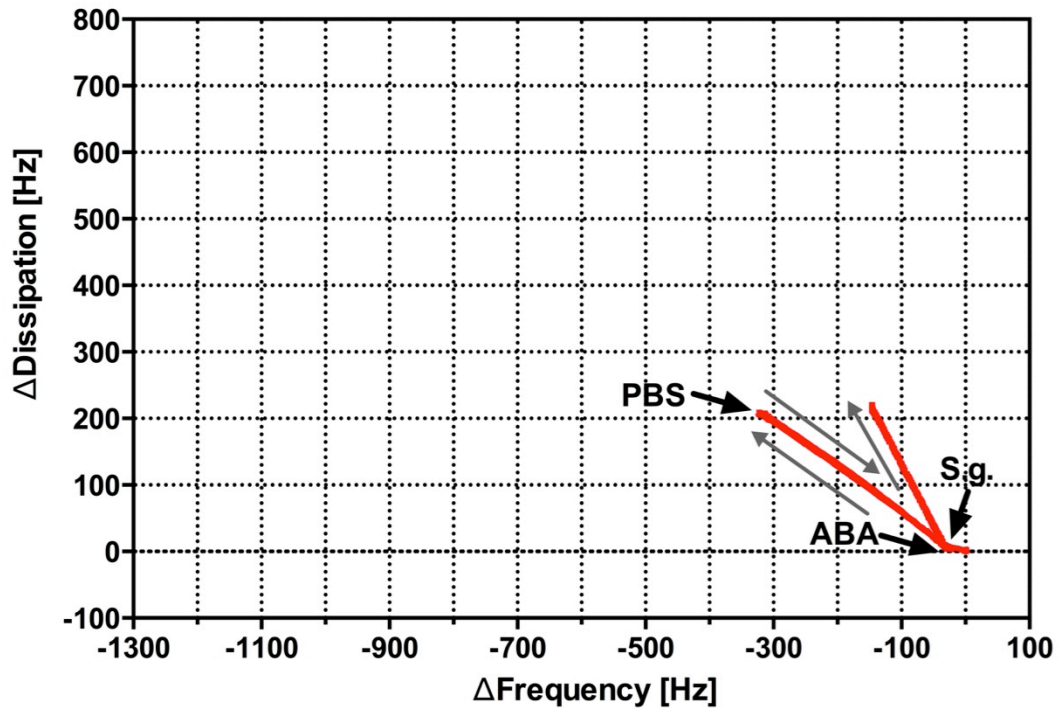


Figure 52: Exemplary ΔD - Δf plots of QCM-D sequence of applying *S. gordonii* on ABA preconditioned Ti-coated sensor surface (protocol C1 in Figure 4: ABA-*S.g.*). The flow sequences of the different solutions were indicated by the gray arrows. [85]

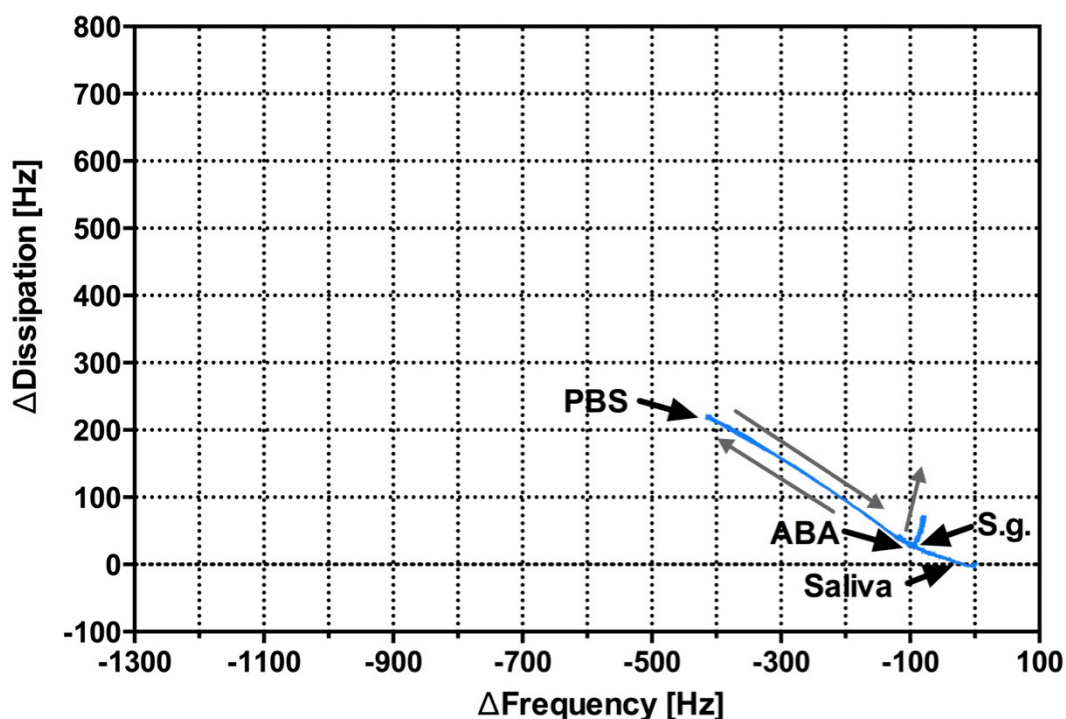


Figure 53: Exemplary ΔD - Δf plots of QCM-D sequence of applying *S. gordonii* on ABA preconditioned saliva-coated biosensor surface (protocol C2 in **Figure 4**: Sal-ABA-S.g.). The flow sequences of the different solutions are indicated by the gray arrows. [85]

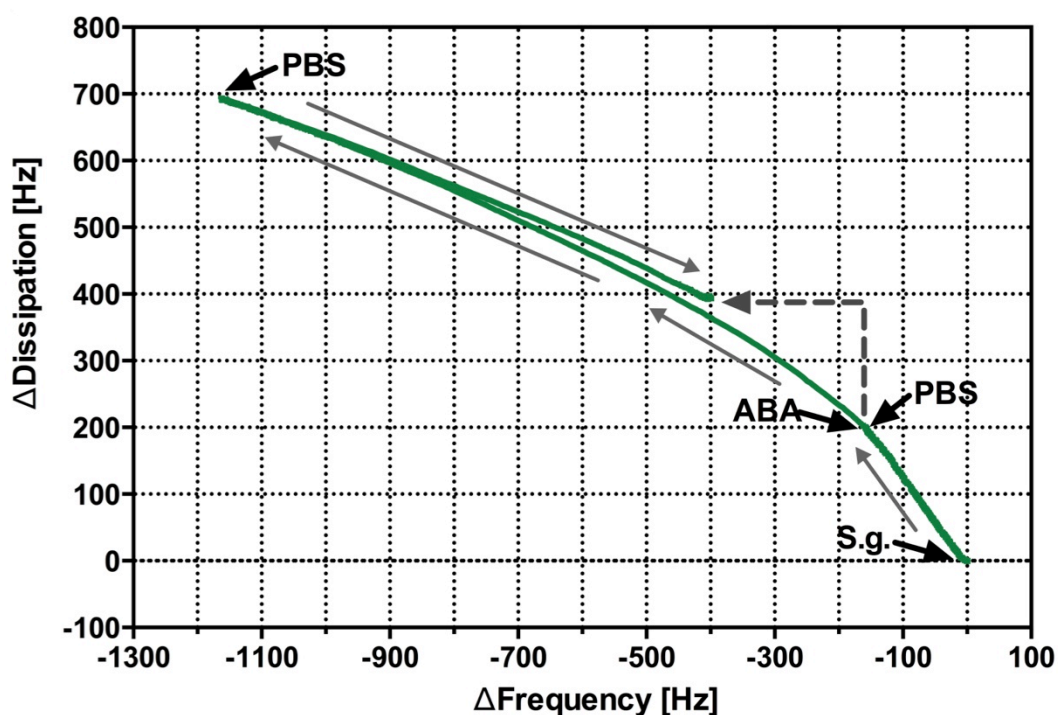


Figure 54: Exemplary ΔD - Δf plots of QCM-D sequence of applying ABA on *S. gordonii* adhered to Ti-coated sensor surface (protocol D1 in **Figure 4**: S.g.-ABA). The flow sequences of different solutions are

3. Results

represented by the gray arrows. The gray dashed lines symbolized the partial irreversibility of ABA and *S. gordonii* interaction, which caused a final mass loading. [85]

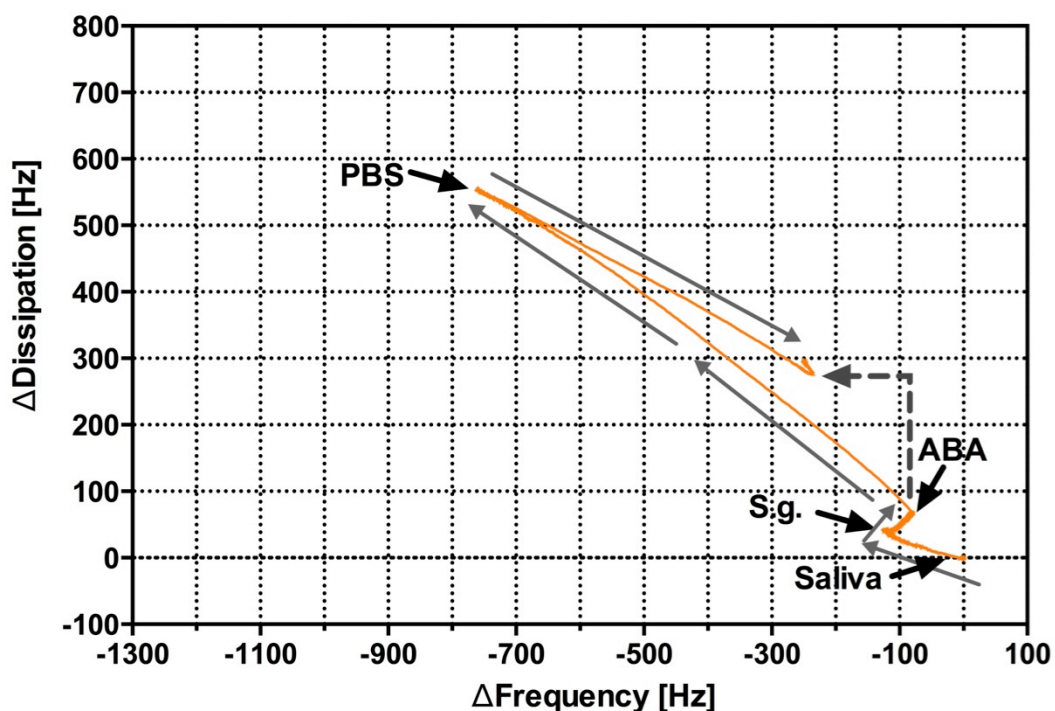


Figure 55: Exemplary ΔD - Δf plots of QCM-D sequence of applying ABA on *S. gordonii* adhered to saliva-coated biosensor surface (protocol D2 in **Figure 4**: Sal-S.g.-ABA). The flow sequences of different solutions are represented by the gray arrows. The gray dashed lines symbolize the partial irreversibility of ABA and *S. gordonii* interaction, which caused a final mass loading. [85]

3.5 QCM-Microscopy set-up construction and application

3.5.1 Microscopic lens selection

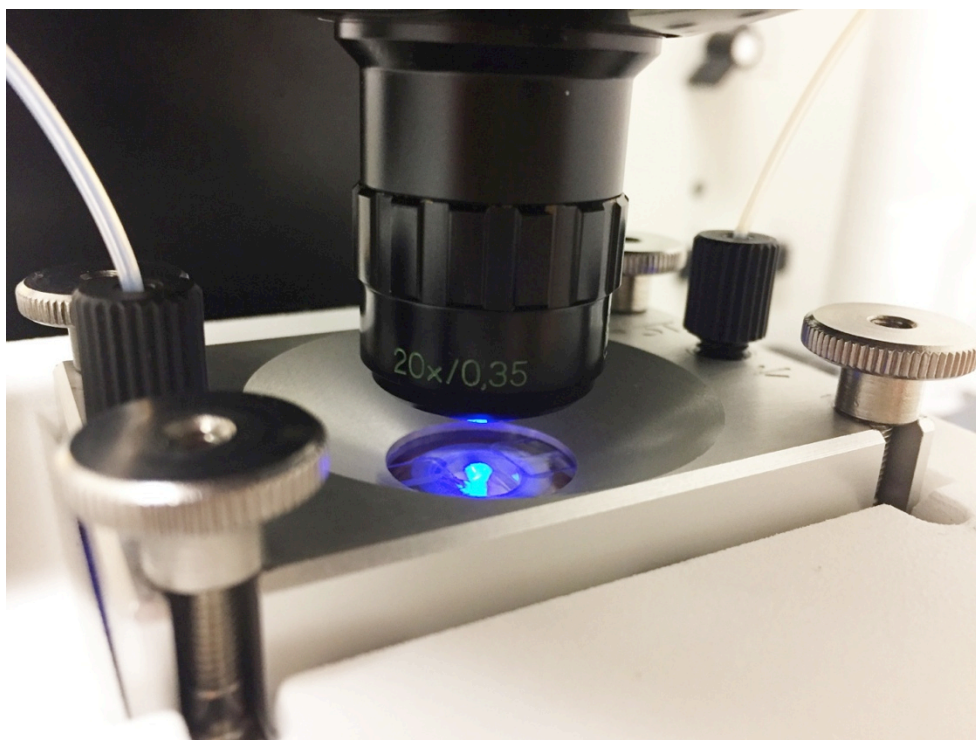


Figure 56: QCM-D flow chamber exposed to fluorescent light for dynamic observation through microscopy. The chamber was fixed with four parallel screws for liquid sealing. Due to the limitation of focusing distance, the enlarged concave indentation of the window of the chamber allows to provide more space for the free movement of the lens of the microscopy. The lens used here is a LDN Achromat 20x 0.35 (Carl Zeiss Jena).

In the process of focusing and after focusing, the 40x lens (**Figure 57 A**) required more horizontal space for movement to observe different regions of the sensor. The other problem was that, the fixation screws (the gray metal screw for fixing and sealing of the chamber) and the tube connector screws restrict this movement. For observing the working region of the quartz surface, a lateral movement of at least 2.5 mm was required (**Figure 57 B**). Actually, the distance between the two tube connector screws (black screws) was 54.98 mm, which was smaller than the sum of the diameter of the 40x lens and the lateral movement distance ($51.66 + 2.5 \times 2 = 56.66$ mm). The height of the tube connector screw (11.53 mm) was larger than the focusing distance from the lens to the flow cell surface (5.35 mm) (**Figure 57 B**), which means when

3. Results

the 40x lens focused, the front part of the lens has already reached the lateral movement limited region caused by the tube connector screws. The distance between the fix screws (gray) was 61.94 mm, which did not interfere with the lateral movement (**Figure 57 C**). Therefore, the 11.53 mm height-tube connector screws were shortened to 2 mm height, which was enough for causing no disturbing to the lateral movement (**Figure 57 D**). In the meantime, the four fix screws were put upside down, which made the lateral movement of the 40x lens more flexible (**Figure 57 D**).

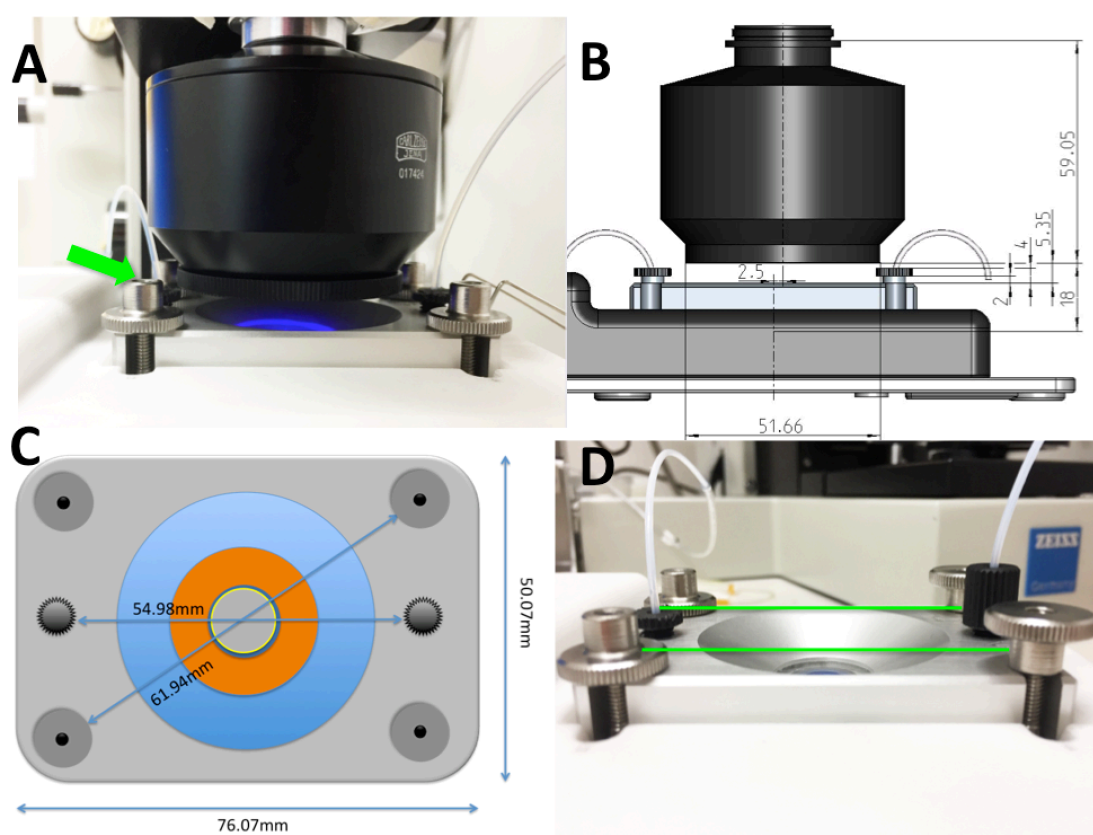


Figure 57: Construction of the mirror lens (40x 0.50, Carl Zeiss Jena) and adjustment of the QCM-D flow chamber. **A:** Focused 40x lens with an additional correction lens in front; **B:** Mode graph for the focused 40x lens with distance and diameter parameters; **C:** Schematic graph of the flow cell, the distance between fixing screws and the tube connection screws interfered with the lateral movement of the lens; **D:** The modification of the flow cell screws (as the green line shows): the right side is the original screw region, the left side is the modified screw region with upside-down fixing screws and cut tube connector screws. This modification aimed at offering more space for the free horizontal and vertical movement of the 40x lens to observe more region of sensor surface and reach the vertical focus distance without being interfered

by the screws or the tube connectors.

A comparison of different image effects between the 20x and 40x lens in different situations was utilized to choose the best focusing method in the online monitoring process for the QCM-D flow chamber. For both the 20x and 40x lens, the company offered an additional correction lens, which could be added to the front of the respective lenses for correcting different thicknesses of the cover glasses. The images were taken in three different situations: directly on the quartz surface outside of the flow chamber, on the quartz surface in the empty flow chamber, and on the quartz surface in the PBS filled flow chamber. For the 20x lens, focusing without additional correction lens was much easier to achieve and the images were sharper than with the correction lens.

However, the images taken with the 40x lens were more blurry and washed-out than with the 20x lens. For direct observation on the quartz surface through the same fluorescent light, the pictures made by 40x lens appeared darker than by the 20x lens (**Figure 58 A, B, C**). When switching to bacteria, which were bound on the quartz surface in an empty flow chamber, the small single bacteria could be clearly observed with the 20x lens, but with 40x lens with or without correction lens, an unclear halo was always observed surrounding the single bacteria (**Figure 58 D, E, F**). In the real condition of observation on bacteria bound quartz in a PBS filled flow chamber, the situation became even worse, with the 20x lens the investigation field turned more blurry than without PBS filling. At least, the focus on bacteria was clear but impaired by a blurry background. The only thing to be seen with 40x lens was a blurry dark and unclear field (**Figure 58 G, H, I**). To simplify the situation of a PBS filled flow chamber, an investigation of the fluorescent marker dots was made on quartz surface and analyzed through different magnification lenses. However, the blurry and halo situation occurred similarly under the 40x lens (**Figure 58 J, K, L**). It was almost impossible to find a focus on the blurry

3. Results

and dark field caused by this 40x lens especially under the real and complicated flowing situation. So the final decision was made to abandon the 40x lens with and without additional correction lens and to use the 20x lens without additional correction lens in the following analyzing process.

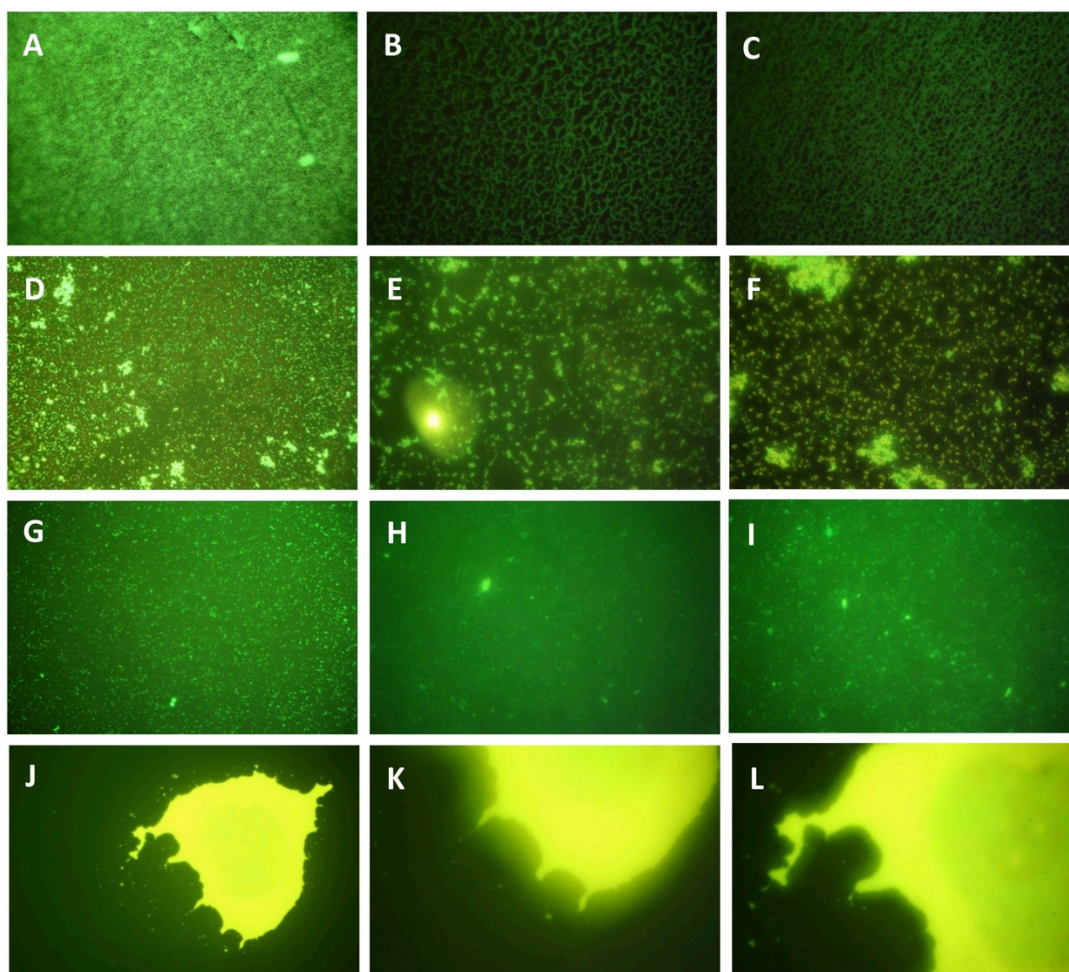


Figure 58: Focused fluorescent images of different situations with different magnification lenses:

A: LDN Achromat 20x: without correction lens, directly on quartz surface;

B: Mirror lens 40x: with correction lens, directly on quartz surface;

C: Mirror lens 40x: without correction lens, directly on quartz surface;

D: LDN Achromat 20x: without correction lens, quartz surface in empty flow chamber;

E: Mirror lens 40x: with correction lens, quartz surface in empty flow chamber

F: Mirror lens 40x: without correction lens, quartz surface in empty flow chamber;

G: LDN Achromat 20x: without correction lens quartz surface in PBS filled flow chamber;

H: Mirror lens 40x: with correction lens, quartz surface in PBS filled flow chamber;

I: Mirror lens 40x: without correction lens, quartz surface in PBS filled flow chamber;

J: LDN Achromat 20x: without correction lens, fluorescent marker dots on quartz surface in PBS filled flow chamber;

K: Mirror lens 40x: with correction lens, fluorescent marker dots on quartz surface in PBS filled flow chamber;

L: Mirror lens 40x: without correction lens, fluorescent marker dots on quartz surface in PBS filled flow chamber.

3.5.2 Consecutive fluorescent microscopic photo making

The 3-hour run of *S. gordonii* over the Ti coated sensor surface ended with a small total increase of both frequency ($\Delta F = +37.7$ Hz) and dissipation ($\Delta D = +72.4$ Hz) (**Figure 59**). For an appropriate online image taking process, a clear focusing of the *S. gordonii* bound to the sensor surface on the bottom of the flow chamber without being influenced by the Live/Dead stained bacteria flow was very important for the success of the experiment. The flow of stained bacteria always contributed to a blurry background in the image taking process. Thus, washing of the stained bacteria was additionally applied after the staining process as shown in **Figure 11**. According to the protocol described in **Figure 11**, the flowing bacteria with the concentration of $OD_{620\text{ nm}} = 0.54$ could reach a high surface density in a very short time, which hinders obtaining a clear focus and taking a consecutive picture with an ascending increase of surface density. Thus, the flow of bacteria with $OD_{620\text{ nm}} = 0.1$ was much more suitable providing enough time to focus and to get the required images of ascending density of surface bound bacteria. The images taken from the stained bacteria without washing procedure showed a better focus situation with clear and shining single bacteria. Therefore, the dilution procedure for the formal experiment was conducted without washing and at a concentration of $OD_{620\text{ nm}} = 0.1$.

In the 3 hour runs of stained *S. gordonii* ($OD_{620\text{ nm}} = 0.1$) over the Ti coated quartz, an increase of both frequency ($\Delta F = +37.7$ Hz) and dissipation

3. Results

($\Delta D = +72.4$ Hz) occurred (**Figure 59**). After successfully focusing on the bacteria bound onto the sensor surface, the images were taken continually every 5 min in the same region. Here, exemplary images of the complete dynamic process are shown (**Figure 60**). The surface bound *S. gordonii* showed a continuous increase of bacterial density over time (**Figure 60, A-H**). When the PBS rinsing started, the background became clearer and the surface density did not change (**Figure 60, H**). Meanwhile, the frequency and dissipation remained at the same equilibrium level after rinsing (**Figure 59**), which indicates that the PBS rinsing process could not remove the surface bound *S. gordonii* from the sensor.

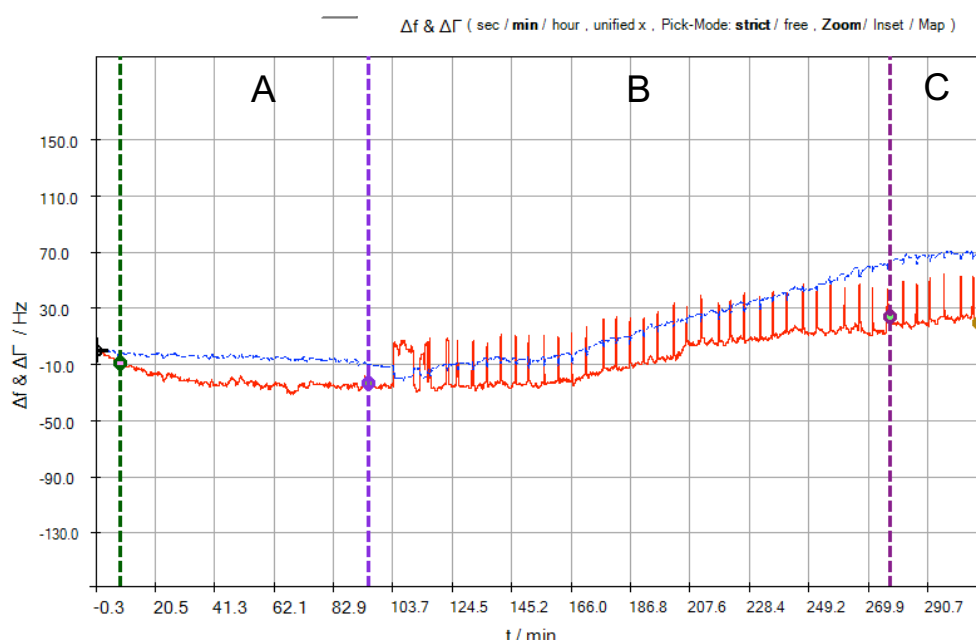
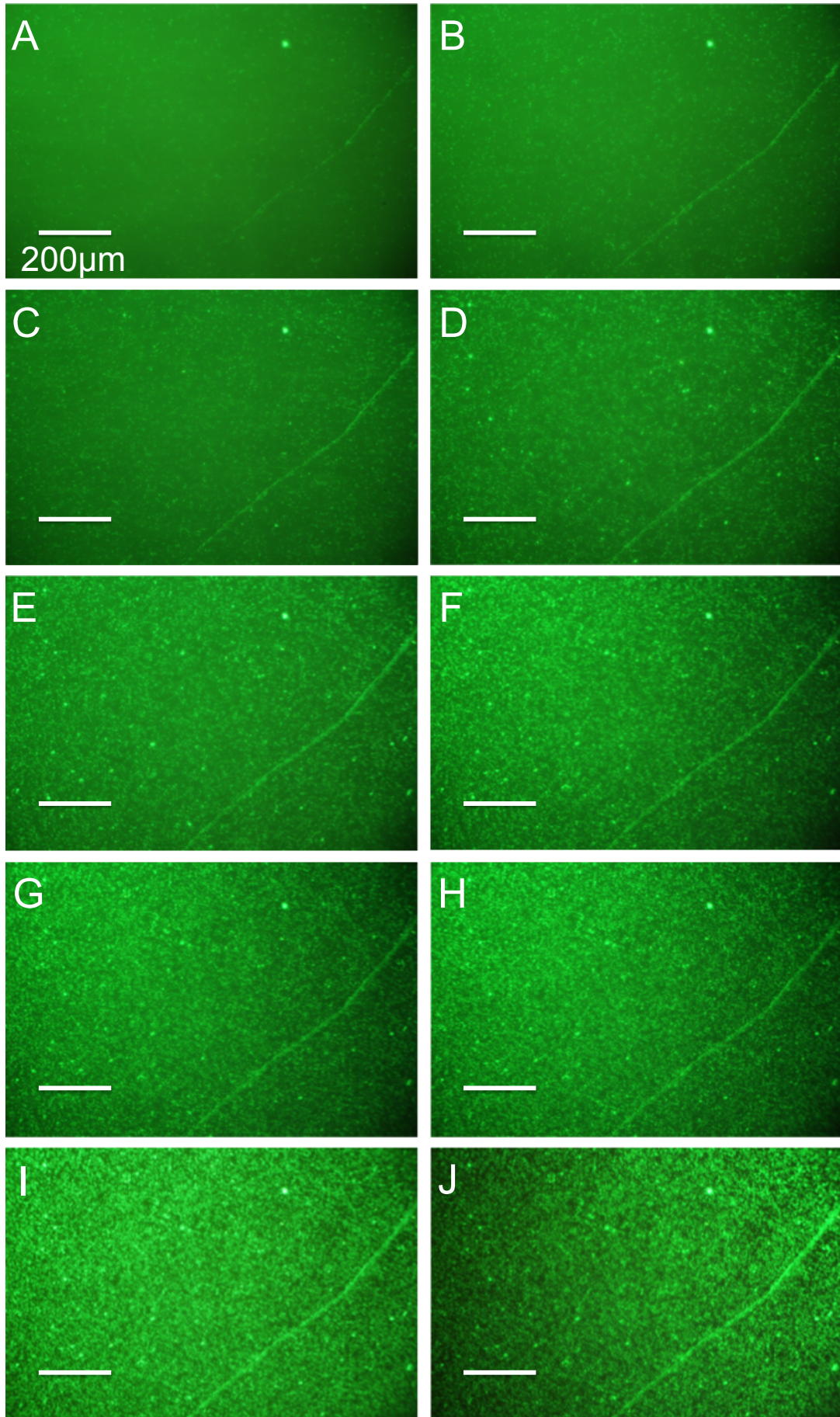


Figure 59: Adhesion experiment of SYTO 9 stained *S. gordonii* ($OD_{620\text{ nm}} = 0.1$) flowing for 3 hours over the Ti coated quartz sensor cleaned with both 70% ethanol ultrasonic bath and 15 min O_2 plasma with photo taking every 5 min under the fluorescent microscope. The binding of *S. gordonii* induced an increase of frequency ($\Delta F = +37.7$ Hz) and an increase of dissipation ($\Delta D = +72.4$ Hz). **A:** PBS baseline; **B:** *S. gordonii* running for 3 hours; **C:** PBS. The fluorescent light caused the spikes on the curve.

3. Results



3. Results

Figure 60: Representative consecutive online fluorescent images of *S. gordonii* ($OD_{620\text{ nm}} = 0.1$) attached to Ti sensor surface cleaned with both 70% ethanol ultrasonic bath and 15 min O_2 plasma at different time points during the *S. gordonii* flow, 200 x. **A:** 15 min, **B:** 35 min, **C:** 55 min, **D:** 75 min, **E:** 95 min, **F:** 115 min, **G:** 135 min, **H:** 155 min, **I:** 175 min, **J:** 195 min (after PBS rinsing). The scale bar represents 200 μm .

However, the flows of $OD_{620\text{ nm}} = 0.1$ fluorescent stained *S. gordonii* over the gold-coated quartz surface induced a decrease of frequency ($\Delta F = -23.2$ Hz) and an almost unchanged dissipation signal ($\Delta D = +1.9$ Hz) (**Figure 61**). At the beginning, there was only a small amount of *S. gordonii* binding on the surface with a relative blurry green background (**Figure 62, A**). The surface density increased gradually with time (**Figure 62, A-F**). Similarly, when PBS rinsing started, the blurry green background became darker and clearer (**Figure 62, F**).

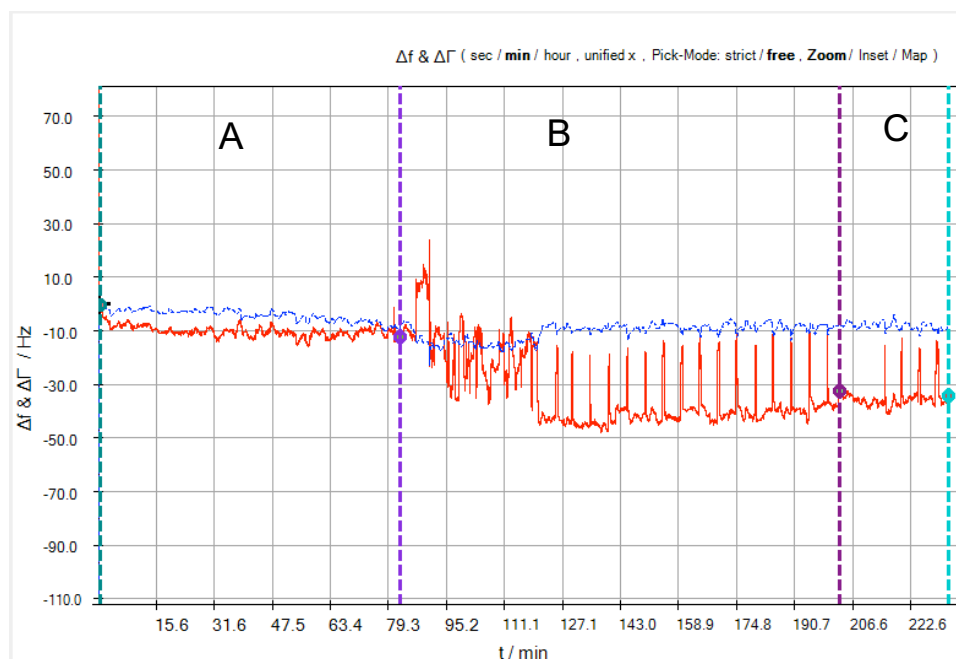


Figure 61: Adhesion experiment of Syto-9 stained *S. gordonii* ($OD_{620\text{ nm}} = 0.1$) flowing for 2 hours over the gold-coated quartz cleaned with both 70% ethanol ultrasonic bath and 15 min of O_2 plasma with images taken every 5 min under the fluorescent microscope. The binding of *S. gordonii* induced a decrease of frequency ($\Delta F = -23.2$ Hz) and an almost unchanged dissipation ($\Delta D = +1.9$ Hz). **A:** PBS baseline; **B:** *S. gordonii* running for 2 hours; **C:** PBS.

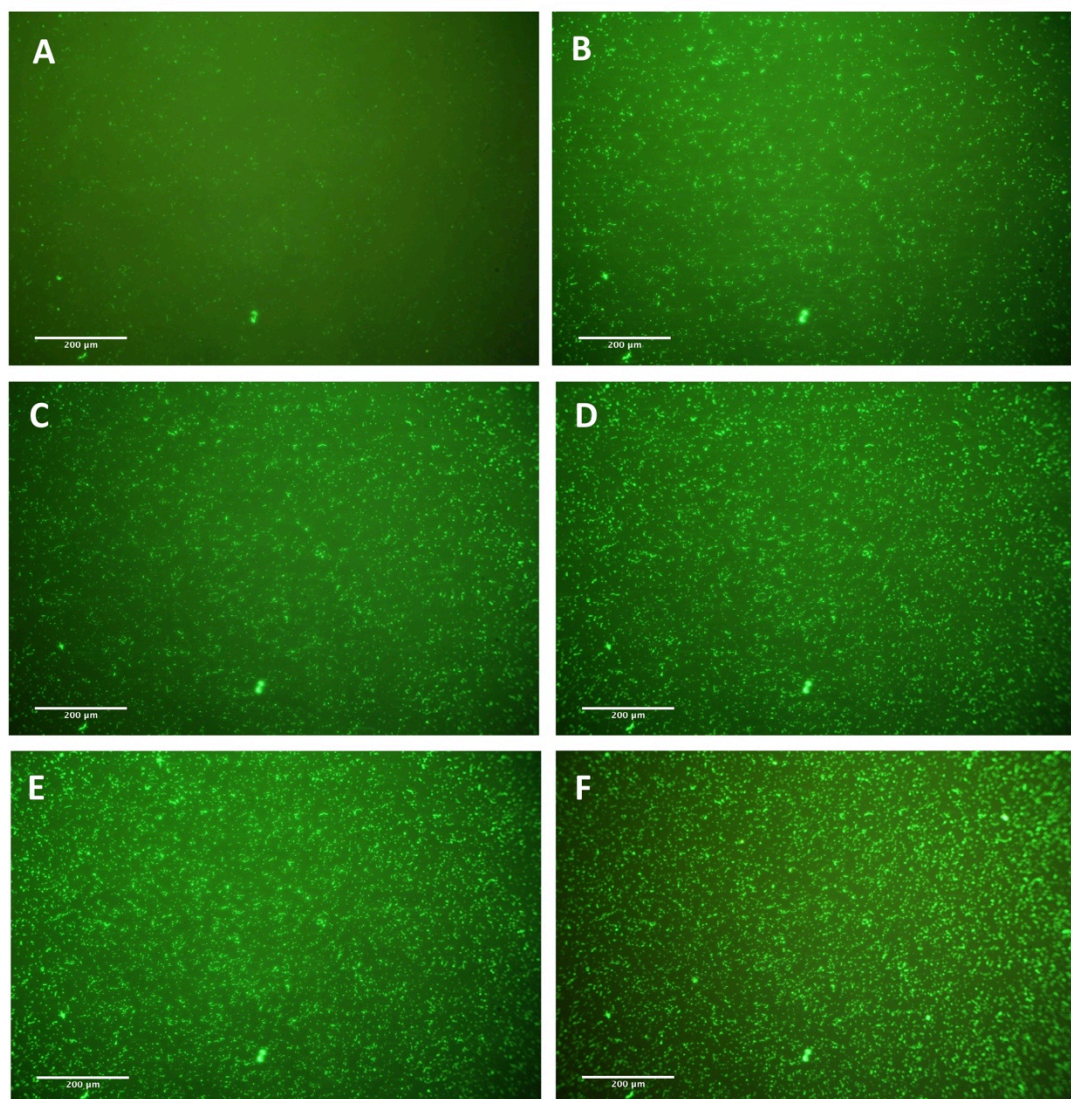


Figure 62: Online consecutive fluorescent images of the attached *S. gordonii* ($OD_{620\text{ nm}} = 0.1$) on gold-coated quartz surface in a 2 hours running period at different time points after switching to *S. gordonii* flow, 200x. **A:** 45 min; **B:** 65 min; **C:** 85 min; **D:** 105 min; **E:** 125 min; **F:** 145 min (after PBS rinsing). The scale bar represents 200 μm .

3.5.3 Combination of bacterial count and QCM-D signal

The data from QCM-D f and D signals and the consecutive pictures were imported into qGraph Viewer (**Figure 63**). The Image J software embedded in the qGraph viewer was used to calculate the amount of the surface bound bacteria, which were further correlated with the corresponding frequency and dissipation curve (**Figure 64**). The numbers of surface-bound *S. gordonii* increased with the increase of both frequency and dissipation (**Figure 65**) [85].

3. Results

After linear regression analysis, the numbers of surface-bound *S. gordonii* were found to be positively correlated with both frequency ($R^2 = 0.8471$) and dissipation ($R^2 = 0.7877$) (**Figure 66**).

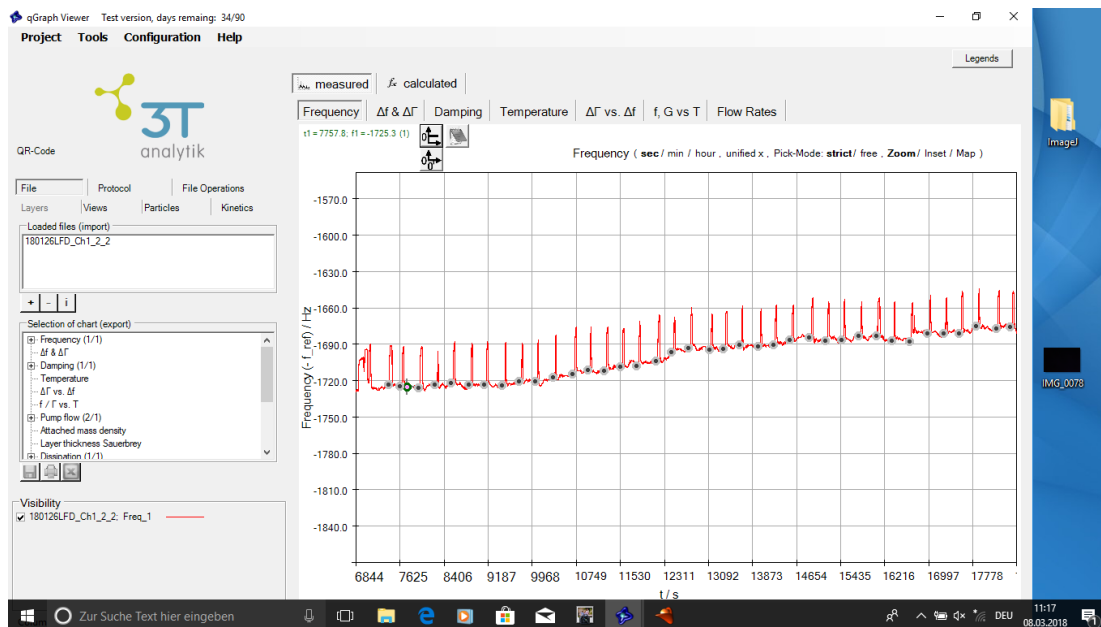


Figure 63: Correlating the consecutive fluorescent images with the same time points on the frequency curve, the gray dots shown at the spike region in the frequency curve represented the correlated image data at the corresponding time points.

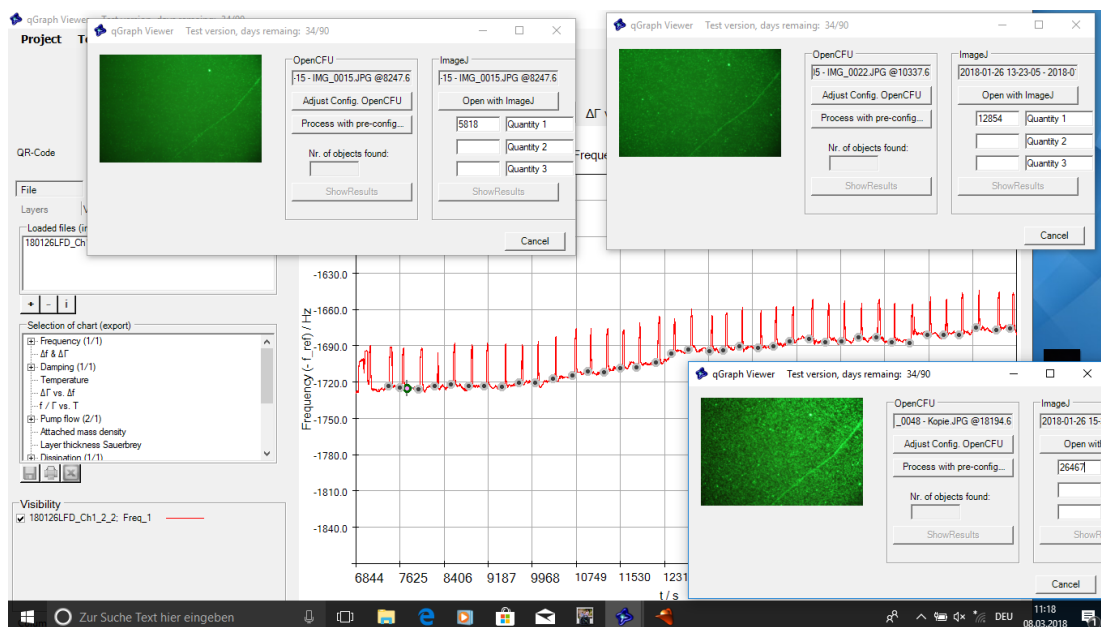


Figure 64: Correlating the number of surface bound bacteria in the imaging

3. Results

field with the frequency change at each time point through the qGraph Viewer software embedded with Image J.

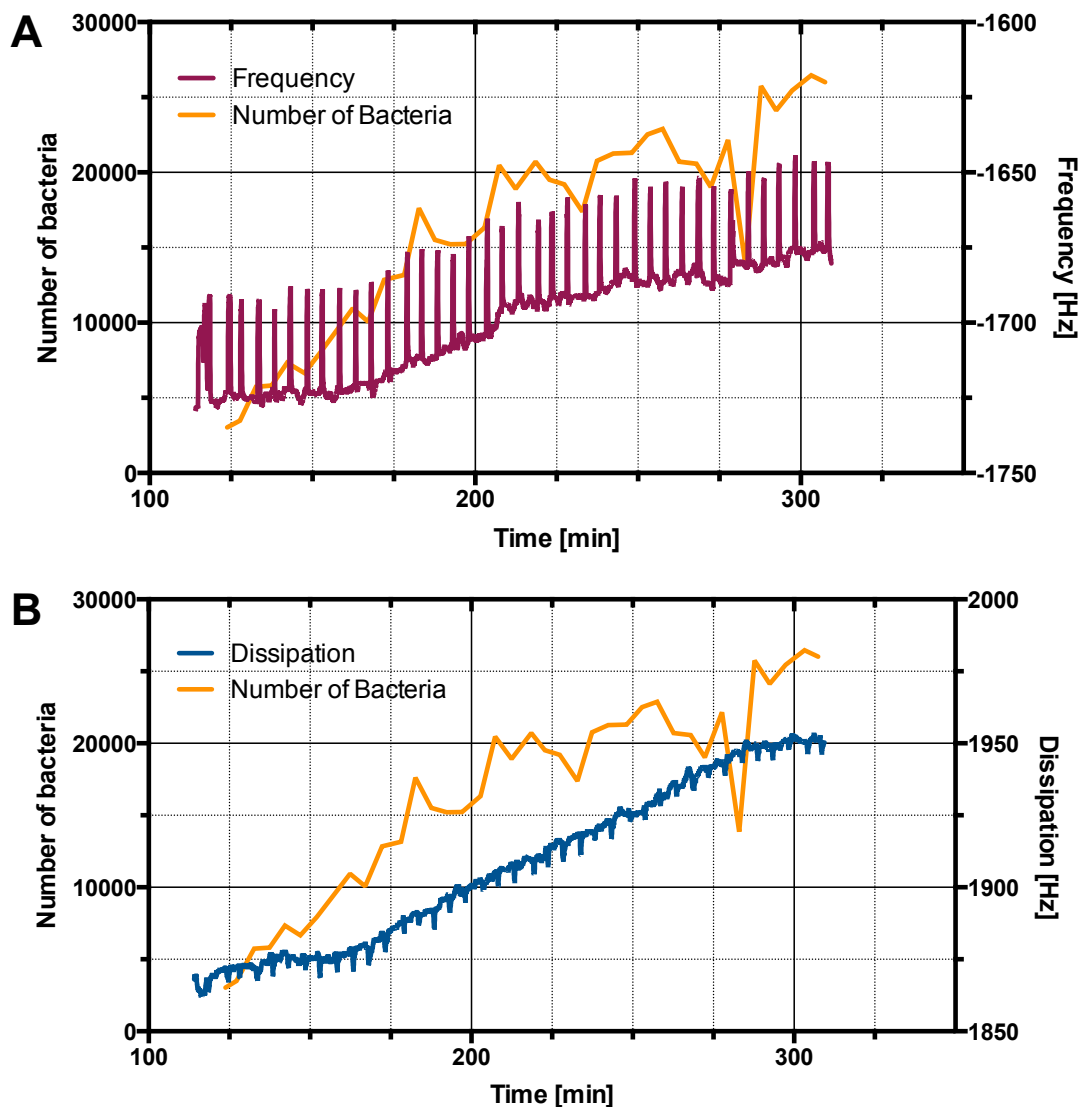


Figure 65: Correlation between the change of QCM-D signal and the amount of Ti sensor surface-bound *S. gordonii* in the imaging field. **A.** The correlation between the increase of frequency and the number of surface-bound bacteria; **B.** The correlation between the increase of dissipation and the number of surface-bound bacteria. The spikes in frequency and dissipation were due to the fluorescent light-induced temperature change during image taking.

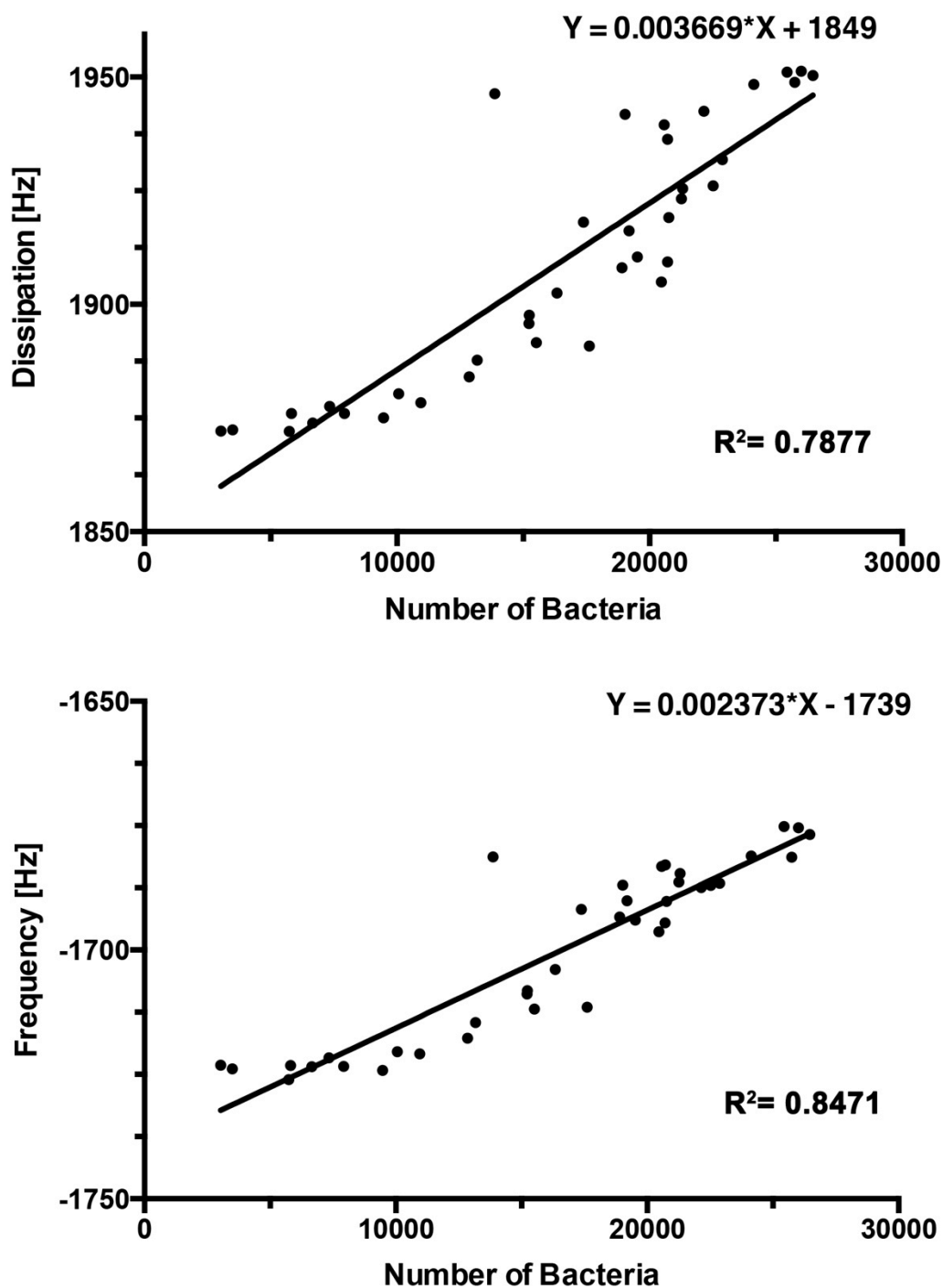


Figure 66: Linear correlation between the number of surface-bound bacteria and frequency or dissipation change. **A.** Positive linear correlation between frequency and number of surface-bound bacteria; **B.** Positive linear correlation between dissipation and number of surface-bound bacteria.

3.5.4 Analysis of antibacterial function

For the purpose of online microscopic observation of the dynamic

3. Results

interaction between bacteria and ABA, stained bacteria were flown over the surface first, then, the flow of ABA solution over the bacterial film was carried out. The emerging question was that when ABA triggered the interaction with the Live/Dead stained bacteria, will the bactericidal effect from ABA solution be indicated online by a color change? Theoretically, the bacteria will stay green even if they were killed, because the bacteria were stained before being killed. According to the mechanism of LIVE/DEAD® BacLight™ Bacterial Viability Kits, SYTO 9 can get into both live and dead bacteria, but propidium iodide (PI) can only get into the dead bacteria with broken membrane. Both SYTO 9 and PI are nucleic acid stain. After Live/Dead staining, no PI could be found inside the living bacteria. When flowing ABA over these living and stained bacteria, even though membrane perforation was expected by the bactericidal effect immediately, there was no additional PI molecule in the flow medium which could infiltrate through the damaged bacteria membrane and induce a red staining. Thus, the killed bacteria would still stay green.

To prove this theory, a simplified glass slide staining experiment was carried out to figure out the possible procedure of monitoring the dynamic bacterial death upon ABA through the Live/Dead staining. **Figure 67 A, B** were similarly green, which proved the previous hypothesis that if make Live/Dead staining of bacteria before using ABA, the bacteria would not show any color change from green to red after being killed. In **Figure 67 C**, when Live/Dead staining was applied after applying ABA, the PI infiltrated through the perforated membrane and stained the bacteria red after being killed. However, this is only a staining process upon the end of the experiment, which could not indicate any dynamic change. In **Figure 67 D**, a modified process was used: a droplet (10 μ L) of PBS washed live stained *S. gordonii* (**Figure 11**) and a droplet of mixture (10 μ L) of ABA and PI were put on a glass slide, when the coverslip was laid on top, the two drop liquids were mixed up. A gradual color change from green to orange was observed in a short time period. This implies that flowing a mixture of ABA and PI into the flow chamber could provide the

3. Results

possibility for dynamically monitoring color changes of the bacteria upon ABA.

This staining procedure was further applied in the dynamic monitoring experiment in the flow chamber. The 30 min flow of *S. gordonii* ($OD_{620\text{ nm}} = 0.74$) over the gold sensor surface induced a frequency decrease of 100 Hz and a dissipation increase of 100 Hz. The following flow of the ABA and PI mixture induced a fast 450 Hz decrease of frequency and a fast 550 Hz increase of dissipation (**Figure 68**). As shown in the dynamic images in the flow chamber, the gradual color change was from a total green to a mixture of green and orange stained bacteria, further to the total orange stained bacteria and finally back to green upon PBS rinsing (**Figure 69**). The single bacterial cells could be detected in the total process.

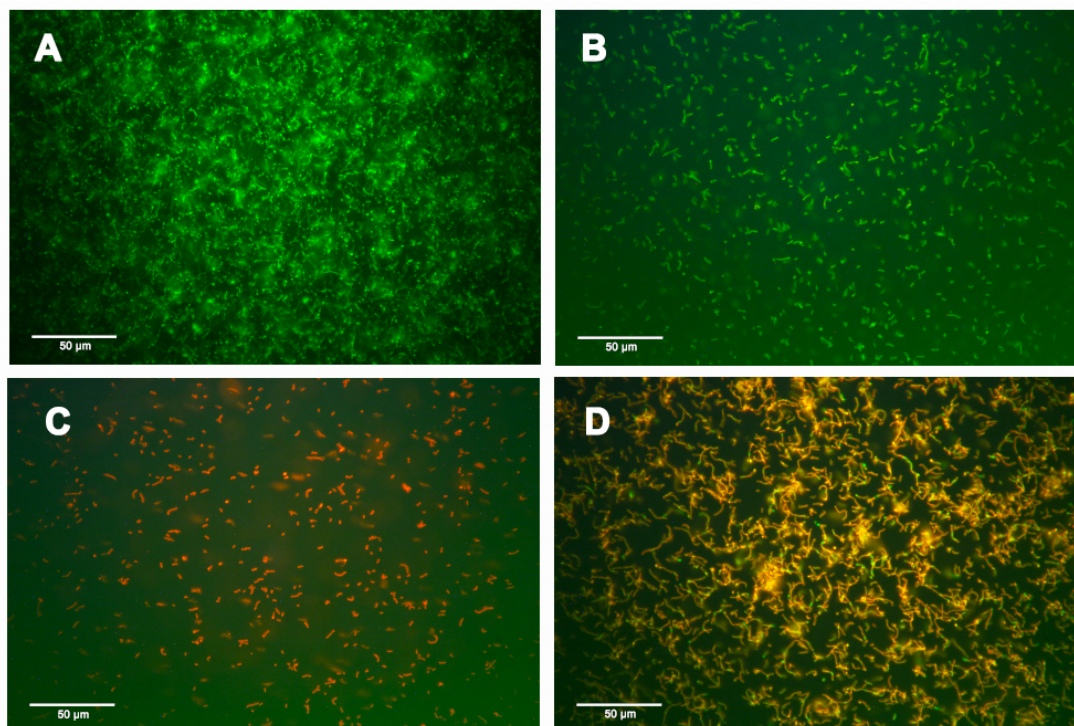


Figure 67: Glass slide test with different ABA and *S. gordonii* Live/Dead stain process under fluorescent microscope (400x):

A: Live (SYTO 9)+Dead (PI) stain *S. gordonii* for 15 min

B: Live (SYTO 9)+Dead (PI) stain *S. gordonii* for 15 min, washed with PBS and centrifugation, then add ABA

C: Live (SYTO 9)+ABA stain *S. gordonii* for 15 min, washed with PBS and centrifugation, then add Dead (PI)

D: Live (SYTO 9) stain *S. gordonii* for 15 min, washed with PBS and centrifugation, then add mixture of ABA and PI (100 μL ABA + 100 μL PI).

PI: propidium iodide; ABA: antibacterial agent.

3. Results

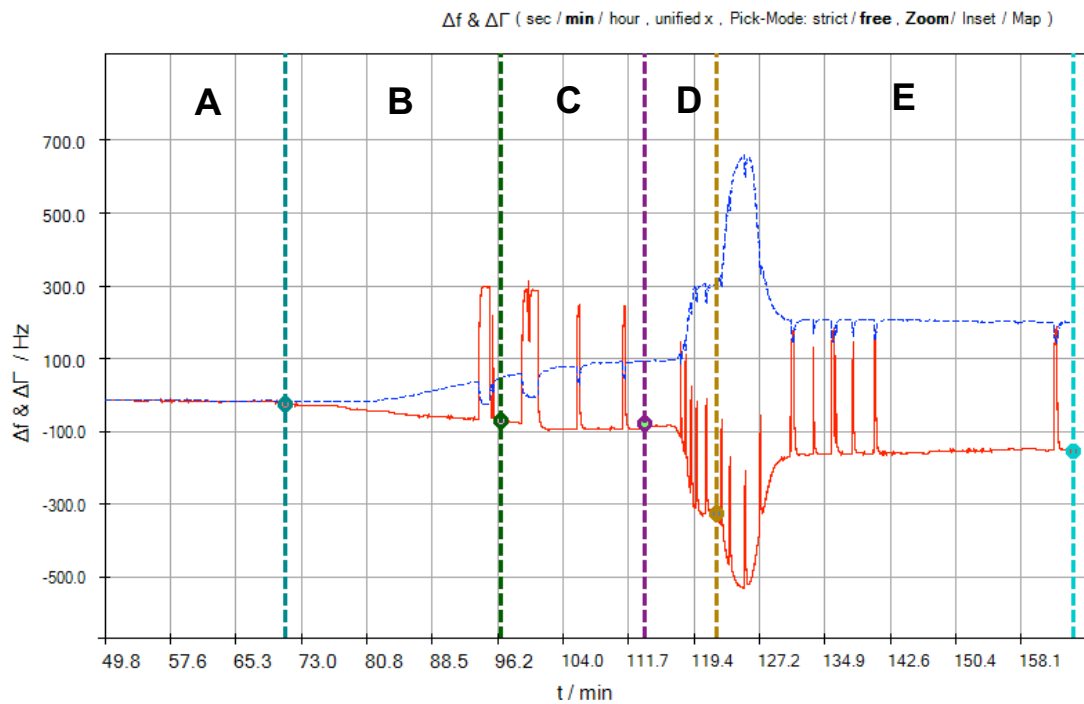


Figure 68: SYTO 9 stained *S. gordonii* ($OD_{620 \text{ nm}} = 0.74$) binding on ultrasonically cleaned gold-coated quartz sensors followed with ABA + PI mixture. **A:** PBS baseline; **B:** *S. gordonii*: 30 min; **C:** PBS: 15 min; **D:** 200 μL ABA + 200 μL PI mixture: 5 min; then stop pump for 5 min incubation; **E:** PBS rinsing 30 min. PI: propidium iodide; ABA: antibacterial agent. (The red line represents the frequency, the blue line represents dissipation).

3. Results

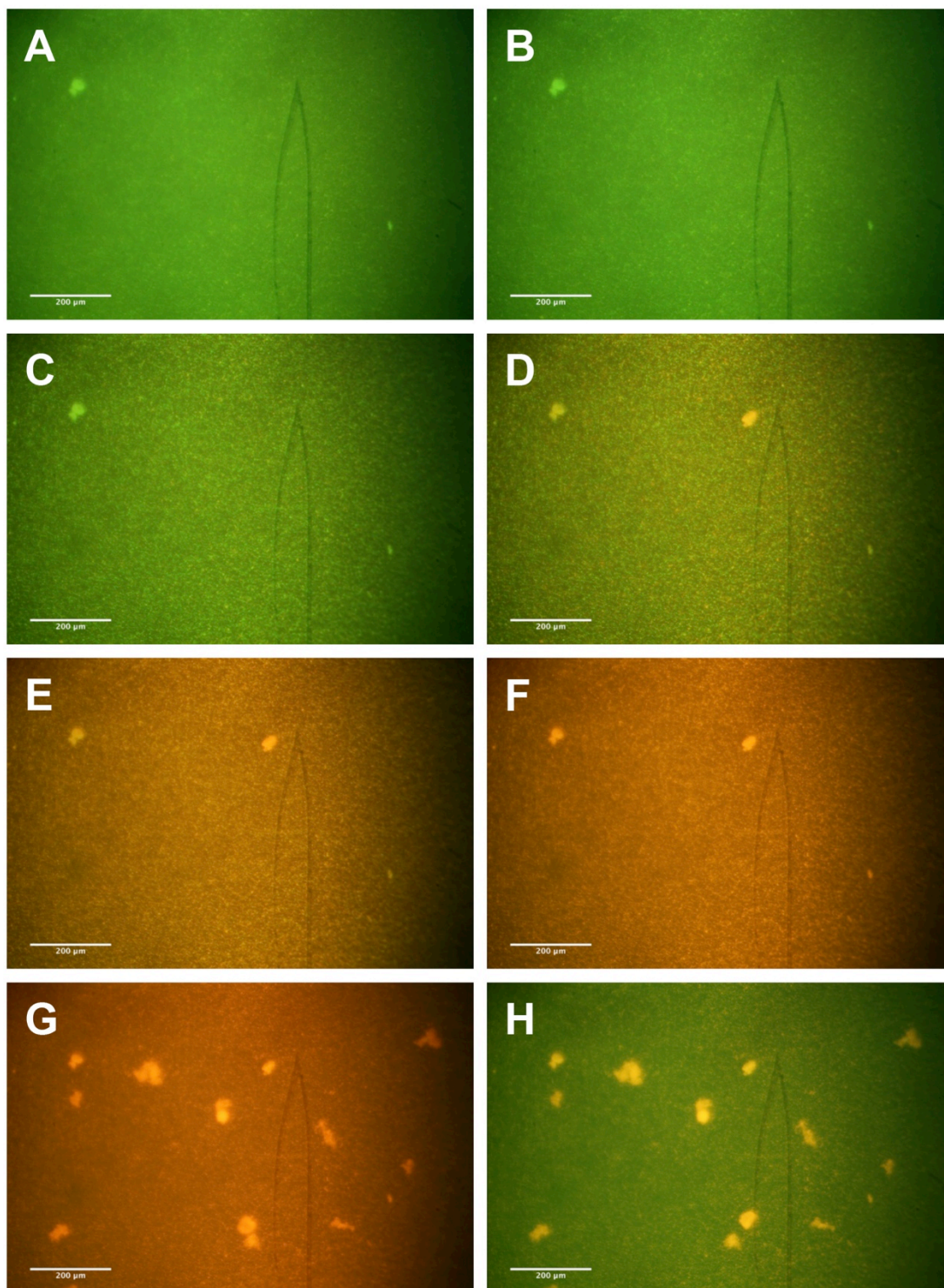


Figure 69: Exemplary online fluorescent images (200 x) of SYTO 9 stained *S. gordonii* ($OD_{620\text{ nm}} = 0.74$) binding on ultrasonically and plasma cleaned gold-coated quartz sensors and interacting with ABA. In the ABA + PI mixture interaction stage, images were taken every 60 s. In PBS rinsing stage, photos were taken every 3 min. **A:** SYTO 9 stained green *S. gordonii*; **B-G:** Upon flowing 200 μL ABA + 200 μL PI mixture, the background and the *S. gordonii* gradually turned red within 5 min.; **H:** Upon PBS rinsing, the background

3. Results

turned back to green, the small red dead single *S. gordonii* could be seen. C-F were the consecutive images taken every 60 s upon start of ABA. PI: propidium iodide; ABA: antibacterial agent. The small scratch in the image was made for keeping the focus in the same region.

The other attempt was the utilization of the bacteria membrane penetrable stain (FDA, fluorescein diacetate, green) and the nucleic acid stain ethidium bromide (EB, red), which only infiltrate through the damaged bacterial membrane indicating the death of bacteria [127]. The FDA stained bacteria flowed into the cell and contributed to a decrease of frequency ($\Delta F = -65$ Hz) and an increase of dissipation ($\Delta D = +371.2$ Hz) (**Figure 70 B**). However, the FDA bleached away very fast accompanied with the blurry background (**Figure 71 A**), which caused the difficulty for focusing on the bacteria. The background and *S. gordonii* gradually turned red upon ABA flowing (**Figure 71 A-D**). The ABA induced a sharp decrease ($\Delta F = -1042$ Hz) and a sharp increase ($\Delta D = +2094$ Hz) of dissipation (**Figure 70 D**). When switched to PBS rinsing, the background turned back to green, the unclear small red *S. gordonii* bacteria could hardly be noticed upon the unclear background (**Figure 71 E, F**). The blurry background occurred in the whole run being worse than the situation with SYTO 9/PI, which led to the blurry and unfocused microscopic images (**Figure 71**). Based on the results and evaluation above, SYTO 9/PI was better for the dynamic microscopic monitoring.

3. Results

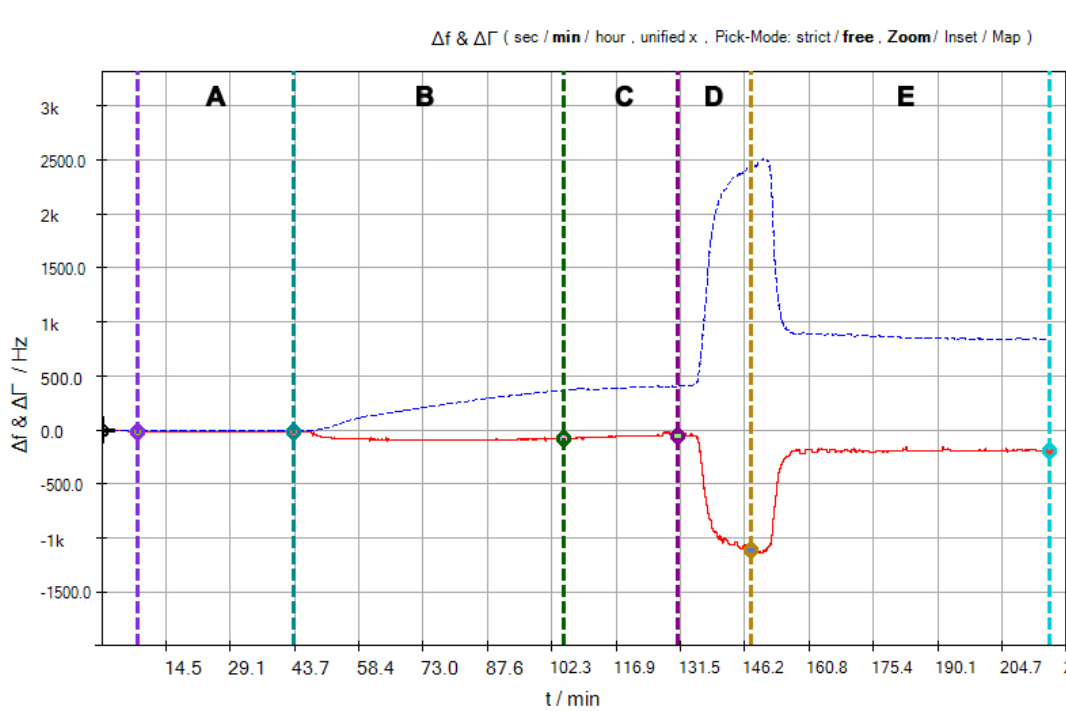


Figure 70: FDA stained *S. gordonii* ($OD_{620\text{ nm}} = 1.4$) binding on ultrasonically and 15 min O_2 plasma cleaned gold-coated quartz sensors and interacting with ABA. A: PBS baseline; B: FDA stained *S. gordonii*: 1 h; C: PBS: 30 min; D: ABA+EB mixture: 16 min; PBS: 30 min. (The red line represents the frequency, the blue line represents dissipation).

3. Results

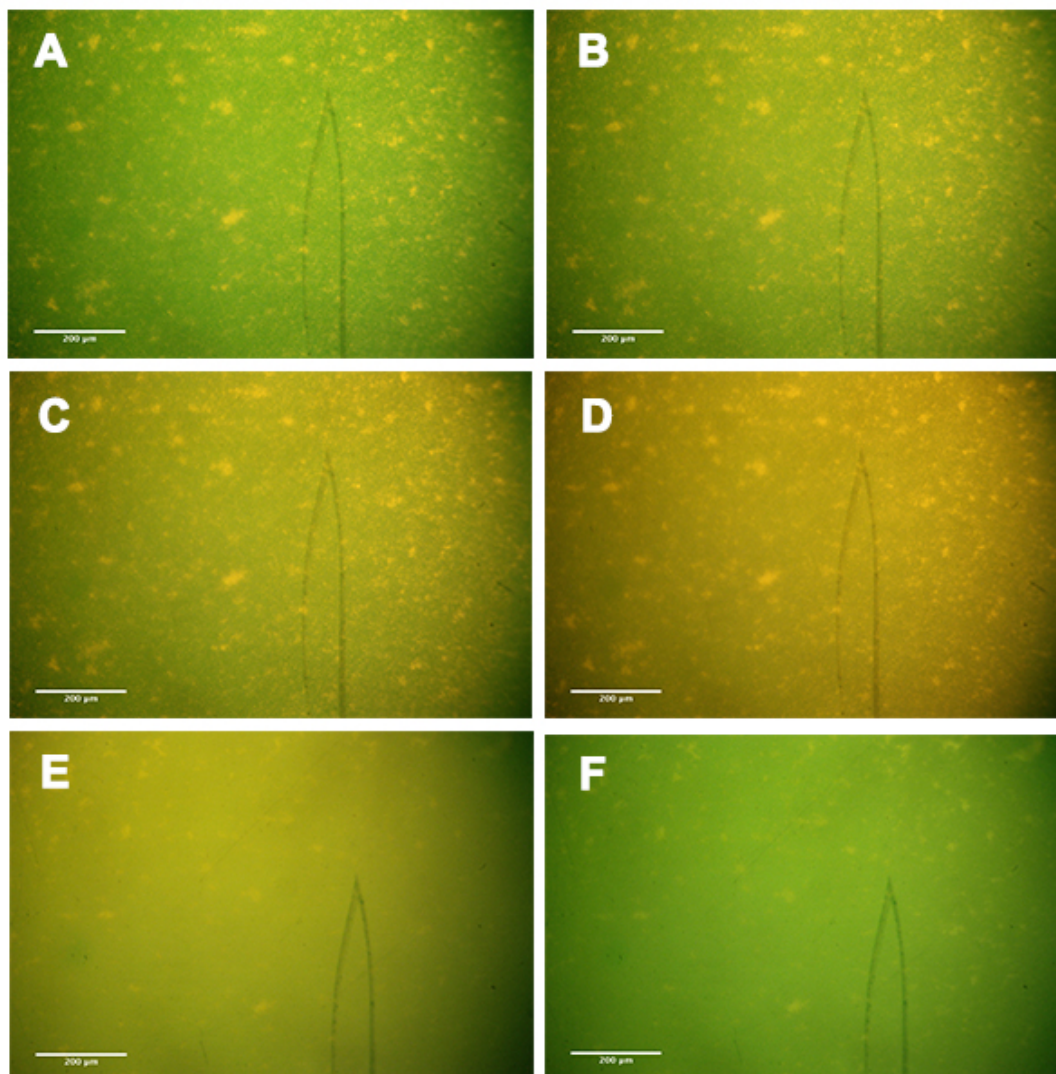


Figure 71: Exemplary online fluorescent photos of FDA/EB stained *S. gordonii* ($OD_{620\text{ nm}} = 1.4$) binding on ultrasonically and 15 min O_2 plasma cleaned gold-coated quartz sensors and interacting with ABA. In the period of application of ABA+EB mixture over the FDA stained bacteria, images were taken every 60 s. In PBS rinsing stage, photos were taken every 5 min. During the whole process, the background was too blurry to take a clear image. **A-D:** when ABA started to flow inside the chamber, the bacteria color changed gradually from green to red; **E-F:** The background turned green upon PBS rinsing, only small unclear red single bacteria could be seen. The small scratch in the image was made for keeping the focus in the same region.

4. Discussion

The bacteria involved infection has become an essential issue, which threatened human health for decades. In the field of dentistry, scientists have spent great efforts searching for an efficient way for controlling the biofilm formation to prevent or limit the progress of dental related infections such as peri-implantitis. A better understanding of the interfacial interaction, involving dental materials, salivary pellicle, attachment of bacteria and antibacterial agents are quite necessary and crucial for the development of novel antibacterial agents and materials.

Our study of interfacial interaction involved the technology of highly sensitive QCM-D, which opens a new door in the field of dentistry. Through these QCM-D studies, models can be improved in terms of binding mechanisms or mass sensitive damage processes. Furthermore, a modified QCM-D, combined with fluorescence microscopy was developed, which could combine online microscopy with the simultaneous QCM-D signal detection, allowing in a first approach correlations of frequency and dissipation with bacterial quantity.

4.1 QCM-D and SPR

Label-free acoustic and optical transducers are commonly used in investigations of biological responses in the interfaces of biomaterial and bio-system. Surface plasmon resonance (SPR), as a kind of label-free optical technology, relies on the binding induced refractive index change to probe the interaction and recognition of element immobilizing on the SPR sensor surface [128]. The quartz crystal microbalance (QCM) method detects for example adsorbed wet mass, i.e, including the mass of solvent. Surface plasmon resonance (SPR) considers mostly the adsorbed dry mass. Both of them have high sensitivity and wide applications. Moreover, the QCM-D technology allows insights into the stiffness of adsorbed films, which is of high interest

when studying the development of elastic/viscoelastic contacts or structures during binding processes [85].

In our studies, the QCM-D technique was applied to investigate and compare the viscoelastic bacterial adhesion referring the stiffness of binding contacts of *S. gordonii* to pure titanium and saliva-coated titanium surface in the contacting sensing zone.

4.2 QCM-D and bacteria adhesion

Compared to the static SEM, AFM, colony counting, and fluorescent staining technologies, the QCM-D technology makes the dynamic and nondestructive analysis of bacterial adhesion, biofilm formation and interfacial bacterial interaction possible. QCM-D has been applied in evaluating factors influencing bacterial adhesion for different stages of the biofilm formation. It was proved by QCM-D measurements that the reversible bacterial adhesion switching to irreversible adhesion occurs in almost 55 s [129]. The QCM-D signal change can also be correlated with the bacterial surface properties. Non-fibrillated “bald” bacteria mostly contribute to a decrease of frequency and a constant dissipation, on the contrary, fibrillated bacteria with long surface fibrils always appeared to have a higher dissipation [85, 129, 130]. The surface hydrophilicity was also evaluated by QCM-D measurement as a parameter influencing the adhesion of bacteria. The hydrophilicity or hydrophobicity of the bacteria will influence the viscoelastic properties of the surface-bacterium bonding [131]. Consistently, hydration and swelling properties of a PVDF grafted surface would also somehow repel the bacterial adhesion [132]. The surface functionalized by –OH is possibly reducing the membrane fouling [133]. Besides, surfaces tailored by polyelectrolyte architecture appeared with high hydrophilicity and coupling with negative surface charges exhibited resistance toward bacterial adhesion [134]. PAMAM-grafted surfaces were proved to inhibit the adhesion of *S. gordonii* and maintained bacterial repulsive capability even after being covered with pellicle [135].

4.3 Chlorhexidine (CHX) and Ti interaction

Oral bacteria can colonize oral titanium implants immediately after their surgical placement, and the colonization pattern of Streptococci species on Ti implant surfaces is distinctively different from that on natural teeth [136]. Though interactions between CHX and biofilms on natural teeth have been intensively studied, there is still limited insight in interactions between CHX and Ti based oral biofilms. Not only with teeth, pellicle and bacteria, CHX can [137] also interact with Ti, as shown in the present study.

Compared with positively charged CHX, in a healthy oral environment with pH 6.7 – pH 7.3 [138], the Ti surface is normally slightly negatively charged [58, 85, 139]. This supports the assumption of CHX binding to Ti surface. CHX in PBS can rapidly adsorb to crystalline TiO₂ reaching equilibrium within 60 s followed by a gradual desorption process [140].

In our study, the fast frequency decrease induced by CHX on pure Ti mainly originated from differences in the viscosity between PBS and CHX, indicated by fast and frequency and dissipation shifts of same size, and only to a limited degree due to CHX molecular adsorption [85]. For smooth Ti sensor surfaces with an average roughness R_a of 1.1 nm [141], 0.12 % CHX adsorbed with a small final residual mass of 128.2 ng/cm² after rinsing. Similarly, studies applying ellipsometry have shown CHX (0.2 %) adsorption of 0.10 µg/cm² and 0.17 µg/cm², respectively, for bare smooth hydrophilic and hydrophobic silicone surfaces, but nearly full reversibility upon rinsing [142]. For anatase ($R_a = 0.136$ µm) [143], 0.1 % CHX caused an adsorption of 0.37 µg/cm² and desorption of 35 % upon water rinsing, ending up with 0.24 µg/cm² CHX [144]. On rutile ($R_a = 0.137$ µm) [143], 0.18 µg/cm² CHX adsorption and 11 % desorption upon rinsing, led to a final amount of 0.16 µg/cm² CHX [144]. For machined smooth Ti ($R_a = 0.36$ µm), 0.1 % CHX and 0.2 % CHX were retained in a final amount of 122.47 µg/cm² and 209.94 µg/cm², respectively [137]. For sandblasted and acid etched microrough Ti ($R_a = 1.78$ µm), 0.1 % CHX and 0.2 % CHX caused final residues of 281.42 µg/cm² and 422.15 µg/cm²,

respectively [137].

Thus, CHX may bind to a higher degree on rough compared to smooth surfaces, due to an increased surface area and a higher number of possible binding sites [137, 142-146]. Smooth Ti sensor surface as used in our study to simulate the trans-gingival part of dental implants seems to offer only a limited number of binding sites for CHX, which may explain the observed minimal bactericidal and also the small binding inhibition effect of Ti sensors pre-conditioned with CHX.

For clinical use, trans-gingival abutment surfaces with $R_a \leq 0.088 \mu\text{m}$ are suggested, which can significantly inhibit the accumulation and maturation of plaque [147]. However, as shown here, a smooth Ti abutment surface with low R_a is not able to retain a functional amount of CHX. To find a balance between enough CHX and lesser plaque accumulation, modifying a relative smooth Ti surface with a topographical feature in the nano scale might be a good possibility and requires further research.

4.4 S. gordonii and pellicle interaction and mass-loss effects

These issues as cited below have been thoroughly discussed in Xu et al [85]:

“The Ti coated sensors used here were moderately hydrophilic allowing simulation of intraoral pellicle formation in this in vitro model. The acquired pellicle is normally formed on any natural and artificial dental material surfaces exposed to the oral salivary environment and consists of spontaneously adsorbing, protein-dominated films [85]. This pellicle plays an irreplaceable role in oral bacterial adhesion and dental plaque formation [2, 9]. In the present study, to simulate the formation of pellicle on a Ti implant surface under clinical conditions, human sterile saliva was adsorbed for entire 30 min on the Ti coated sensors.”[85]

“The QCM-D results showed that saliva adsorbed irreversibly onto Ti

without obvious desorption upon PBS rinsing. The preconditioning with saliva resulted in 537 ng/cm² of retained mass, confirming earlier results [9]. As depicted in **Figure 72**, saliva derived pellicle is a heterogeneous multilayered structure with an inner denser basal layer and a highly hydrated outermost layer [13] comprising larger proteins. In a previous study, we quantified the thickness of such pellicle films on Ti by Kelvin-Voigt modelling of QCM-D data to be <30 nm [9].”[85]

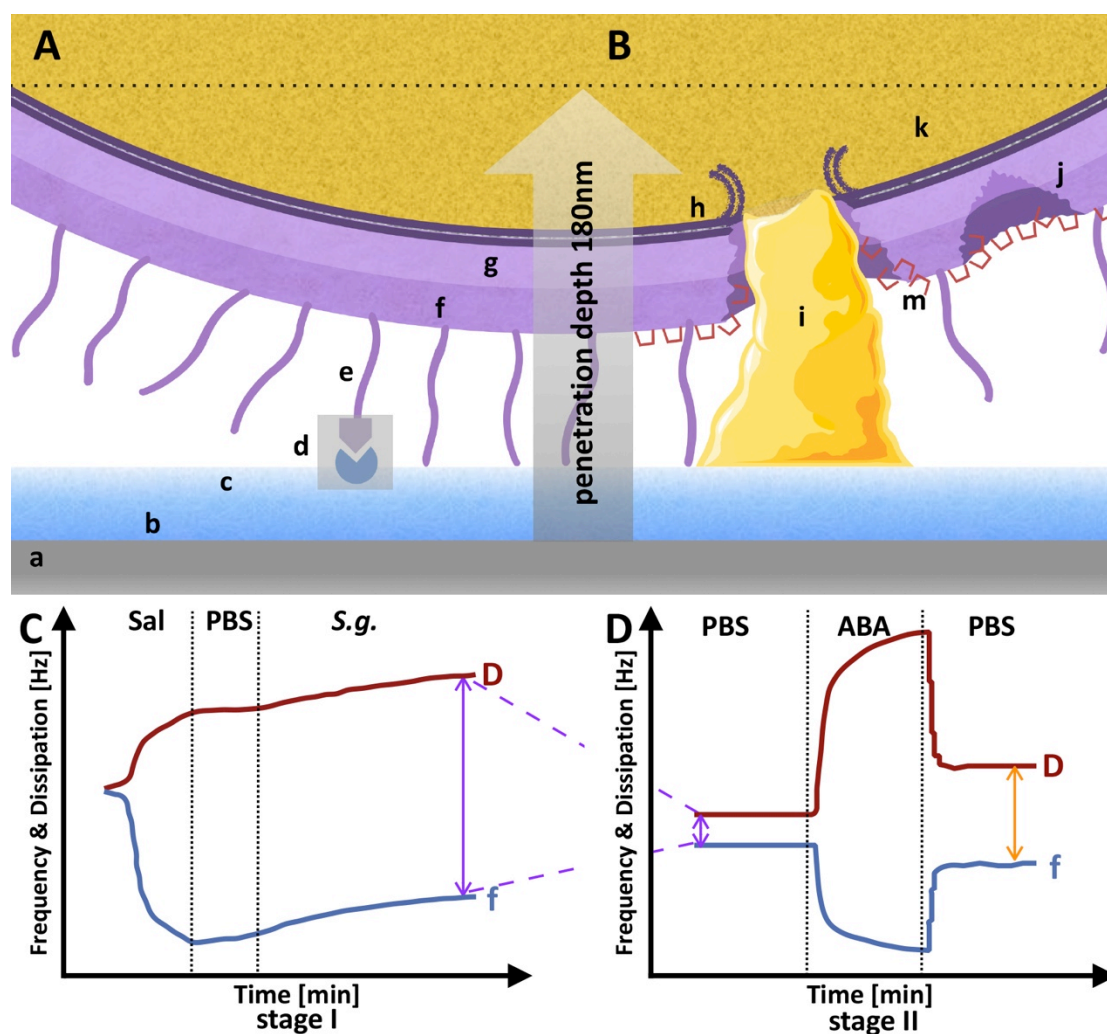


Figure 72: Schematic illustration of QCM-D signal patterns during two physiologically important oral situations: First, specific interaction of *S. gordonii* and pellicle (A) and the respective QCM-D signals (C) are shown. Second, the impact of the bactericidal agent ABA on *S. gordonii* pre-adsorbed to pellicle (B) with the observed characteristic QCM-D response (D) are presented [85]. Please note that C and D highlight two consecutive parts (**stage I** and **stage II**) of one connected online measurement as shown in **Figure 33**; therefore, the purple arrows in C and D represent the same gap between D and *f*. The gap is widened by the interaction of ABA with *S. gordonii*. Details: the transparent

4. Discussion

grey central arrow subdividing A and B illustrates the penetration depth of the evanescent acoustic shear wave into the biological interface, which is about 180 nm [114]. **a.** Ti coated sensor surface; **b and c.** salivary pellicle coating with a dense basal layer (b) and a highly hydrated outermost layer (c) with entire pellicle thickness of < 30 nm [9]; **d.** exemplary specific interaction of bacterial adhesin and pellicle receptor; **e.** peritrichous fibrils of *S. gordonii* 60-80 nm in length [114, 148]; **f.** peptidoglycan (outer wall zone) 15 to 30 nm thick; **g.** peptidoglycan (inner wall zone, periplasmic space) 16 to 22 nm thick [149]; **h.** bacterial plasma phospholipid bilayer membrane, about 4 nm thick; **i.** disintegration of both peptidoglycan cell wall and plasma membrane causing leakage of bacterial plasmatic components; **j.** perforation of bacterial peptidoglycan; **k.** bacterial plasma (not shown are intracellular components like DNA and ribosomes); **m.** U-shaped, red colored ABA molecules interacting with the outer cell wall [85]. **Stage I** in **C** represents the specific binding of *S. gordonii* onto the saliva coated biosensor (modeled in A) characterized by mass-loss (coincident increase of frequency and dissipation) and explained by the coupled-oscillator model. **Stage II** in **D** represents the impact of ABA on pellicle-bound *S. gordonii*, with the characteristic final frequency decrease and dissipation increase which indicates contrary to stage I mass loading. As outlined in the text, mass loading may reflect coincident cell damage and cytoplasm release (modeled in B). ABA (antibacterial agent), *S.g.* (*S. gordonii*), Sal (saliva), Ti (titanium).”[85]

“As shown in our results, *S. gordonii* adhered to a slightly lesser degree onto pellicle than on pure Ti. *S. gordonii* adhesion to a pellicle induced a simultaneous small increase of both frequency and dissipation, which formally represents mass-loss. Apparent mass-loss in the face of microscopically proven surface-adhered bacteria points to specific interactions between *S. gordonii* and the pellicle film. Similar frequency increases were reported recently for *S. gordonii* adhesion to gold pre-conditioned with saliva [114]. Our results indicate that the applied biosensors constitute a sensing probe for specific adhesion of *S. gordonii* by exposing receptors at their outermost surface complementary to adhesins of *S. gordonii*. Whether this biosensor allows specific adhesion of other bacteria has to be proven in further studies.”[85]

“Compared to two-layer viscoelastic models of cells, mass-loss during adhesion of rigid, particle-like bacteria might better be explained

based on a coupled-oscillator model [150]: particle-resonator systems can mathematically be modeled as a pair of coupled oscillators, which show for weak particle binding an increase of system frequency [151]. This soft contact is based, due to this model, on a resonance frequency of the particle below the resonance frequency of the QCM sensor due to a low stiffness (low spring constant) of the bacterium-sensor binding [152]. Positive frequency shifts of bacteria were observed on *Streptococcus salivarius mutants* with surface appendages of different length, with mass loading for bare bacteria and frequency increase up to positive shifts dependent on the type of appendages [153]. Such bacteria do not directly contact the sensor surface and are kept in a certain distance.”[85]

“Approximately 35 % of *S. gordonii* DL1 (wild type) cells are equipped with short peritrichous fibrils (fibrillae) having a length of an estimated 60 to 80 nm [148]. In addition, the pre-adsorbed viscoelastic salivary film increased the distance between the bound bacteria and the oscillating sensor surface. Furthermore, gram positive *S. gordonii* has a 30 to 50 nm thick peptidoglycan cell wall structure [149]. Thus, most bulk parts of the bacterium are outside the penetration depth of the applied 10 MHz QCM-D evanescence shear wave, which in an aqueous system amounts to about 180 nm. Therefore, mass loading and viscoelastic properties cannot be fully detected by the acoustic QCM-D sensor **Figure 72** [114].” [85]

“According to the coupled resonator model, positive frequency shifts require small-point contacts between micrometer-sized adsorbed particles and the sensor surface [154]. *S. gordonii* binds to constituents of the pellicle by proteinaceous adhesins, whereby their specific stereochemical binding mechanism contributed to small contact areas [155-157]: In *S. gordonii*, variants of serine-rich (Srr) protein adhesins or adhesins belonging to the antigen I/II family bind to salivary receptors [17, 85]. It is still unclear why different bacteria show partially adhesion to pure

substrates such as gold or titanium by conventional mass loading with frequency related to the adsorbed mass, e.g., *S. gordonii* on gold [114] and Ti (current study), *S. salivarius* without surface appendages on gold [153], and partially according to the coupled oscillator model, where the frequency represents the contact stiffness and mass-loss effects can be observed, e.g., *S. salivarius* with surface appendages on gold [153], *S. gordonii* on pellicle (current study), and *P. aeruginosa* on hydrophilic silica or more hydrophobic polyvinylidene fluoride [125].”[85]

“The increase of dissipation during bacterial interaction is large on pure Ti but very low with pellicle as an intermediate film. Bacterial films formed by unspecific binding seem to be more dissipative, whereas specific binding increases film stiffness. This might once more be due to the limited detection of the bacteria by the shear wave. Furthermore, coupled oscillators reflect now the interfacial binding between bacteria and the sensor rather than the attached particle mass or dissipation.”[85]

“As highlighted in **Figure 72**, bacteria binding primarily to the surface of a heterogeneous pellicle film lead to a perpendicularly heterogeneous layer with increasing complexity by additional colonizing bacterial species. Furthermore, there is also inhomogeneity horizontally to the sensor surface due to at least initially inhomogeneously distributed bacteria in the lateral direction. Currently, there are no models available which are able to quantitatively describe the respective QCM data upon such complex layer formation [101].”[85]

4.5 Surface interaction of antibacterial agent and its impact on bacterial adhesion and vitality

As discussed above, due to the different charge characteristics, CHX and other cationic bactericidal agents such as CPC are able to bind to the Ti surface. As shown below, these points have already been discussed in Xu et al [85].

“According to our QCM-D results, ABA causes a typical fast frequency decrease and dissipation increase for different surface conditions, i.e., pure Ti, pellicle-coated Ti, or adhered *S. gordonii* films. The fast frequency decrease induced by ABA on pure Ti mainly originates from differences in the viscosity between the bactericidal solution and PBS, indicated by fast and symmetrical frequency and dissipation shifts, and only to a limited degree due to molecular adsorption. The observed QCM signal development, including its reversibility on pellicle, is in line with a previous study using ellipsometry [142].”[85]

“Joiner et al. reported that CHX adsorbs to the pellicle and contributes to modified pellicle properties, such as increased electrostatic attractions and interactions between cationic CHX and negatively charged components [158]. After rinsing with CHX, saliva itself exerts antibacterial activity for up to 5 hours, the persistence in oral surfaces could suppress salivary bacterial counts for over 12 hours [159] showing the reversibility of CHX binding towards saliva [158].”[85]

“CHX inhibits bacterial aggregation and attachment through binding to oral surfaces and precipitating agglutination molecules in saliva by the displacement of Ca^{2+} [160-162], which explains the lower bacterial density and diminished frequency changes in our study observed upon ABA/bacteria mixtures.”[85]

“The mechanisms of CHX and CPC for killing bacteria include adsorption to the negatively charged bacterial cell wall, damaging the permeability barriers which form the entrance of bactericides to the cytoplasm, precipitation and leakage of the cytoplasm, and inhibition of cell wall and membrane rehabilitation [163-166].”[85]

“Bactericidal effects have been confirmed in our study by the observed efficient killing of planktonic as well as surface-adhered *S. gordonii* by bactericidal agent. For interaction of the ABA with the pre-adsorbed bacteria, QCM-D disclosed partial irreversibility of both

frequency and dissipation. By a final decrease in frequency and an increase in dissipation, this indicated mass loading, independent if bacteria adhered unspecifically on pure Ti or specifically on salivary films. Simultaneously, the bacteria-pellicle multilayer becomes slightly stiffer by the bactericidal solution as shown by the decreased slope of the ΔD - Δf plots. These QCM-D results may be indications of the outlined irreversible microbial cell wall damage and cytoplasm release, common mechanisms of biocide interaction [85]. Thus, the observed increase of detectable mass upon ABA may likely be due to leakage of cell content through breached, damaged sites of the cell wall and the ruptured membrane **Figure 72**. Similar to our findings, Olsson et al. have shown that *Staphylococcus epidermis* adheres to gold sensor surfaces according to the coupled oscillator theory and shows conventional mass-loading in course of leakage of extracellular polymeric substances [152]. Ultrastructural studies by transmission electron microscopy (TEM) have shown that CHX caused membrane rupturing and blebbing to a minor part of bacteria within oral biofilms, while CHX did not contribute to a significant disintegration of mature oral biofilms [167]. In contrast to TEM, and in agreement with our FE-SEM and HIM results, no CHX caused cellular damage could be observed in the study of Vitkov et al.”[85]

4.6 HIM and applications

The Helium ion microscope (HIM) is a recently developed nano-scale microscope with various advantages compared to the traditional SEM. Owing to its low energy spread of $\Delta E/E$ up to 2×10^{-5} , the small diffraction effects with $\lambda \sim 80$ fm and high source brightness with B more than 4×10^9 A/cm²sr, the HIM could reach a sub-nanometer resolution of focusing spot size accurate to 0.25 nm [168]. The HIM imaging technology has been applied in more and more biological samples analysis. The analysis of the model plant *Arabidopsis thaliana* through HIM revealed fine surface cuticle structures 163 kX (478 nm

field of view) [124]. As for the explorations of the mammalian neural crest-derived stem cells (NCSCs), the nanodomains of the ultrastructure of the cell membrane, which could not be detected by the traditional SEM, were visualized by HIM at a resolution of 1.5 nm. Without metal coating layer, the HIM images showed the native state of the cell membranes characterized with various diameters of inhomogeneous pits [169]. Moreover, HIM was also applied for the analysis of other mammalian cells such as human liver cells [170], HeLa cells [124], human colon cancer cells [171], similarly, more ultra-structures were revealed than with the traditional coating procedures necessary for SEM.

Additionally, with the development of the technology, HIM was also applied in microbial imaging. HIM was used for studying different stages of the organic-mineral aggregation process of the Fe (II)-oxidizing bacteria, showing delicate nano-scale structures [172]. The HIM imaging also provides a new possibility for the investigation of the interactions between bacteriophages and bacteria. Under HIM, *E. coli* cells involved with ongoing phage infections could be visualized, showing the phages with spreading contracted tails inducing the active infection, which would be covered or damaged by the metal coating and could not be detected by the traditional SEM technology. The lysis of *E. coli* induced by the bursting of new phages could also be detected through HIM [173]. However, in our study the predicted perforation and lysis of the *S. gordonii* membrane could not be visualized so far under HIM due to the shrinkage problem described above. A further modification of the HIM parameters or the sample preparation procedures could be a possibility of getting rid of the bacterial shrinkage after exposure to the He beam. When this issue is resolved, the HIM could shed light on the nanoscale view of the interfacial interactions of bacterial colonization and also of the bacteria-ABA interaction, which opened up new horizons for this important field of dentistry.

4.7 Real-time monitoring with QCM and the QCM-Microscopy set-up

Various attempts have been carried out to correlate microscopic images with the QCM-D signals, to have a better understanding of the kinetics of signal changes and bacterial attachment. The QCM-D sensing combined with simultaneous fluorescent microscopic observation through the window module (QWM401, Q-sense) was applied for detecting the cytoskeletal change of the living cells toward different cytomorphic agents [118]. Besides, it was further utilized in online monitoring and sensing the morphological change, detachment and death of cancer cells (MCF-7) upon different concentrations of drugs to quantify the drug effect and to build up a real-time QCM-D model for detecting the sensitivity of cancer cell toward drugs [117]. For the field of microbiological analysis, the integration of microscopic image taking with bacteria induced QCM-D signal changes was also investigated in several studies [152, 153].

In order to gain a better signal interpretation and more information, QCM-D was combined with AFM, SEM, or fluorescent microscopy. According to the principle of sauerbrey, due to the viscos properties of the bacterial adhesion, the bacteria induced mass loading cannot be directly calculated with the sauerbrey equation based on pure frequency changes. Therefore, quantifying the sensor surface bound bacteria could not be realized by the traditional method. Correlating the online microscopic quantification with the frequency and dissipation shifts might offer a new calculation model in the situation of bacterial adhesion.

However, one of the main difficulties to improve this combined device was the staining and focusing procedure. The key point for a favorable experimental beginning was to find a suitable microscopic lens with a large depth of field, which could focus through the glass window and the liquid layer on the sensor surface. The quality of the image making process was low because of the hardship of keeping focusing through the glass window on the

same adhered bacteria during the 2 to 3 h of consecutive dynamic bacterial flow. The flow of the stained bacteria induced the described blurry and green background, which made the single green stained already adhered bacteria more indistinguishable under the fluorescent light. Concerning the blurry background problem, the possible reasons could be: 1) high concentration of stained bacteria in the flow; 2) the free SYTO 9 molecules in PBS; 3) the inner height of the flow chamber caused inner liquid thickness; 4) the adhesion of bacteria on the inner surface of the flow cell glass lid. However, if the free SYTO 9 molecules in PBS were washed away through the washing procedure, the stained bacteria appeared to have a weaker fluorescent signal, which also made the stained adhered single bacteria hard to distinguish. The situation involving the ABA interaction showed worse background problems, and the red stained dead bacteria were much more inconspicuous than the green stained bacteria. In order to get a sharp clear image of the stained bacteria adhered on the sensor surface, the blue fluorescent light should possess sufficient intensity to activate enough fluorescent signal from the stained bacteria. Nevertheless, the high-intensity fluorescent light irradiating the sensor surface, would concurrently generate the observed spike in the signal curve owing to the local temperature elevation of the region exposed to the fluorescent light. As measured, an elevation of 1 °C will induce a frequency increase of 22 Hz in this system. To find a balance between a distinguishable bacterial image and a minimized signal disturbing is a real challenge. Thus, future possible device improvements could be to modify the staining procedure into higher efficiency, to decrease the inner height of the flow chamber and the replacement of the glass window with a low bacterial binding material to match lenses with higher magnification.

Overall, this QCM-D microscopy set up is a prototype for the new research trend of Lab-on-a-chip [174, 175]. Additionally, repeating tests are encouraged to carry out in different QCM-D systems to prove the signal interpretation and the correlation of this model.

5. Conclusion

“The QCM-D online system with saliva-coated biosensors provides a useful assay to investigate in vitro dynamic interfacial processes located in the oral environment, such as salivary pellicle formation, bacterial adhesion, and effects of antibacterial agents.” [85]

“This assay provides mechanistic insight not only for conventional mass loading processes; additionally, important information about binding mechanisms of bacteria is provided in the case of dissipative events. Due to missing-mass effects and strong influence of a complex viscoelastic multilayer system, bacteria that colonize implant surfaces cannot be simply counted by QCM-D. Important complementary information about microbial film formation can be received by microscopy. Missing-mass effects as observed during bacteria/pellicle interaction indicate specific adhesion mechanisms between bacterial adhesins and complementary salivary receptors.” [85]

“During killing of the model bacterium *S. gordonii* by the applied antibacterial agent, QCM-D could sense mass adsorption, most likely due to concurrent release of cell content towards the sensor caused by cell wall and membrane rupture. Therefore, QCM-D is bearing potential for further mass and dissipation sensitive studies concerning the impact of antibacterial agents on the integrity of gram-positive and gram-negative bacteria.” [85]

“To provide controlled parameters for high reproducibility, suspensions of a single bacterium in standardized buffer solutions were investigated in a basic model system. In future experiments, the adhesion of different bacteria suspended additionally in processed or natural human saliva instead in simple buffer solutions have to be investigated to highlight adhesion directly from this bioliquid and to expand this assay.” [85]

5. Conclusion

Additionally, the further developed QCM-D microscopy set-up combining the *S. gordonii* adhesion induced frequency and dissipation change with the real-time fluorescent imaging, made the quantitative interpretation of QCM-D bacterial adhesion signal possible. The methods for obtaining dynamic images of bactericidal effects of ABA need to be further modified. QCM-D is a suitable online instrumentation to shed light on how antibacterial agents modify regular bacterial adhesin-receptor binding [85]. The applications of QCM-D in building up dental interfacial interaction models provide a very high research potential in the future.

6. Zusammenfassung

Bakterien, die an medizinischen Implantaten anhaften, können invasive mikrobielle Infektionen verursachen, z.B. im Bereich von Haut, Lunge oder Blut. In der Zahnheilkunde ist *Streptococcus gordonii* ein früher oraler Besiedler, der die Bildung von Zahnbiofilmen initiiert und auch an der lebensbedrohlichen infektiösen Endokarditis beteiligt ist. Zur Behandlung von oralen Biofilmen werden häufig antibakterielle Mundspülungen verwendet. Solche initialen Wechselwirkungen zwischen Biomaterialien und Bakterien sowie der Einfluss antibakterieller Behandlungen wurden hier in situ mit der Quarzkristall-Mikrowaage mit Dissipationsüberwachung (QCM-D) eingehend untersucht.

Ein mit Speichel beschichteter Titan (Ti) -Biosensor wurde verwendet, um mögliche spezifische Signalmuster zu analysieren, die auf mikrobielle Bindungsmechanismen und bakterizidbedingte Veränderungen der Bakterienfilmsteifigkeit oder Zelleckage hinweisen, die durch ein klinisch relevantes antibakterielles Mittel (ABA), d.h. eine Mundspülung (Chlorhexidin (CHX) und Cetylpyridiniumchlorid (CPC)), verursacht werden. Offensichtlich fehlende Masseneffekte bei der Bildung von mikroskopisch nachgewiesenen dichten und vitalen Bakterienfilmen deuteten auf eine punktuelle, spezifische Bindung von *S. gordonii* an den mit Speichel beschichteten Biosensor im Vergleich zu einer unspezifischen Haftung an reinem Ti hin.

Gleichzeitig mit der ABA-induzierten Abtötung von an der Oberfläche haftenden Bakterien konnte im Gegensatz zum vorherigen Massenverlust eine Zunahme der adsorbierten dissipativen Masse festgestellt werden. Dies legt die akustische Erfassung des Auslaufens von Zellinhalt nahe, der durch das Aufbrechen der bakteriellen Zellwand und die Beschädigung der Membran beim bakteriziden Angriff verursacht wurde. Diese Ergebnisse haben signifikante Auswirkungen auf die Prüfung der bakteriellen Adhäsionsmechanismen und der zellulären Integrität während der

Wechselwirkung mit antibakteriellen Mitteln.

Zusätzlich wurde in dieser Studie ein QCM-D-Mikroskopie-Aufbau weiterentwickelt, durch den die durch die Adhäsion von *S. gordonii* induzierte Frequenz und Dissipationsänderung mit den Echtzeit-Fluoreszenzbildern korreliert werden konnte, was die quantitative Interpretation des QCM-D-Bakterienadhäsionssignals ermöglicht hat. Die Anwendung von QCM-D beim Aufbau eines dentalen Grenzflächen-Interaktionsmodells bietet in Zukunft ein sehr hohes Forschungspotenzial.

7. References

- [1] J.O.Tenovuo, B. Nauntofte, F. Lagerlöf., Secretion and composition of saliva. In: Dental Caries: The disease and its clinical management, Eds: O. Fejerskov, E. A.M. Kidd, Blackwell Munkgaard (2003) 7-27.
- [2] U. Lendenmann, J. Grogan, F.G. Oppenheim, Saliva and dental pellicle--a review, *Adv Dent Res* 14 (2000) 22-8.
- [3] R. Gocke, F. Gerath, H. von Schwanewede, Quantitative determination of salivary components in the pellicle on PMMA denture base material, *Clin Oral Investig* 6(4) (2002) 227-35.
- [4] S.D. Bradway, E.J. Bergey, P.C. Jones, M.J. Levine, Oral mucosal pellicle. Adsorption and transpeptidation of salivary components to buccal epithelial cells, *Biochem J* 261(3) (1989) 887-96.
- [5] S.D. Bradway, E.J. Bergey, F.A. Scannapieco, N. Ramasubbu, S. Zawacki, M.J. Levine, Formation of salivary-mucosal pellicle: the role of transglutaminase, *Biochem J* 284 (Pt 2) (1992) 557-64.
- [6] M. Hannig, Transmission electron microscopic study of in vivo pellicle formation on dental restorative materials, *Eur J Oral Sci* 105(5 Pt 1) (1997) 422-33.
- [7] W.L. Siqueira, W. Custodio, E.E. McDonald, New insights into the composition and functions of the acquired enamel pellicle, *J Dent Res* 91(12) (2012) 1110-8.
- [8] A.T. Hara, M. Ando, C. Gonzalez-Cabezas, J.A. Cury, M.C. Serra, D.T. Zero, Protective effect of the dental pellicle against erosive challenges in situ, *J Dent Res* 85(7) (2006) 612-6.
- [9] F. Rupp, M. Haupt, M. Eichler, C. Doering, H. Klostermann, L. Scheideler, S. Lachmann, C. Oehr, H.P. Wendel, E. Decker, J. Geis-Gerstorfer, C. von Ohle, Formation and photocatalytic decomposition of a pellicle on anatase surfaces, *J Dent Res* 91(1) (2012) 104-9.
- [10] K.K. Skjørland, M. Rykke, T. Sønju, Rate of pellicle formation in vivo, *Acta Odontologica Scandinavica* 53(6) (1995) 358-362.
- [11] O. Santos, L. Lindh, T. Halthur, T. Arnebrant, Adsorption from saliva to silica and hydroxyapatite surfaces and elution of salivary films by SDS and delmopinol, *Biofouling* 26(6) (2010) 697-710.
- [12] L. Vitkov, M. Hannig, Y. Nekrashevych, W.D. Krautgartner, Supramolecular pellicle precursors, *European journal of oral sciences* 112(4) (2004) 320-325.
- [13] M. Cárdenas, T. Arnebrant, A. Rennie, G. Fragneto, R.K. Thomas, L. Lindh, Human saliva forms a complex film structure on alumina surfaces, *Biomacromolecules* 8(1) (2007) 65-69.
- [14] L. Macakova, G.E. Yakubov, M.A. Plunkett, J.R. Stokes, Influence of ionic strength changes on the structure of pre-adsorbed salivary films. A response of a natural multi-component layer, *Colloids and Surfaces B: Biointerfaces* 77(1) (2010) 31-39.

7. References

- [15] D. Kohavi, A. Klinger, D. Steinberg, M.N. Sela, Adsorption of salivary proteins onto prosthetic titanium components, *J Prosthet Dent* 74(5) (1995) 531-4.
- [16] F.E. Dewhirst, T. Chen, J. IZard, B.J. Paster, A.C. Tanner, W.-H. Yu, A. Lakshmanan, W.G. Wade, The human oral microbiome, *Journal of bacteriology* 192(19) (2010) 5002-5017.
- [17] A.H. Nobbs, H.F. Jenkinson, N.S. Jakubovics, Stick to your gums: mechanisms of oral microbial adherence, *J Dent Res* 90(11) (2011) 1271-8.
- [18] D. Takamatsu, B.A. Bensing, A. Prakobphol, S.J. Fisher, P.M. Sullam, Binding of the streptococcal surface glycoproteins GspB and Hsa to human salivary proteins, *Infection and immunity* 74(3) (2006) 1933-1940.
- [19] L.J. Brady, S.E. Maddocks, M.R. Larson, N. Forsgren, K. Persson, C.C. Deivanayagam, H.F. Jenkinson, The changing faces of Streptococcus antigen I/II polypeptide family adhesins, *Molecular microbiology* 77(2) (2010) 276-286.
- [20] A. Jonasson, C. Eriksson, H.F. Jenkinson, C. Källestål, I. Johansson, N. Strömberg, Innate immunity glycoprotein gp-340 variants may modulate human susceptibility to dental caries, *BMC infectious diseases* 7(1) (2007) 57.
- [21] S. Sekine, K. Kataoka, M. Tanaka, H. Nagata, T. Kawakami, K. Akaji, S. Aimoto, S. Shizukuishi, Active domains of salivary statherin on apatitic surfaces for binding to *Fusobacterium nucleatum* cells, *Microbiology* 150(7) (2004) 2373-2379.
- [22] J.W. Costerton, P.S. Stewart, E.P. Greenberg, Bacterial biofilms: a common cause of persistent infections, *Science* 284(5418) (1999) 1318-22.
- [23] K. Subramani, R.E. Jung, A. Molenberg, C.H. Hammerle, Biofilm on dental implants: a review of the literature, *Int J Oral Maxillofac Implants* 24(4) (2009) 616-26.
- [24] R. Saini, Oral biofilm and dental implants: A brief, *National journal of maxillofacial surgery* 2(2) (2011) 228.
- [25] J. Costerton, L. Montanaro, C.R. Arciola, Biofilm in implant infections: its production and regulation, *The International journal of artificial organs* 28(11) (2005) 1062-1068.
- [26] E. Tacconelli, E. Carrara, A. Savoldi, S. Harbarth, M. Mendelson, D.L. Monnet, C. Pulcini, G. Kahlmeter, J. Kluytmans, Y. Carmeli, Discovery, research, and development of new antibiotics: the WHO priority list of antibiotic-resistant bacteria and tuberculosis, *The Lancet Infectious Diseases* 18(3) (2018) 318-327.
- [27] I. Fedtke, F. Gotz, A. Peschel, Bacterial evasion of innate host defenses--the *Staphylococcus aureus* lesson, *Int J Med Microbiol* 294(2-3) (2004) 189-94.
- [28] P.S. Stewart, J.W. Costerton, Antibiotic resistance of bacteria in biofilms, *The lancet* 358(9276) (2001) 135-138.
- [29] N. Jakubovics, P. Kolenbrander, The road to ruin: the formation of disease-associated oral biofilms, *Oral diseases* 16(8) (2010) 729-739.
- [30] H. Wolfe, Biofilm plaque formation on tooth and root surfaces,

7. References

- Periodontology, Stuttgart: Thieme (2005) 24-30.
- [31] C. Saxton, Scanning electron microscope study of the formation of dental plaque, *Caries research* 7(2) (1973) 102-119.
- [32] M. Cowan, K. Taylor, R. Doyle, Kinetic analysis of *Streptococcus sanguis* adhesion to artificial pellicle, *Journal of dental research* 65(10) (1986) 1278-1283.
- [33] C.J. Whittaker, C.M. Klier, P.E. Kolenbrander, Mechanisms of adhesion by oral bacteria, *Annu Rev Microbiol* 50 (1996) 513-52.
- [34] J.W. Costerton, Z. Lewandowski, D.E. Caldwell, D.R. Korber, H.M. Lappin-Scott, Microbial biofilms, *Annu Rev Microbiol* 49 (1995) 711-45.
- [35] M. Wilson, B. O'Connor, H. Newman, Isolation and identification of bacteria from subgingival plaque with low susceptibility to minocycline, *Journal of Antimicrobial Chemotherapy* 28(1) (1991) 71-78.
- [36] A. Tanner, M. Maiden, K. Lee, L. Shulman, H. Weber, Dental implant infections, *Clinical infectious diseases* 25(Supplement_2) (1997) S213-S217.
- [37] T. Rams, T. Roberts, D. Feik, A. Molzan, J. Slots, Clinical and microbiological findings on newly inserted hydroxyapatite-coated and pure-titanium human dental implants, *Clinical oral implants research* 2(3) (1991) 121-127.
- [38] Å. Leonhardt, K. Gröndahl, C. Bergström, U. Lekholm, Long-term follow-up of osseointegrated titanium implants using clinical, radiographic and microbiological parameters, *Clinical oral implants research* 13(2) (2002) 127-132.
- [39] M. Quirynen, N. Van Assche, RCT comparing minimally with moderately rough implants. Part 2: microbial observations, *Clinical oral implants research* 23(5) (2012) 625-634.
- [40] P. Murray, A. Prakobphol, T. Lee, C. Hoover, S. Fisher, Adherence of oral streptococci to salivary glycoproteins, *Infection and immunity* 60(1) (1992) 31-38.
- [41] G.S. Cook, J.W. Costerton, R.J. Lamont, Biofilm formation by *Porphyromonas gingivalis* and *Streptococcus gordonii*, *Journal of periodontal research* 33(6) (1998) 323-327.
- [42] G. Nakazato, H. Tsuchiya, M. Sato, M. Yamauchi, In vivo plaque formation on implant materials, *International Journal of Oral & Maxillofacial Implants* 4(4) (1989).
- [43] J.S. Foster, P.E. Kolenbrander, Development of a multispecies oral bacterial community in a saliva-conditioned flow cell, *Appl Environ Microbiol* 70(7) (2004) 4340-8.
- [44] S.W. Kerrigan, D. Cox, Platelet-bacterial interactions, *Cell Mol Life Sci* 67(4) (2010) 513-23.
- [45] A. Mombelli, M. Marxer, T. Gaberthüel, U. Grander, N.P. Lang, The microbiota of osseointegrated implants in patients with a history of periodontal disease, *Journal of clinical periodontology* 22(2) (1995) 124-130.
- [46] T. Berglundh, S. Jepsen, B. Stadlinger, H. Terheyden, Peri-implantitis and

7. References

- its prevention, *Clinical oral implants research* 30(2) (2019) 150-155.
- [47] A. Mombelli, N.P. Lang, Microbial aspects of implant dentistry, *Periodontology* 2000 4(1) (1994) 74-80.
- [48] J. Gerber, D. Wenaweser, L. Heitz-Mayfield, N.P. Lang, G. Rutger Persson, Comparison of bacterial plaque samples from titanium implant and tooth surfaces by different methods, *Clinical oral implants research* 17(1) (2006) 1-7.
- [49] M.M. Fürst, G.E. Salvi, N.P. Lang, G.R. Persson, Bacterial colonization immediately after installation on oral titanium implants, *Clinical oral implants research* 18(4) (2007) 501-508.
- [50] A. Han, J.K. Tsoi, F.P. Rodrigues, J.G. Leprince, W.M. Palin, Bacterial adhesion mechanisms on dental implant surfaces and the influencing factors, *International Journal of Adhesion and Adhesives* 69 (2016) 58-71.
- [51] L. Rimondini, S. Farè, E. Brambilla, A. Felloni, C. Consonni, F. Brossa, A. Carrassi, The effect of surface roughness on early in vivo plaque colonization on titanium, *Journal of periodontology* 68(6) (1997) 556-562.
- [52] D.R. Drake, J. Paul, J.C. Keller, Primary bacterial colonization of implant surfaces, *International Journal of Oral and Maxillofacial Implants* 14(2) (1999) 226-232.
- [53] F. Mabboux, L. Ponsonnet, J.-J. Morrier, N. Jaffrezic, O. Barsotti, Surface free energy and bacterial retention to saliva-coated dental implant materials—an in vitro study, *Colloids and Surfaces B: Biointerfaces* 39(4) (2004) 199-205.
- [54] S. Sardin, J.J. Morrier, G. Benay, O. Barsotti, In vitro streptococcal adherence on prosthetic and implant materials. Interactions with physicochemical surface properties, *Journal of Oral Rehabilitation* 31(2) (2004) 140-148.
- [55] R. Bos, H.C. Van der Mei, H.J. Busscher, Physico-chemistry of initial microbial adhesive interactions—its mechanisms and methods for study, *FEMS microbiology reviews* 23(2) (1999) 179-230.
- [56] S. Baliga, S. Muglikar, R. Kale, Salivary pH: A diagnostic biomarker, *Journal of Indian Society of Periodontology* 17(4) (2013) 461.
- [57] C.Y. Guo, J.P. Matinlinna, A.T.H. Tang, Effects of surface charges on dental implants: past, present, and future, *International journal of biomaterials* 2012 (2012).
- [58] T. Preočanin, N. Kallay, Point of zero charge and surface charge density of TiO₂ in aqueous electrolyte solution as obtained by potentiometric mass titration, *Croatica chemica acta* 79(1) (2006) 95-106.
- [59] T.P. Schaer, S. Stewart, B.B. Hsu, A.M. Klibanov, Hydrophobic polycationic coatings that inhibit biofilms and support bone healing during infection, *Biomaterials* 33(5) (2012) 1245-1254.
- [60] K. Narendrakumar, M. Kulkarni, O. Addison, A. Mazare, I. Junkar, P. Schmuki, R. Sammons, A. Igljč, Adherence of oral streptococci to nanostructured titanium surfaces, *Dental Materials* 31(12) (2015) 1460-1468.
- [61] C.R. Arciola, D. Campoccia, P. Speziale, L. Montanaro, J.W. Costerton,

7. References

Biofilm formation in Staphylococcus implant infections. A review of molecular mechanisms and implications for biofilm-resistant materials, *Biomaterials* 33(26) (2012) 5967-5982.

[62] H. Lv, Z. Chen, X. Yang, L. Cen, X. Zhang, P. Gao, Layer-by-layer self-assembly of minocycline-loaded chitosan/alginate multilayer on titanium substrates to inhibit biofilm formation, *Journal of dentistry* 42(11) (2014) 1464-1472.

[63] S.J. Lee, D.N. Heo, H.R. Lee, D. Lee, S.J. Yu, S.A. Park, W.-K. Ko, S.W. Park, S.G. Im, J.-H. Moon, Biofunctionalized titanium with anti-fouling resistance by grafting thermo-responsive polymer brushes for the prevention of peri-implantitis, *Journal of Materials Chemistry B* 3(26) (2015) 5161-5165.

[64] Y. Wu, J. Geis-Gerstorf, L. Scheideler, F. Rupp, Photocatalytic antibacterial effects on TiO₂-anatase upon UV-A and UV-A/VIS threshold irradiation, *Biofouling* 32(5) (2016) 583-595.

[65] H. Chourifa, H. Bouloussa, V. Migonney, C. Falentin-Daudré, Review of titanium surface modification techniques and coatings for antibacterial applications, *Acta biomaterialia* (2018).

[66] R. Adell, B.O. Hansson, P.I. Branemark, U. Breine, Intra-osseous anchorage of dental prostheses. II. Review of clinical approaches, *Scand J Plast Reconstr Surg* 4(1) (1970) 19-34.

[67] P.I. Branemark, R. Adell, U. Breine, B.O. Hansson, J. Lindstrom, A. Ohlsson, Intra-osseous anchorage of dental prostheses. I. Experimental studies, *Scand J Plast Reconstr Surg* 3(2) (1969) 81-100.

[68] G. Granstrom, Craniofacial osseointegration, *Oral Dis* 13(3) (2007) 261-9.

[69] M. Niinomi, T. Kobayashi, N. Sasaki, Toughness and microstructural factors of Ti-6Al-4V alloy, *Materials Science and Engineering* 100 (1988) 45-55.

[70] R. Osman, M. Swain, A critical review of dental implant materials with an emphasis on titanium versus zirconia, *Materials* 8(3) (2015) 932-958.

[71] M. McCracken, Dental implant materials: commercially pure titanium and titanium alloys, *Journal of prosthodontics* 8(1) (1999) 40-43.

[72] N.U. Zitzmann, T. Berglundh, Definition and prevalence of peri-implant diseases, *J Clin Periodontol* 35(8 Suppl) (2008) 286-91.

[73] F. Schwarz, J. Derks, A. Monje, H.L. Wang, Peri-implantitis, *Journal of clinical periodontology* 45 (2018) S246-S266.

[74] A. Mombelli, N. Muller, N. Cionca, The epidemiology of peri-implantitis, *Clin Oral Implants Res* 23 Suppl 6 (2012) 67-76.

[75] H. Dreyer, J. Grischke, C. Tiede, J. Eberhard, A. Schweitzer, S.E. Toikkanen, S. Glockner, G. Krause, M. Stiesch, Epidemiology and risk factors of peri-implantitis: A systematic review, *J Periodontal Res* 53(5) (2018) 657-681.

[76] L. Sbordone, C. Bortolaia, Oral microbial biofilms and plaque-related diseases: microbial communities and their role in the shift from oral health to disease, *Clin Oral Investig* 7(4) (2003) 181-8.

7. References

- [77] T. Berglundh, G. Armitage, M.G. Araujo, G. Avila-Ortiz, J. Blanco, P.M. Camargo, S. Chen, D. Cochran, J. Derks, E. Figuero, Peri-implant diseases and conditions: Consensus report of workgroup 4 of the 2017 World Workshop on the Classification of Periodontal and Peri-Implant Diseases and Conditions, *Journal of periodontology* 89 (2018) S313-S318.
- [78] M. Esposito, M. Grusovin, P. Coulthard, H. Worthington, The efficacy of interventions to treat peri-implantitis: a Cochrane systematic review of randomised controlled clinical trials, *European journal of oral implantology* 9(2) (2016) 111-125.
- [79] S. Renvert, J. Lessem, G. Dahlén, C. Lindahl, M. Svensson, Topical minocycline microspheres versus topical chlorhexidine gel as an adjunct to mechanical debridement of incipient peri-implant infections: a randomized clinical trial, *Journal of clinical periodontology* 33(5) (2006) 362-369.
- [80] L.J. Heitz-Mayfield, A. Mombelli, The therapy of peri-implantitis: a systematic review, *International Journal of Oral & Maxillofacial Implants* 29 (2014).
- [81] K. Subramani, D. Wismeijer, Decontamination of titanium implant surface and re-osseointegration to treat peri-implantitis: a literature review, *International Journal of Oral & Maxillofacial Implants* 27(5) (2012).
- [82] M. Muthukuru, A. Zainvi, E.O. Esplugues, T.F. Flemmig, Non-surgical therapy for the management of peri-implantitis: a systematic review, *Clinical Oral Implants Research* 23 (2012) 77-83.
- [83] N. Sahm, J. Becker, T. Santel, F. Schwarz, Non-surgical treatment of peri-implantitis using an air-abrasive device or mechanical debridement and local application of chlorhexidine: a prospective, randomized, controlled clinical study, *Journal of clinical periodontology* 38(9) (2011) 872-878.
- [84] S. Jepsen, T. Berglundh, R. Genco, A.M. Aass, K. Demirel, J. Derks, E. Figuero, J.L. Giovannoli, M. Goldstein, F. Lambert, Primary prevention of peri-implantitis: Managing peri-implant mucositis, *Journal of clinical periodontology* 42 (2015) S152-S157.
- [85] Z. Xu, L. Coriand, R. Loeffler, J. Geis-Gerstorfer, Y. Zhou, L. Scheideler, M. Fleischer, F.K. Gehring, F. Rupp, Saliva-coated titanium biosensor detects specific bacterial adhesion and bactericide caused mass loading upon cell death, *Biosensors and Bioelectronics* 129 (2019) 198-207.
- [86] P. Marsh, Microbiological aspects of the chemical control of plaque and gingivitis, *Journal of Dental Research* 71(7) (1992) 1431-1438.
- [87] J.E. Stoeken, S. Paraskevas, G.A. Van Der Weijden, The long-term effect of a mouthrinse containing essential oils on dental plaque and gingivitis: a systematic review, *Journal of periodontology* 78(7) (2007) 1218-1228.
- [88] R.P. Allaker, C.I. Douglas, Novel anti-microbial therapies for dental plaque-related diseases, *International journal of antimicrobial agents* 33(1) (2009) 8-13.
- [89] P.D. Marsh, Controlling the oral biofilm with antimicrobials, *Journal of dentistry* 38 (2010) S11-S15.

7. References

- [90] M. Brading, P. Marsh, The oral environment: the challenge for antimicrobials in oral care products, *International dental journal* 53(S6P1) (2003) 353-362.
- [91] S. Haps, D. Slot, C. Berchier, G. Van der Weijden, The effect of cetylpyridinium chloride-containing mouth rinses as adjuncts to toothbrushing on plaque and parameters of gingival inflammation: a systematic review, *International journal of dental hygiene* 6(4) (2008) 290-303.
- [92] S. Haps, D.E. Slot, C.E. Berchier, G.A. Van der Weijden, The effect of cetylpyridinium chloride-containing mouth rinses as adjuncts to toothbrushing on plaque and parameters of gingival inflammation: a systematic review, *Int J Dent Hyg* 6(4) (2008) 290-303.
- [93] C.G. EMILSON, Susceptibility of various microorganisms to chlorhexidine, *European Journal of Oral Science* 85(4) (1977) 255-265.
- [94] M.E. Barbour, S.E. Maddocks, N.J. Wood, A.M. Collins, Synthesis, characterization, and efficacy of antimicrobial chlorhexidine hexametaphosphate nanoparticles for applications in biomedical materials and consumer products, *Int J Nanomedicine* 8 (2013) 3507-19.
- [95] C.G. Jones, Chlorhexidine: is it still the gold standard?, *Periodontol* 2000 15 (1997) 55-62.
- [96] D.A. Van Strydonck, D.E. Slot, U. Van der Velden, F. Van der Weijden, Effect of a chlorhexidine mouthrinse on plaque, gingival inflammation and staining in gingivitis patients: a systematic review, *Journal of clinical periodontology* 39(11) (2012) 1042-1055.
- [97] G. P., Chlorhexidine and related compounds, *journal of dental research* 68 (1989) 1602-1608.
- [98] K.-S. Lim, P. Kam, Chlorhexidine-pharmacology and clinical applications, *Anaesthesia and intensive care* 36(4) (2008) 502-512.
- [99] A. Scheie, F. Petersen, *Antimicrobials in caries control, Dental Caries–The disease and its clinical management*. 2nd ed. UK: Blackwell Munksgaard Ltd (2008) 266-76.
- [100] P.C. Pan, S. Harper, D. Ricci-Nittel, R. Lux, W. Shi, In-vitro evidence for efficacy of antimicrobial mouthrinses, *Journal of dentistry* 38 (2010) S16-S20.
- [101] I. Reviakine, D. Johannsmann, R.P. Richter, Hearing what you cannot see and visualizing what you hear: interpreting quartz crystal microbalance data from solvated interfaces, *Anal Chem* 83(23) (2011) 8838-48.
- [102] M.C. Dixon, Quartz crystal microbalance with dissipation monitoring: enabling real-time characterization of biological materials and their interactions, *J Biomol Tech* 19(3) (2008) 151-8.
- [103] M. Rodahl, F. Höök, A. Krozer, P. Brzezinski, B. Kasemo, Quartz crystal microbalance setup for frequency and Q-factor measurements in gaseous and liquid environments, *Review of Scientific Instruments* 66(7) (1995) 3924-3930.
- [104] D. Johannsmann, *Methods of Read-Out, The Quartz Crystal Microbalance in Soft Matter Research*, Springer2015, pp. 23-31.
- [105] M. Pax, J. Rieger, R.H. Eibl, C. Thielemann, D. Johannsmann,

7. References

- Measurements of fast fluctuations of viscoelastic properties with the quartz crystal microbalance, *Analyst* 130(11) (2005) 1474-1477.
- [106] G. Sauerbrey, Verwendung von Schwingquarzen zur Wägung dünner Schichten und zur Mikrowägung, *Z. Physik*, 155, 206–222, 1959.
- [107] A. Janshoff, H.J. Galla, C. Steinem, Piezoelectric mass-sensing devices as biosensors—an alternative to optical biosensors?, *Angewandte Chemie International Edition* 39(22) (2000) 4004-4032.
- [108] B. Becker, M.A. Cooper, A survey of the 2006-2009 quartz crystal microbalance biosensor literature, *J Mol Recognit* 24(5) (2011) 754-87.
- [109] M. Hussain, F. Rupp, H.P. Wendel, F.K. Gehring, Bioapplications of acoustic crystals, a review, *TrAC Trends in Analytical Chemistry* (2018).
- [110] M. Hussain, H. Northoff, F.K. Gehring, QCM-D providing new horizon in the domain of sensitivity range and information for haemostasis of human plasma, *Biosens Bioelectron* 66 (2015) 579-84.
- [111] T.E. Alexander, L.D. Lozeau, T.A. Camesano, QCM-D Characterization of Time-Dependence of Bacterial Adhesion, *The Cell Surface* (2019) 100024.
- [112] R. Hao, D. Wang, X.e. Zhang, G. Zuo, H. Wei, R. Yang, Z. Zhang, Z. Cheng, Y. Guo, Z. Cui, Rapid detection of *Bacillus anthracis* using monoclonal antibody functionalized QCM sensor, *Biosensors and Bioelectronics* 24(5) (2009) 1330-1335.
- [113] Z.-Q. Shen, J.-F. Wang, Z.-G. Qiu, M. Jin, X.-W. Wang, Z.-L. Chen, J.-W. Li, F.-H. Cao, QCM immunosensor detection of *Escherichia coli* O157: H7 based on beacon immunomagnetic nanoparticles and catalytic growth of colloidal gold, *Biosensors and Bioelectronics* 26(7) (2011) 3376-3381.
- [114] S. Krajewski, J. Rheinlaender, P. Ries, D. Canjuga, C. Mack, L. Scheideler, T.E. Schaffer, J. Geis-Gerstorfer, H.P. Wendel, F. Rupp, Bacterial interactions with proteins and cells relevant to the development of life-threatening endocarditis studied by use of a quartz-crystal microbalance, *Anal Bioanal Chem* 406(14) (2014) 3395-406.
- [115] A.L. Olsson, M.R. Mitzel, N. Tufenkji, QCM-D for non-destructive real-time assessment of *Pseudomonas aeruginosa* biofilm attachment to the substratum during biofilm growth, *Colloids Surf B Biointerfaces* 136 (2015) 928-34.
- [116] T. Leino, M. Raulio, M. Salkinoja-Salonen, P. Stenius, J. Laine, Adsorption of bacteria and polycations on model surfaces of cellulose, hemicellulose and wood extractives studied by QCM-D, *Colloids and Surfaces B: Biointerfaces* 86(1) (2011) 131-139.
- [117] L. Nowacki, J. Follet, M. Vayssade, P. Vigneron, L. Rotellini, F. Cambay, C. Egles, C. Rossi, Real-time QCM-D monitoring of cancer cell death early events in a dynamic context, *Biosensors and Bioelectronics* 64 (2015) 469-476.
- [118] J. Fatisson, F. Azari, N. Tufenkji, Real-time QCM-D monitoring of cellular responses to different cytomorphic agents, *Biosensors and Bioelectronics* 26(7) (2011) 3207-3212.

7. References

- [119] A. Duparre, J. Ferre-Borrull, S. Gliech, G. Notni, J. Steinert, J.M. Bennett, Surface characterization techniques for determining the root-mean-square roughness and power spectral densities of optical components, *Applied optics* 41(1) (2002) 154-171.
- [120] L. Coriand, M. Mitterhuber, A. Duparré, A. Tünnermann, Definition of roughness structures for superhydrophobic and hydrophilic optical coatings on glass, *Applied optics* 50(9) (2011) C257-C263.
- [121] M. Hussain, F.K. Gehring, S. Sinn, H. Northoff, A straightforward detection of HIT type II via QCM-D, *UK J. Pharm. Biosci* 3(6) (2015) 18-29.
- [122] S.A.L. Center for Light-Matter Interaction, Abbildung der Oberfläche: HIM -HeliumIonenmikroskop.<[https://uni-tuebingen.de/forschung/forschungsinfrastuktur/lisa/einrichtungen/duennfilm-oberflaechen-analyse/abbildung-der-oberflaeche/ - c383699](https://uni-tuebingen.de/forschung/forschungsinfrastuktur/lisa/einrichtungen/duennfilm-oberflaechen-analyse/abbildung-der-oberflaeche/-c383699)>, (2019).
- [123] F.B. Bidlack, C. Huynh, J. Marshman, B. Goetze, Helium ion microscopy of enamel crystallites and extracellular tooth enamel matrix, *Frontiers in physiology* 5 (2014) 395.
- [124] M.S. Joens, C. Huynh, J.M. Kasuboski, D. Ferranti, Y.J. Sigal, F. Zeitvogel, M. Obst, C.J. Burkhardt, K.P. Curran, S.H. Chalasani, Helium Ion Microscopy (HIM) for the imaging of biological samples at sub-nanometer resolution, *Scientific reports* 3 (2013) 3514.
- [125] I.M. Marcus, M. Herzberg, S.L. Walker, V. Freger, *Pseudomonas aeruginosa* attachment on QCM-D sensors: the role of cell and surface hydrophobicities, *Langmuir* 28(15) (2012) 6396-402.
- [126] G.A. McCubbin, S. Praporski, S. Piantavigna, D. Knappe, R. Hoffmann, J.H. Bowie, F. Separovic, L.L. Martin, QCM-D fingerprinting of membrane-active peptides, *Eur Biophys J* 40(4) (2011) 437-46.
- [127] M. Miyamoto, Y. Morimoto, Y. Nozawa, A. Balamurugan, B. Xu, K. Inoue, Establishment of fluorescein diacetate and ethidium bromide (FDAEB) assay for quality assessment of isolated islets, *Cell transplantation* 9(5) (2000) 681-686.
- [128] J. Homola, Present and future of surface plasmon resonance biosensors, *Analytical and bioanalytical chemistry* 377(3) (2003) 528-539.
- [129] A.L. Olsson, H.C. van der Mei, H.J. Busscher, P.K. Sharma, Novel analysis of bacterium– substratum bond maturation measured using a Quartz Crystal Microbalance, *Langmuir* 26(13) (2010) 11113-11117.
- [130] A.L. Olsson, H.C. Van der Mei, H.J. Busscher, P.K. Sharma, Influence of cell surface appendages on the bacterium– substratum interface measured real-time using QCM-D, *Langmuir* 25(3) (2008) 1627-1632.
- [131] J. Gutman, S.L. Walker, V. Freger, M. Herzberg, Bacterial attachment and viscoelasticity: physicochemical and motility effects analyzed using quartz crystal microbalance with dissipation (QCM-D), *Environmental science & technology* 47(1) (2012) 398-404.
- [132] M. Herzberg, A. Sweity, M. Bрами, Y. Kaufman, V. Freger, G. Oron, S. Belfer, R. Kasher, Surface properties and reduced biofouling of

7. References

- graft-copolymers that possess oppositely charged groups, *Biomacromolecules* 12(4) (2011) 1169-1177.
- [133] A.E. Contreras, Z. Steiner, J. Miao, R. Kasher, Q. Li, Studying the role of common membrane surface functionalities on adsorption and cleaning of organic foulants using QCM-D, *Environmental science & technology* 45(15) (2011) 6309-6315.
- [134] S. Guo, M.Y. Kwek, Z.Q. Toh, D. Pranantyo, E.-T. Kang, X.J. Loh, X. Zhu, D. Jańczewski, K.G. Neoh, Tailoring polyelectrolyte architecture to promote cell growth and inhibit bacterial adhesion, *ACS applied materials & interfaces* 10(9) (2018) 7882-7891.
- [135] M. Eichler, V. Katzur, L. Scheideler, M. Haupt, J. Geis-Gerstorfer, G. Schmalz, S. Ruhl, R. Müller, F. Rupp, The impact of dendrimer-grafted modifications to model silicon surfaces on protein adsorption and bacterial adhesion, *Biomaterials* 32(35) (2011) 9168-9179.
- [136] M.M. Furst, G.E. Salvi, N.P. Lang, G.R. Persson, Bacterial colonization immediately after installation on oral titanium implants, *Clinical oral implants research* 18(4) (2007) 501-8.
- [137] A. Kozlovsky, Z. Artzi, O. Moses, N. Kamin-Belsky, R.B. Greenstein, Interaction of chlorhexidine with smooth and rough types of titanium surfaces, *J Periodontol* 77(7) (2006) 1194-200.
- [138] S. Baliga, S. Muglikar, R. Kale, Salivary pH: A diagnostic biomarker, *Journal of Indian Society of Periodontology* 17(4) (2013) 461-5.
- [139] J.P.M. Cecilia Yan Guo, Alexander Tin HongTang, Effects of Surface Charges on Dental Implants: Past, Present, and Future, *International Journal of Biomaterials* 2012 (2012) 5.
- [140] D.J.O.S. Michele E. Barbour, Daryll C. Jagger, Chlorhexidine adsorption to anatase and rutile titanium dioxide, *Colloids and Surfaces A* 307 (2007) 116-120.
- [141] F. Rupp, M. Haupt, H. Klostermann, H.S. Kim, M. Eichler, A. Peetsch, L. Scheideler, C. Doering, C. Oehr, H.P. Wendel, S. Sinn, E. Decker, C. von Ohle, J. Geis-Gerstorfer, Multifunctional nature of UV-irradiated nanocrystalline anatase thin films for biomedical applications, *Acta biomaterialia* 6(12) (2010) 4566-77.
- [142] L.B. Freitas, N. Vassilakos, T. Arnebrant, Interactions of chlorhexidine with salivary films adsorbed at solid/liquid and air/liquid interfaces, *J Periodontal Res* 28(2) (1993) 92-7.
- [143] M.E. Barbour, N. Gandhi, A. el-Turki, D.J. O'Sullivan, D.C. Jagger, Differential adhesion of *Streptococcus gordonii* to anatase and rutile titanium dioxide surfaces with and without functionalization with chlorhexidine, *J Biomed Mater Res A* 90(4) (2009) 993-8.
- [144] M.E. Barbour, D.J. O'Sullivan, D.C. Jagger, Chlorhexidine adsorption to anatase and rutile titanium dioxide, *Colloids and Surfaces A: Physicochemical and Engineering Aspects* 307(1-3) (2007) 116-120.
- [145] M. Morra, C. Cassinelli, G. Cascardo, A. Carpi, M. Fini, G. Giavaresi, R.

7. References

- Giardino, Adsorption of cationic antibacterial on collagen-coated titanium implant devices, *Biomedicine & pharmacotherapy* 58(8) (2004) 418-422.
- [146] H.S. Ryu, Y.I. Kim, B.S. Lim, Y.J. Lim, S.J. Ahn, Chlorhexidine Uptake and Release From Modified Titanium Surfaces and Its Antimicrobial Activity, *Journal of periodontology* 86(11) (2015) 1268-75.
- [147] L. Rimondini, S. Fare, E. Brambilla, A. Felloni, C. Consonni, F. Brossa, A. Carrassi, The effect of surface roughness on early in vivo plaque colonization on titanium, *J Periodontol* 68(6) (1997) 556-62.
- [148] R. McNab, H. Forbes, P.S. Handley, D.M. Loach, G.W. Tannock, H.F. Jenkinson, Cell wall-anchored CshA polypeptide (259 kilodaltons) in *Streptococcus gordonii* forms surface fibrils that confer hydrophobic and adhesive properties, *J Bacteriol* 181(10) (1999) 3087-95.
- [149] W. Vollmer, D. Blanot, M.A. de Pedro, Peptidoglycan structure and architecture, *FEMS Microbiol Rev* 32(2) (2008) 149-67.
- [150] N. Tymchenko, E. Nileback, M.V. Voinova, J. Gold, B. Kasemo, S. Svedhem, Reversible changes in cell morphology due to cytoskeletal rearrangements measured in real-time by QCM-D, *Biointerphases* 7(1-4) (2012) 43.
- [151] D.G. L, A sensitive new method for the determination of adhesive bonding between a particle and a substrate, *Journal of Applied Physics* 58(7) (1985) 2789-2790.
- [152] A.L. Olsson, H.C. van der Mei, H.J. Busscher, P.K. Sharma, Acoustic sensing of the bacterium-substratum interface using QCM-D and the influence of extracellular polymeric substances, *J Colloid Interface Sci* 357(1) (2011) 135-8.
- [153] A.L. Olsson, H.C. van der Mei, H.J. Busscher, P.K. Sharma, Influence of cell surface appendages on the bacterium-substratum interface measured real-time using QCM-D, *Langmuir* 25(3) (2009) 1627-32.
- [154] A. Pomorska, D. Shchukin, R. Hammond, M.A. Cooper, G. Grundmeier, D. Johannsmann, Positive frequency shifts observed upon adsorbing micron-sized solid objects to a quartz crystal microbalance from the liquid phase, *Analytical chemistry* 82(6) (2010) 2237-2242.
- [155] S.J. Ahn, H.S. Kho, K.K. Kim, D.S. Nahm, Adhesion of oral streptococci to experimental bracket pellicles from glandular saliva, *Am J Orthod Dentofacial Orthop* 124(2) (2003) 198-205.
- [156] S. Ruhl, A.L. Sandberg, J.O. Cisar, Salivary receptors for the proline-rich protein-binding and lectin-like adhesins of oral actinomyces and streptococci, *J Dent Res* 83(6) (2004) 505-10.
- [157] D.L. Stevens, E.L. Kaplan, *Streptococcal infections: clinical aspects, microbiology, and molecular pathogenesis*, Oxford University Press, USA2000.
- [158] A. Joiner, U.M. Elofsson, T. Arnebrant, Adsorption of chlorhexidine and black tea onto in vitro salivary pellicles, as studied by ellipsometry, *Eur J Oral Sci* 114(4) (2006) 337-42.
- [159] W.R. Roberts, M. Addy, Comparison of the in vivo and in vitro

7. References

antibacterial properties of antiseptic mouthrinses containing chlorhexidine, alexidine, cetyl pyridinium chloride and hexetidine. Relevance to mode of action, *J Clin Periodontol* 8(4) (1981) 295-310.

[160] G. Rolla, B. Melsen, On the mechanism of the plaque inhibition by chlorhexidine, *J Dent Res* 54 Spec No B (1975) B57-62.

[161] M.J. Winrow, Metabolic studies with radiolabelled chlorhexidine in animals and man, *J Periodontal Res Suppl* 12 (1973) 45-8.

[162] E.-M. Decker, R. Weiger, C. Von Ohle, I. Wiech, M. Brex, Susceptibility of planktonic versus attached *Streptococcus sanguinis* cells to chlorhexidine, *Clinical oral investigations* 7(2) (2003) 98-102.

[163] A. Davies, The mode of action of chlorhexidine, *J Periodontal Res Suppl* 12 (1973) 68-75.

[164] S.P. Denyer, Mechanisms of action of antibacterial biocides, *International biodeterioration & biodegradation* 36(3-4) (1995) 227-245.

[165] H.-Y. Cheung, M.M.-K. Wong, S.-H. Cheung, L.Y. Liang, Y.-W. Lam, S.-K. Chiu, Differential actions of chlorhexidine on the cell wall of *Bacillus subtilis* and *Escherichia coli*, *PLoS One* 7(5) (2012) e36659.

[166] K.A. Pitten FA, Efficacy of Cetylpyridinium Chloride Used as Oropharyngeal Antiseptic, *Arzneim Forsch/ Drug Research* 51(7) (2001) 588-595.

[167] L. Vitkov, A. Hermann, W. Krautgartner, M. Herrmann, K. Fuchs, M. Klappacher, M. Hannig, Chlorhexidine-induced ultrastructural alterations in oral biofilm, *Microscopy research and technique* 68(2) (2005) 85-89.

[168] B. Ward, J.A. Notte, N. Economou, Helium ion microscope: A new tool for nanoscale microscopy and metrology, *Journal of Vacuum Science & Technology B: Microelectronics and Nanometer Structures Processing, Measurement, and Phenomena* 24(6) (2006) 2871-2874.

[169] M. Schürmann, N. Frese, A. Beyer, P. Heimann, D. Widera, V. Mönkemöller, T. Huser, B. Kaltschmidt, C. Kaltschmidt, A. Gölzhäuser, Helium ion microscopy visualizes lipid nanodomains in mammalian cells, *Small* 11(43) (2015) 5781-5789.

[170] X. Chen, C.N. Udalagama, C.-B. Chen, A.A. Bettiol, D.S. Pickard, T. Venkatesan, F. Watt, Whole-cell imaging at nanometer resolutions using fast and slow focused helium ions, *Biophysical journal* 101(7) (2011) 1788-1793.

[171] D. Bazou, G. Behan, C. Reid, J. Boland, H. Zhang, Imaging of human colon cancer cells using He-Ion scanning microscopy, *Journal of microscopy* 242(3) (2011) 290-294.

[172] J.M. Byrne, M. Schmidt, T. Gauger, C. Bryce, A. Kappler, Imaging Organic–Mineral Aggregates Formed by Fe (II)-Oxidizing Bacteria Using Helium Ion Microscopy, *Environmental Science & Technology Letters* 5(4) (2018) 209-213.

[173] M. Leppänen, L.R. Sundberg, E. Laanto, G.M. de Freitas Almeida, P. Papponen, I.J. Maasilta, Imaging Bacterial Colonies and Phage–Bacterium Interaction at Sub-Nanometer Resolution Using Helium-Ion Microscopy,

7. References

Advanced Biosystems 1(8) (2017) 1700070.

[174] A.L. Olsson, P. Braun, J. Zhang, H. Drechsel, A. Sterck, G. Prepens, T. Reiner, F.K. Gehring, Mikrofluidischer Chip vereint QCM-D und mikroskopische Messungen, BIOSpektrum 25(3) (2019) 300-302.

[175] A.L. Olsson, Z. Xu, P. Braun, J. Zhang, H. Drechsel, A. Sterck, G. Prepens, T. Reiner, S. Krajewski, F. Rupp, Erratum zu „Mikrofluidischer Chip vereint QCM-D und mikroskopische Messungen“, BIOSpektrum 25(5) (2019) 541-541.

Declaration of Contribution

This research was carried out in the Section Medical Materials Science and Technology, University Hospital Tübingen (MWT), under the supervision of Prof. Dr. Frank Rupp.

Prof. Dr. Frank Rupp, Prof. Dr. Jürgen Geis-Gerstorfer and Dr. Lutz Scheideler were involved in hypothesis development, the project design and the project application. Prof. Dr. Frank Rupp has supervised the work, corrected the doctoral thesis, reviewed the manuscript and submission of the publication. Dr. Lutz Scheideler has helped with the experimental strategy modification, the construction of the QCM-microscopy set-up and review of the manuscript.

Ms. Ingrid Stephan (MWT) provided the instruction of contact angle measurement, saliva preparation, and the procedure of the QCM-D measurement. Mr. Ernst Schweizer (MWT) helped with the SEM measurements of the bacteria on the sensor surface. Ms. Evi Kimmerle-Müller (MWT) offered her help with the bacterial preparation and bacterial staining. Ms. Barbara Illing helped with correcting the thesis manuscript.

Dr. Bernd Neumann (Department of Thoracic, cardiac and vascular surgery, University Hospital Tübingen) helped with the critical point drying of the samples. Dr. Luisa Coriand (Fraunhofer Institute for Applied Optics and Precision Engineering, Jena) made the AFM and WLI measurements for the surface characterization. Prof. Dr. Monika Fleischer and Dr. Ronny Loeffler (Core Facility LISA+, Eberhard Karls University Tübingen) offered the high-resolution analysis of bacteria on sensor surface through FE-SEM and HIM. Dr. Frank Gehring (3T analytic, Tuttlingen) and Mr. Thomas Reiner (3T analytic, Tuttlingen) offered the technical support for the QCM-D instrument and were involved in the construction and development of the QCM-Microscopy set-up. Dr. Adam. J. Olsson (3T analytic, Tuttlingen) helped with the calculation theory support and Mr. Jin Zhang (3T analytic, Tuttlingen)

helped with the software development for the QCM-Microscopy set-up. Dr. Yi Zhou (Prosthodontic department, School & Hospital of Stomatology, Wuhan University, (Hubei-MOST)) offered the clinical suggestions to the modification of the manuscript.

Zeqian Xu has done all the experiments, data evaluation, statistic analysis and also written the whole publication by herself. Thus, I declare that the submitted thesis is my own independent work. All indirect or direct sources used in this thesis are acknowledged as references.

Tuebingen, D-72076,

Zeqian Xu

Signature: *Zeqian Xu*

Publication of the content of the dissertation

Here I would like to declare that, before finishing this doctoral thesis, some figures and some relevant text from the dissertation have already been published in “Z. Xu, L. Coriand, R. Loeffler, J. Geis-Gerstorfer, Y. Zhou, L. Scheideler, M. Fleischer, F.K. Gehring, F. Rupp, Saliva-coated titanium biosensor detects specific bacterial adhesion and bactericide caused mass loading upon cell death, *Biosensors and Bioelectronics* 129 (2019) 198-207” and as a conference paper in “Z. Xu, I. Stephan, L. Scheideler, J. Geis - Gerstorfer, F. Rupp, QCM analysis of chlorhexidine interaction with salivary and *S. gordonii* films on titanium implant surfaces, *Clinical Oral Implants Research* 29 (2018) 237-237.”

Acknowledgment

First of all, I would like to thank my supervisor, Prof. Dr. Frank Rupp, for offering the enormous support to my research work and guiding me rambling into the world of science. A new idea of innovation and attempts are always encouraged. Under his rigorous supervision mode of “teach me to fish rather than give me fish,” I have gained considerable progress in my research work. I want to thank my supervisor for opening a new door in my research career, and I will keep walking forward no matter how difficult it is.

Then, I would like to show my gratitude to the head of our lab, Prof. Dr. Jürgen Geis-Gerstorfer, who offered me the chance to stay in this research section with excellent experimental conditions and various scientific resources. He always enthusiastically offered me help for the problems I met in both research work and also daily life.

After that, I want to thank Dr. Lutz Scheideler, who helped me a lot with the design and modification of the experiment. I greatly benefited from his profound academic background, positive and optimistic character and the curious attitude toward exploring something new.

Furthermore, I would like to thank Ms. Ingrid Stephan, who offered me lots of help with my experiment with the QCM-D machine, the wettability test and daily life. I also want to thank my colleagues, Mr. Ernst Schweizer, who offered SEM analysis and also lots of jokes; Ms. Christine Schille, who offered many important suggestions; Ms. Evi Kimmerle-Müller, who helped me in the bio-lab; Mr. Sebastian Spintzyk who worked with 3D printing, surface roughness and was always willing to help; and Ms. Barbara Illing, who helped me with my doctoral thesis writing. I would like to thank my Chinese colleagues, Ms. Xingting Han, Mr. Ping Li, Dr. Yichen Xu, Ms. Jintao Dai, Dr. Lanchen Liang and Dr. Yanyun Wu who provide great concern, pleasure, accompany, help and support to my research work and daily life.

And my special acknowledgment is for the Chinese Scholarship Council

for offering financial support during my study in Germany.

Besides, I acknowledge my sincere gratitude to Prof. Dr. Heiner Weber and Priv. Doz. Dr. Eva Engel for offering the possibility to join the clinical work and to be involved in the DGPro program “Specialist for Prosthetics” in the department of prosthodontics and implantology.

Moreover, I am grateful to Prof. Dr. Monika Fleischer, Dr. Ronny Loeffler, Dr. Yi Zhou, Dr. Luisa Coriand, Prof. Dr. Hans Peter Wendel, Dr. Stefanie Krajewski, Dr. Bernd Neumann, Dr. Frank Gehring, Dr. Adam. J. Olsson, Mr. Thomas Reiner, Mr. Jin Zhang for the nice and successful cooperation.

Finally, I profoundly appreciate my beloved parents, Xiao’e Chen and Yuefan Xu, who respect my decision to study abroad in this crucial turning point of my life, constantly express their care to my daily life and share my pressure, sadness and happiness. I am also grateful to my other family members and my best friends, for offering me the mental support.

Curriculum Vitae

Personal Information

Name: Zeqian Xu

Gender: Female

Date of Birth: 13. 04.1993

Nationality: Chinese



Education

- | | |
|---------------------|--|
| 09. 2009 – 06. 2014 | School & Hospital of Stomatology Wuhan University,
Bachelor Degree, China |
| 09. 2014 – 06. 2016 | School & Hospital of Stomatology Wuhan University,
Department of Prosthodontics,
Master Degree, China |
| 08. 2015 | National Dental Board Examinations, China |
| 11.2016 – Present | University Hospital Tübingen,
Department of Prosthodontics,
Section “Medical Materials and Technology”
Doctor Degree, Germany |

Science Activities and Scholarships

- Poster presentation of “QCM analysis of chlorhexidine interaction with salivary and *S. gordonii* films on titanium implant surfaces” at the 27th Annual Scientific Meeting of the European Association for Osseointegration (EAO), Vienna, Austria, 2018.
- Join the International Osteology Symposium Barcelona, Spain, 2019.
- Poster presentation of “Novel QCM-D/microscopy set-up for real-time analysis of bacterial binding onto biomaterial- coated sensors” at the 5th European Symposium and Exhibition on Biomaterials and related Areas (Euro BioMAT) held by Deutsche Gesellschaft für Materialkunde (DGM), Weimar, Germany, 2019.

- Oral presentation of “Multi-disciplinary therapy combined with soft and hard -tissue augmentation for implant restoration in the esthetic-zone” at the 18th Biennial Meeting of the ICP Meeting Jointly with the European Prosthodontic Association (EPA), Amsterdam, Netherlands, 2019.
- Oral presentation of “Natural antibacterial coating on dental implants and/or abutments for the prevention and treatment of peri- implantitis” at the 30th Annual Conference of the European Society for Biomaterials (ESB) together with the 26th Annual Conference of the German Society for Biomaterials (DGBM), Dresden, Germany, 2019.
- Poster presentation of “The Application of Natural Antibacterial Coating for the Surface Modification of Dental Implants and Abutments” at 28th Annual Scientific Meeting of the European Association for Osseointegration (EAO), Lisbon, Portugal, 2019.

- Scholarship from the Chinese Scholarship Council, 2017-2020
- Scholarship from the Wuhan University, 2009-2014

Academic Competition:

- 2016. 5 BITC implantology clinical case competition (Hubei Region)
the third prize
- 2016. 9 National BITC implant clinical case competition
the third prize
- 2016. 9 National multi-disciplinary clinical case competition in dentistry
hold by CSA (the Chinese Stomatological Association)
the third prize

List of Publications:

1. Z. Xu, L. Coriand, R. Loeffler, J. Geis-Gerstorfer, Y. Zhou, L. Scheideler, M. Fleischer, F.K. Gehring, F. Rupp, Saliva-coated titanium biosensor detects specific bacterial adhesion and bactericide caused mass loading upon cell death, *Biosensors and Bioelectronics* 129 (2019) 198-207.
2. X. Han, N. Sharma, Z. Xu, L. Scheideler, J. Geis-Gerstorfer, F. Rupp, F.M. Thieringer, S. Spintzyk, An In Vitro Study of Osteoblast Response on Fused-Filament Fabrication 3D Printed PEEK for Dental and Cranio-Maxillofacial Implants, *Journal of clinical medicine* 8(6) (2019) 771.
3. A.L. Olsson, Z. Xu, P. Braun, J. Zhang, H. Drechsel, A. Sterck, G. Prepens, T. Reiner, S. Krajewski, F. Rupp, F.K. Gehring. Erratum zu „Mikrofluidischer Chip vereint QCM-D und mikroskopische Messungen“, *BIOspektrum* 25(5) (2019) 541-541.
4. **[Conference paper]** Z. Xu, I. Stephan, L. Scheideler, J. Geis-Gerstorfer, F. Rupp, QCM analysis of chlorhexidine interaction with salivary and *S. gordonii* films on titanium implant surfaces, *Clinical Oral Implants Research* 29 (2018) 237-237.
5. **[Conference paper]** Z. Xu, S. Krajewski, T. Weindl, X. Han, E. Kimmerle-Müller, E. Schweizer, J. Geis-Gerstorfer, L. Scheideler, H. Peter Wendel, F. Rupp, The application of natural antibacterial coating for the surface modification of dental implants and abutments, *Clinical Oral Implants Research* 30(S19) (2019) 132-132.